MARTIN MARIETTA ENERGY SYSTEMS LIBRARIES

3 4456 0380305 2

ORNL/TM-12466

ornl

OAK RIDGE
NATIONAL
LABORATORY

MARTIN MARIETTA

MCNP Analysis of the FOEHN Critical Experiment

October 1993

OAK RIDGE NATIONAL LABORATORY
CENTRAL RESEARCH LIBRARY
CIRCULATION SECTION
4500N ROOM 175
LIBRARY LOAN COPY
DO NOT TRANSFER TO ANOTHER PERSON
If you wish someone else to see this report, send in name with report and the library will arrange a loan.
ornl-6151 (3-96)

Advanced Neutron Source

MANAGED BY
MARTIN MARIETTA ENERGY SYSTEMS, INC.
FOR THE UNITED STATES
DEPARTMENT OF ENERGY

This report has been reproduced directly from the best available copy.

Available to DOE and DOE contractors from the Office of Scientific and Technical Information, P.O. Box 62, Oak Ridge, TN 37831; prices available from (615) 576-8401, FTS 626-8401.

Available to the public from the National Technical Information Service, U.S. Department of Commerce, 5285 Port Royal Rd., Springfield, VA 22161.

This report was prepared as an account of work sponsored by an agency of the United States Government. Neither the United States Government nor any agency thereof, nor any of their employees, makes any warranty, express or implied, or assumes any legal liability or responsibility for the accuracy, completeness, or usefulness of any information, apparatus, product, or process disclosed, or represents that its use would not infringe privately owned rights. Reference herein to any specific commercial product, process, or service by trade name, trademark, manufacturer, or otherwise, does not necessarily constitute or imply its endorsement, recommendation, or favoring by the United States Government or any agency thereof. The views and opinions of authors expressed herein do not necessarily state or reflect those of the United States Government or any agency thereof.

ORNL/TM-12466

MCNP ANALYSIS OF THE FOEHN CRITICAL EXPERIMENT

A. M. Ougouag
C. A. Wemple
G. A. Rubio
J. M. Ryskamp

Idaho National Engineering Laboratory
EG&G IDAHO, Inc., P.O. Box 1625
Idaho Falls, Idaho 83415-3885

October 1993

Prepared by
OAK RIDGE NATIONAL LABORATORY
Oak Ridge, Tennessee 37831-6285
managed by
MARTIN MARIETTA ENERGY SYSTEMS, INC.
for the
U.S. DEPARTMENT OF ENERGY
under contract DE-AC05-84OR21400

MARTIN MARIETTA ENERGY SYSTEMS LIBRARIES

3 4456 0380305 2

CONTENTS

LIST OF FIGURES vii

LIST OF TABLES ix

ACKNOWLEDGEMENTS xi

EXECUTIVE SUMMARY xiii

ABSTRACT xvii

1. INTRODUCTION 1

1.1 MOTIVATION 1

1.2 SCOPE AND LIMITATIONS OF THE STUDY 1

1.3 ORGANIZATION OF THE REPORT 1

2. THE FOEHN EXPERIMENT 3

2.1 INTRODUCTION 3

2.2 DESCRIPTION OF THE FOEHN EXPERIMENT 3
2.2.1 Reactor Components and Geometry 3
2.2.1.1 Reactor Core 3
2.2.1.2 Reflector and Internal Stack Geometry 4
2.2.1.3 Control Elements and Safety System 4
2.2.1.4 Safety Rods 4
2.2.1.5 Solid Boron End Zones 4
2.2.2 Experimental Facilities 4
2.2.2.1 Reflector Internal Components 4
2.2.2.2 Cold Source Facility Mock-up 5
2.2.2.3 Hot Source Facility Mock-up 5
2.2.2.4 Loops 5
2.2.3 Materials 5

2.3 RESULTS OF THE FOEHN EXPERIMENT 5
2.3.1 Quantities Measured 6
2.3.1.1 Core Multiplication Factor (k_{eff}) 6
2.3.1.2 Fluxes and Spectrum 6
2.3.1.3 Flux Efficiency (Rendement) 6
2.3.1.4 Power Distribution 7
2.3.1.5 Gamma Heating in the Reflector 7
2.3.2 Normalization of Tabulated Results 7
2.3.2.1 FOEHN Experiment Normalization Method 7

2.3.2.2 Single Table Normalization 8
2.3.2.3 Multiple Tables with Missing Data 8
2.3.2.4 Normalization of Fluxes 9

2.4 ERROR ANALYSIS OF FOEHN RESULTS 11
2.4.1 Error Reporting in the FOEHN Experiment 11
2.4.2 Sources of Errors 11
2.4.2.1 Geometric Tolerances 11
2.4.2.2 Materials Data 11
2.4.2.3 Counting Geometry, Statistics, and Times 11
2.4.3 Estimates of the Error on Select Quantities 12
2.4.3.1 Cadmium Ratio, R_{Cd} 12
2.4.3.2 Thermal Flux 12
2.4.3.3 Powers 13
2.4.3.4 Rendement 14

2.5 SUMMARY 14

3. MCNP MODEL OF THE FOEHN EXPERIMENT 15

3.1 INTRODUCTION 15

3.2 MAJOR APPROXIMATIONS AND ASSUMPTIONS 15
3.2.1 Homogenous Core, Geometry Details, and Fidelity 15
3.2.2 Assumptions on Materials Data 16

3.3 MCNP MODEL DESCRIPTION 17
3.3.1 The Core and Surrounding Structures 17
3.3.2 Reflector Internals 28
3.3.3 Safety Rods 28
3.3.4 The Coordinate System 29
3.3.5 Materials 29

3.4 MCNP TALLIES AND COMPUTATION OF k_{eff} AND RENDEMENT 29
3.4.1 Fluxes 29
3.4.2 Powers 30
3.4.3 Effective Multiplication Factor 30
3.4.4 Determination of Rendement 30

3.5 SUMMARY 30

4. RESULTS 31

4.1 INTRODUCTION 31

4.2 SIMPLE REACTOR MODEL 31
4.2.1 Core Multiplication Factors (k_{eff}) 31
4.2.2 Thermal Flux 31

4.2.3 Rendement 34
4.2.4 Power 34

4.3 INTERMEDIATE COMPLEXITY REACTOR MODEL 41
4.3.1 Core Multiplication Factor (k_{eff}) 41
4.3.2 Thermal Flux 41
4.3.3 Rendement 54
4.3.4 Power 61

4.4 FULL COMPLEXITY REACTOR MODEL 61
4.4.1 Core Multiplication Factor (k_{eff}) 61
4.4.2 Thermal Flux 61
4.4.3 Rendement 71
4.4.4 Power 71

4.5 SUMMARY 78

5. CONCLUSIONS 79

6. REFERENCES 81

Appendix A. MCNP MODEL INPUT FILE 83

LIST OF FIGURES

Figure		Page
ES-1	Computed vs measured axial power distribution at three radial positions of the FOEHN critical experiment	xv
3.1a	SABRINA printout of the current ANS reactor design MCNP model	18
3.1b	SABRINA printout of the FOEHN experiment MCNP model (front view)	19
3.2	SABRINA printout of the FOEHN experiment MCNP model (left view)	20
3.3	SABRINA printout of the FOEHN experiment MCNP model (right view)	21
3.4	SABRINA printout of the FOEHN experiment MCNP model (top view)	22
3.5	SABRINA printout of the FOEHN experiment MCNP model (lower view)	23
3.6	SABRINA printout of the FOEHN experiment MCNP model (back view)	24
3.7a	Axial view of the FOEHN core and its surrounding cask	25
3.7b	Radial view of the FOEHN core and its surrounding cask	26
3.8	Axial diagram of the FOEHN core and surrounding structures	27
4.1	MCNP prediction of k_{eff} for a set of critical states of the simple FOEHN reactor configuration	33
4.2	Control rod position perturbation effect on k_{eff} in the simple FOEHN reactor configuration	35
4.3	Comparison of experimental and computed axial flux shapes at r = 235 mm in the simple FOEHN configuration	38
4.4	Comparison of experimental and computed axial flux shapes at r = 355 mm in the simple FOEHN configuration	39
4.5	Comparison of experimental and computed axial flux shapes at r = 835 mm in the simple FOEHN configuration	40
4.6	Comparison of normalized experimental and computed axial power distribution in the simple FOEHN configuration at r = 143.5 mm	44
4.7	Comparison of normalized experimental and computed axial power distribution in the simple FOEHN configuration at r = 167.5 mm	45
4.8	Comparison of normalized experimental and computed axial power distribution in the simple FOEHN configuration at r = 193.95 mm	46
4.9	Comparison of normalized experimental and computed axial power distribution in the simple FOEHN configuration at H = 2.5 mm	47
4.10	Comparison of normalized experimental and computed radial power distribution in the simple FOEHN configuration at H = 50 mm	48
4.11	Comparison of normalized experimental and computed radial power distribution in the simple FOEHN configuration at H = 175 mm	49
4.12	Comparison of normalized experimental and computed radial power distribution in the simple FOEHN configuration at H = 400 mm	50
4.13	Comparison of normalized experimental and computed radial power distribution in the simple FOEHN configuration at H = 625 mm	51
4.14	Comparison of normalized experimental and computed radial power distribution in the simple FOEHN configuration at H = 750 mm	52
4.15	Comparison of normalized experimental and computed radial power distribution in the simple FOEHN configuration at H = 797.5 mm	53

Figure		Page

4.16 MCNP prediction of k_{eff} for a set of critical states of the intermediate FOEHN reactor configuration 55
4.17 Comparison of experimental and computed axial flux shapes at r = 235 mm in the intermediate FOEHN configuration 58
4.18 Comparison of experimental and computed axial flux shapes at r = 355 mm in the intermediate FOEHN configuration 59
4.19 Comparison of experimental and computed axial flux shapes at r = 835 mm in the intermediate FOEHN configuration 60
4.20 Comparison of normalized experimental and computed axial power distribution in the intermediate FOEHN configuration at r = 143.5 mm 65
4.21 Comparison of normalized experimental and computed axial power distribution in the intermediate FOEHN configuration at r = 167.5 mm 66
4.22 Comparison of normalized experimental and computed axial power distribution in the intermediate FOEHN configuration at r = 193.95 mm 67
4.23 MCNP prediction of k_{eff} for a set of critical states of the full-featured FOEHN reactor configuration 70
4.24 Comparison of normalized experimental and computed axial power distribution in the full-featured FOEHN configuration at r = 143.5 mm 74
4.25 Comparison of normalized experimental and computed axial power distribution in the full-featured FOEHN configuration at r = 167.5 mm 75
4.26 Comparison of normalized experimental and computed axial power distribution in the full-featured FOEHN configuration at r = 193.95 mm 76

LIST OF TABLES

Table		Page
2.1	FOEHN experiment fuel plates characteristics	3
2.2	Experimental power production distribution in FOEHN	10
3.1	Composition of Zircaloy-4 used in the model	16
3.2	Composition of the AG3-NE aluminum alloy	17
4.1	MCNP computed core effective multiplication factors (k_{eff}) for various critical states of the simple reactor configuration	32
4.2	Effect of control rod perturbations on the core effective multiplication factor for three critical states of the simple reactor configuration	34
4.3	Computed thermal fluxes for the simple reactor configuration	36
4.4	MCNP error estimate (2σ, absolute) for the thermal fluxes for the simple reactor configuration	37
4.5	Normalized MCNP power production (F7:n tallies) for the simple reactor configuration	42
4.6	MCNP error estimate (2σ, absolute) for the normalized MCNP power production for the simple reactor configuration	43
4.7	MCNP computed core effective multiplication factors (k_{eff}) for various critical states of the intermediate complexity reactor configuration	54
4.8	Computed thermal fluxes for the intermediate reactor configuration	56
4.9	MCNP error estimate (2σ, absolute) for the thermal fluxes for the intermediate reactor configuration	57
4.10	Normalized MCNP power production (F7:n tallies) for the intermediate reactor configuration	62
4.11	MCNP error estimate (2σ, absolute) for the normalized MCNP power production for the intermediate reactor configuration	63
4.12	Experimental power production distribution in the intermediate reactor configuration	64
4.13	Points of nonmatching power production density in the intermediate reactor configuration	68
4.14	MCNP-computed core effective multiplication factors (k_{eff}) for various critical states of the full complexity reactor configuration	69
4.15	Normalized MCNP power production (F7:n tallies) for the full complexity reactor configuration	72
4.16	MCNP error estimate (2σ, absolute) for the normalized MCNP power production for the full complexity reactor configuration	73
4.17	Points of nonmatching power production density in the full complexity reactor configuration	77

ACKNOWLEDGEMENTS

We would like to thank Oak Ridge National Laboratory personnel C. D. West, Advanced Neutron Source (ANS) project director, and D. L. Selby, ANS research and development manager, for encouraging this work and providing the necessary funding. We also thank D. L. Selby and B. A. Worley for reviewing the draft report.

P. Ageron of the Institut Laue-Langevin in Grenoble, France, and K. Böning and A. Rohrmoser of the Technische Universität München, in Munich, Germany, provided J. M. Ryskamp with valuable insights that were not included in the original FOEHN report. In addition, Rohrmoser spent one week in Idaho assisting on the FOEHN model. We sincerely appreciate the help these scientists provided on this project.

EXECUTIVE SUMMARY

In the research and development plan of the Advanced Neutron Source (ANS) reactor, the second phase planned for neutronics design methods validation is to compare computational model results and experimental results for a critical facility exhibiting similarities to the ANS reactor.[1] One such facility is the FOEHN experiment.[2] In this report, an MCNP model of the FOEHN experiment is developed, and its results are compared to experimental data from the literature. The MCNP[3] model reproduces measured quantities of interest with a high level of agreement.

FOEHN is a critical experiment performed in the course of the design of the Franco-German High Flux Reactor [Institut Laue-Langevin (ILL)]. The experiment was conducted at CEN-Cadarache in the French EOLE reactor, which was modified for this purpose. The reactor core is a hollow cylinder made of 90% enriched uranium-aluminum (U-Al) alloy circular involute fuel plates. The plates have a thickness of ~1.27 mm. The core is heavy water moderated and reflected. Other components in the FOEHN experiment include loops, beam tubes, and boron axial end plates. Many of these features are similar to the currently envisioned design of the ANS reactor.[4] Design methods capable of properly modeling FOEHN would be well suited for the design and analysis of the ANS reactor.

The core effective multiplication factor (k_{eff}), the thermal flux in the reflector, and the core power distribution were measured in FOEHN. In addition, the rendement, a neutron efficiency defined as the ratio of the maximum thermal flux in the reflector to the total power, was evaluated. All of these quantities are compared to their MCNP-computed equivalents. The fluxes and the spectrum were measured using foil activation. They correspond to MCNP F4:n tallies. The power distribution was measured using fission probes of the same material as the reactor fuel plates, yielding a quantity that essentially mirrors the core fission power production shape. This is compared to MCNP F7:n tallies. The effective multiplication factors were measured via the stable period, the continuous run, and the neutron pulse damping methods.[2] The MCNP KCODE option is used to estimate k_{eff}.

In the FOEHN report[2] estimates of the errors associated with the measured quantities are given without detailed justification. In the present work, the error estimates are reassessed. Thermal flux measurement errors are believed to range from 3.3% to as much as 22.8% vs the 2% claimed in the FOEHN report. The power distribution measurement error is believed to be 4–8% vs the 1% claimed in the FOEHN report. A major omission in the FOEHN report is the nearly 4% uncertainty on the fission probe volume.

The MCNP model developed here represents the reactor with a very high level of geometric fidelity. Since the thickness of the fuel plates and intervening heavy water channels is very small in terms of neutron mean-free paths, the core is modeled as a homogenous region. This is verified, a posteriori, to be a good approximation. The reflector internals[5] (loops, beam tubes, hot and cold sources) are modeled explicitly. The material compositions are defined in ref. 5. The nuclear data are those included in the MCNP ENDF/B-V library.

The effective multiplication factor was computed for all three configurations[2] of FOEHN for a large number of control rod positions and corresponding experimental critical boron concentrations. In the simplest configuration (no boron end caps, no reflector internals), the agreement between the MCNP-computed k_{eff} and the experimental value of 1.0 is achieved within two MCNP standard deviations (2σ) for two experimental situations and within three standard deviations (3σ) for five more. In the intermediate configuration (with boron end caps, no reflector internals), four cases agree with the experimental value within 2σ and the two other cases within 3σ. In the most complex configuration (with boron end caps and reflector internals), the agreement is still remarkably good, with three matches within 2σ and all the other cases displaying matches within 3σ.

The MCNP-computed power distribution was normalized to the same average core power density of 1.0 as the FOEHN data. Typical of the results obtained, the normalized axial power distribution at three radial positions is shown in Fig. ES-1. The experimental error bars of 4% are based on the discussion presented above. The bars on the computational curve assume errors of 2σ. Similar curves were generated for radial power distributions. In this way, every experimental data point was plotted at least once. The graphs show that nearly all the computational results coincide with their experimental counterparts within the error bounds established above. In the simple reactor configuration, only two points, <2% of the total number (122), do not display any overlap. This is remarkably compatible with the statistical interpretation that 95% of the points lie within the $\pm 2\sigma$ "error band." A similar high level of agreement is observed for the thermal fluxes and for the rendement. This work shows that the use of MCNP for the neutronics design of a reactor with features similar to the FOEHN experiment can be achieved successfully.

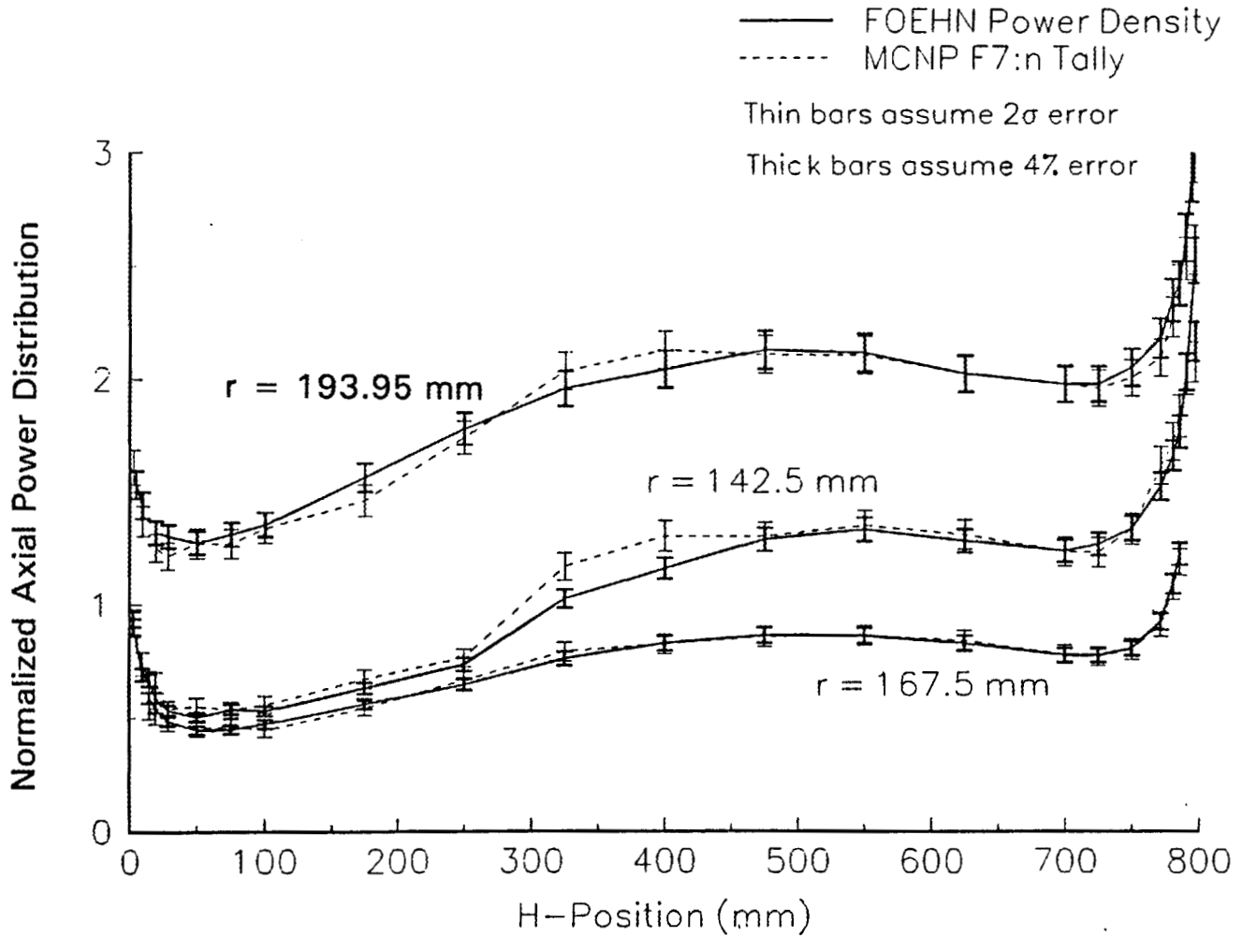

Fig. ES-1. Computed vs measured axial power distribution at three radial positions of the FOEHN critical experiment.

ABSTRACT

A very high fidelity MCNP model of the Franco-German FOEHN critical experiment has been developed. The results obtained show a high degree of agreement with each of the three configurations of the experiment. In particular, it is shown that the model reproduces the power density production distribution for all but a few of the experimental points internal to the core. Agreement for points of the axial ends at the core is less comprehensive. In the configurations that include boron axial core end covers, the agreement is similar within the core, but a few additional disagreement points arise at the axial ends of the core. The results remain consistent, however, with the statistical interpretation of MCNP tallies. The quantities computed also include the thermal flux in the reflector and the core multiplication factor for various critical configurations. It is found that the fluxes agree with the experiment within the experimental error bounds and two computational standard deviations. Most of the core multiplication results agree within three MCNP standard deviations. The overall conclusion of this study is that MCNP is an appropriate and valid computational tool for the static neutronic design of plate-fueled, heavy-water-moderated reactors, such as FOEHN or the Advanced Neutron Source.

1. INTRODUCTION

1.1 MOTIVATION

In the research and development plan of the Advanced Neutron Source (ANS) reactor, the second phase of validation for the neutronics design methods is to compare model (i.e., computational) results and experimental (i.e., measured) results for a critical facility exhibiting similarities with the ANS reactor.[1] One such facility is FOEHN,[2] a critical experiment performed in the course of the design of the Franco-German High Flux Reactor (FGHFR) at the Institut Laue-Langevin (ILL) in Grenoble, France. The experiment was conducted in the French EOLE reactor, which was modified for this purpose. FGHFR is a heavy water reactor with many features similar to those of the proposed ANS reactor. In particular, they both use (or would use) heavy water as moderator and coolant, and they both use (or would use) highly enriched uranium with aluminum plate fuel. The similarity between the two reactors can be seen further from the description of the FOEHN experiment in Chap. 2 and by a graphic rendition of their respective MCNP models in Chap. 3. These similarities in the characteristics of the two reactors suggest that benchmarking MCNP[3] calculations against FOEHN experimental results will enhance the current level of confidence in the computational results and will contribute to the validation of the computational approach chosen for the neutronics design of the ANS reactor.

1.2 SCOPE AND LIMITATIONS OF THE STUDY

In this work, an MCNP model of the FOEHN experiment is developed and its results are compared to experimental data from the literature. It is found that the MCNP model reproduces measured quantities of interest with a high level of agreement. A validation of the method used for computing power generation in the ANS reactor is inferred from the successful comparison of computational results using this method and experimental results in the case of the FOEHN[2] experiment. The extent to which this validation is achieved is limited only by the lack of availability of comprehensive documentation on the details of the experimental setup and on the experimental results. The main sources of differences between the experiment and the model developed in this work stem from the lack of some geometric data about the reactor and in the lack of more detailed information about the materials used than that supplied in the FOEHN report (e.g., impurities information). The results obtained in the course of this study show that the omission of these data leads to no significant difference from the experimental results.

The MCNP model developed here is extensive. It conforms to a high level of fidelity in the representation of the various features of the reactor. The approximations made, when not dictated by the lack of information on the experiment, are explained and their justifications given in Chap. 3. The main items of comparison in the current work are (1) the core multiplication factor for several soluble boron concentration/control rod position combinations, (2) the thermal flux, (3) the core power distribution, and (4) the rendement (neutron efficiency).[4]

1.3 ORGANIZATION OF THE REPORT

In Chap. 2, a review of the FOEHN experiment is presented. Following a brief description of the experiment, a survey of the measured quantities is given. The method of data normalization used in the FOEHN report is explained, and a compatible one for the MCNP computational results is

presented. Finally, the error analysis of the FOEHN experiment is reviewed and complemented. In Chap. 3, the MCNP model developed in this work is presented. In Sect. 3.2, the approximations made are discussed. In Sect. 3.3, the modeling of the reactor features is presented. In Sect. 3.4, the choice of tallies and the methods for computing the elements of the comparison with the experiment are given. Chapter 4 documents the results of the comparisons between the experiment and the model. In Chap. 5, the main results and conclusions of this study are summarized. The references cited in this work are listed in Chap. 6.

2. THE FOEHN EXPERIMENT

2.1 INTRODUCTION

The FOEHN experiment was conducted with three levels of complexity. The first level involves mock-up of only the core surrounded by a reflector, without boron end caps and without the reflector internal structures (internals). The second includes boron end caps (top and bottom of core) but no reflector internals. The third level includes the boron end caps and mock-ups of the features internal to the reflector. A description of the experimental setup (core, reflector, and experimental facilities of the reactor), the method used in reporting the results, and an analysis of the experimental error estimates are presented in this chapter.

2.2 DESCRIPTION OF THE FOEHN EXPERIMENT

2.2.1 Reactor Components and Geometry

The components and geometry of the FOEHN experiment are described in the report by Scharmer and Eckert.[2] A brief review of the elements necessary to the construction of an MCNP model is given in this section.

2.2.1.1 Reactor Core

The fuel zone is a hollow cylinder of height 0.80 m, with outer and inner radii of 0.195 and 0.14 m, respectively. The fuel plates were fabricated out of a uranium-aluminum alloy and shaped as circular involutes with a 134.855-mm generating radius. The fuel plates did not have any cladding along their outer edges. A gap of 1.8 mm is maintained between the assembled plates. Other characteristics of the fuel plates are summarized in Table 2.1. The core structures were all fabricated from the AG3-NE aluminum alloy described in Sect. 3.2.2.

Table 2.1. FOEHN experiment fuel plates characteristics

Fuel	U-A1 alloy (90% ^{235}U)
Load (kg $^{235}U/m^2$)	0.568
Total ^{235}U mass (kg)	8.556
Number of plates in core	276
Plate length (mm)	800.0 ± 0.5
Plate width (mm)	68.3 ± 0.2
Plate thickness (mm)	1.27 ± 0.05
Thickness of lateral A1 cladding (mm)	0.1

The coolant channel volume in the fuel zone was determined in ref. 2 on the basis of the dimensions of the fuel plates and the core structures as measured after fabrication. The borated heavy water volume thus contained in the core was 0.027 m^3 (ref. 2). The total free column volume in the core barrel, including the gaps around the fuel zone, was reported as 0.02885 m^3 (ref. 2).

2.2.1.2 Reflector and Internal Stack Geometry

The core is located in the center of a cylindrical tank of 2.30-m diam and 2.21-m height. The tank is filled with D_2O. A stack passes through the tank axially. The stack extends to the upper rotating plug and has the function of isolating the core and preventing the entire heavy water inventory in the reflector from being contaminated by boron in the event of a leak in the core barrel.

2.2.1.3 Control Elements and Safety System

The excess reactivity of the reactor is compensated for partly by the boron dissolved in the moderator and partly by a control rod that is inserted from below into the central flux trap. The absorber section of this control rod is a nickel tube 5-mm thick, 1.0-m long, and of outer radius 0.126 m.

2.2.1.4 Safety Rods

Six dummy safety rods were used. They were supported by upright aluminum guide tubes of 0.04-m diam and a wall thickness of 4 mm. The safety rods consisted of 2-mm thick cadmium tubes of 90-mm OD and 1.50-m length, clad in 0.5-mm stainless steel.

2.2.1.5 Solid Boron End Zones

A portion of the excess reactivity is compensated for by boron plates above and below the fuel zone. The boron end zones consist of horizontal, 1-mm thick, borated aluminum plates and pure aluminum plates.

2.2.2 Experimental Facilities

A variety of experimental components are included in the reflector of the FOEHN critical facility. These include 16 beam tubes, a hot source, a cold source, and pneumatic tubes for material irradiations. These assemblies closely resemble the facilities originally designed for the FGHFR and are described more fully in the FOEHN report and in ref. 6. A brief description of the main reflector components is given below.

2.2.2.1 Reflector Internal Components

Sixteen beam tubes comprise the bulk of the reflector components. These are used for functions ranging from isotope production and neutron extraction for scattering experiments to conversion electron and/or photon extraction. The beam tubes in FOEHN are of three main shapes: cylindrical, rectangular, and truncated conical. Beam tube orientations range from horizontal to vertical. All beam tube walls are composed of the AG3-NE aluminum alloy and are evacuated within. Two pneumatic tubes for material irradiations are also present in the reflector. These vertical cylindrical tubes are 0.04-m diam and made of the AG3-NE aluminum alloy. One tube nose is located at the core midplane,

and the other is 0.2-m above the midplane. The beta spectrometry vertical channel has an ID of 0.20 m and a wall thickness of 2 mm. It passes through the full height of the reflector. The pneumatic transport systems are simulated by vertical aluminum tubes with 0.04-m ID and 2-mm wall thickness.

2.2.2.2 Cold Source Facility Mock-up

The cold source is simulated by an aluminum vessel of 0.40-m ID and 0.50-m height. The wall thickness is 5 mm. The effect of the cold moderator on neutron absorption in the wall is simulated via an increase in the wall thickness. In the experiment, this was achieved using an aluminum bell 3-mm thick that fit over the cold source.

2.2.2.3 Hot Source Facility Mock-up

The FOEHN hot source mock-up consisted of a cylindrical block of graphite inside a Zircaloy-4 vessel, surrounded by an AG3-NE tube. Two probe holes, one horizontal and one vertical, extend through the center of the graphite block to provide access for measurements within the hot source. The hot source mock-up was located at a radius of 0.496 m from the core centerline, and its centerline was 0.1-m below the core midplane.

2.2.2.4 Loops

The FOEHN critical facility contains three separate loops. The core loop serves to isolate the core region and allows for addition of borated heavy water to the core for reactivity control. The stack loop seals off the primary coolant loop from the reflector. The reflector loop provides cooling for the reflector components. Both the stack and reflector loops can be independently heated and cooled.

2.2.3 Materials

The materials used in the FOEHN experiment are described in great detail in ref. 2, and some of their properties are summarized in Sect. 2.2.1.1 above. The description of the materials does not include quantification of any impurity content. In Sect. 3.2.2, the differences between experiment and model materials are enumerated.

2.3 RESULTS OF THE FOEHN EXPERIMENT

The FOEHN experiment is summarized in a report by Scharmer and Eckert.[2] The main results of interest to the current study are those related to benchmarking an MCNP simulation against the experiment. These results are the spatial distribution of power production, the fluxes, the effective core multiplication factor (k_{eff}), and the rendement. The quantities of interest (limited to the static parameters) are reviewed below, and their actual meanings in the FOEHN experiment are clarified. The actual results of the FOEHN experiment are reviewed in Chap. 4 in conjunction with their comparison to the model.

2.3.1 Quantities Measured

2.3.1.1 Core Multiplication Factor (k_{eff})

The reactivity was measured in the FOEHN experiment via three methods: (1) the stable period method for slightly supercritical states, (2) the continuous reactivity measurement method for cases with large reactivity, and (3) the pulsed neutron source method for subcritical states. The experimental results reported include both critical and off-critical states.

2.3.1.2 Fluxes and Spectrum

The fluxes and the spectrum were measured in the FOEHN experiment using the well known method of foil activation. For the thermal flux measurements, the cadmium ratio, R_{Cd}, was evaluated using a manganese (Mn) probe irradiated at the same location in the experiment and at the same power, once without a cover (Mn) and once under a thick cadmium (Cd) cover (Mn/Cd). From R_{Cd} and the total activity (Mn case), the thermal flux can be computed. The epithermal flux was measured using gold (Au) and indium (In) resonance probes under Cd covers. The fast flux was measured using the threshold reactions of sulfur (S) and phosphorus (P) probes.

The flux spectrum in the FOEHN experiment was measured using paired probes of uranium-plutonium (U/Pu) and lutetium-manganese (Lu/Mn) in addition to the manganese and Mn/Cd probes used for R_{Cd}. The activation ratios obtained from these pairs were then used to obtain a discrete neutron spectrum (thermal, epithermal, and fast neutron energy groups).

2.3.1.3 Flux Efficiency (Rendement)

The rendement is defined in the FOEHN report as the ratio of the maximum thermal flux in the reflector to the total power produced in the core,

$$r = \frac{\phi_{th}^{max}}{P_{tot}} \quad . \tag{1}$$

For experimental determination, this expression is rewritten in terms of experimentally available quantities,

$$r = \frac{A_{Mn,max}}{A_{Mn,R}} \cdot \frac{\mathrm{v}}{\mathrm{v}_o} \cdot \frac{A_{U,R}}{A_{U,C}} \cdot \frac{1}{\Sigma_{f,th,}^{U} V_c \, Q} \quad , \tag{2}$$

where $A_{mn,max}$, $A_{Mn,R}$, $A_{U,R}$, and $A_{U,C}$ are measured activations, respectively, of manganese at the maximum of the flux, of manganese in the reflector, of uranium in the reflector, and of uranium in the core. V_c is the core volume, v is the mean neutron velocity at the location of the maximum of the flux, and v_o is

$$\mathrm{v}_o = \frac{2}{(\pi)^{1/2}} \cdot 2200 \; m/s \quad . \tag{3}$$

The ratio v/v_0 and the effective microscopic fission cross section $\sigma_{f,eff}$ (503 barns at the point of the measurement located at a radius of 0.50 m from the centerline of the reactor) were evaluated using the code THERMOS. The evaluation of r in the FOEHN report also assumes that the recoverable energy released per fission event, Q, is 199.73 MeV.

2.3.1.4 Power Distribution

In the FOEHN report, it is claimed that the power distribution is measured. In reality, the fission power production density (understood to include all the recoverable energy, then normalized to a unit average power density throughout the core) is measured and reported. The fission power production is measured using fission probes of composition similar to that of the reactor material (fuel plates) and cut right into the plates. This choice has the advantage of not significantly disturbing the system studied. The fission foils are irradiated; then the gamma activity above 511 keV is measured. The measured activity is deemed proportional to the power released in the probe during irradiation. The measurements necessarily include all gammas above 511 keV and, hence, may include activity contributed by nonfission events. The results reported do not describe the power distribution as it would result from the combined effects of power production, transport, and deposition. Gamma heating is also reported and is discussed in the next subsection.

2.3.1.5 Gamma Heating in the Reflector

Gamma heating of structural and other materials is the result of the transfer of energy via gamma radiation and the subsequent deposition of the gamma radiation. It is measured in the FOEHN experiment using glass dosimeters and an ionization chamber. The glass dosimetry technique relies on the measurement of the fluorescence induced by the formation of optical centers (i.e., defects) in the glass as a consequence of irradiation by the gamma rays. The effect of the neutron-induced centers is subtracted by comparison to activation measurements. The method is suitable for the measurement of the photon flux and of the energy deposition in the glass probe. A prediction for the energy deposition in other materials (e.g., reflector materials) can be inferred from their respective energy absorption coefficients. The ionization chamber method is fully described in classical references, such as *The Atomic Nucleus* by R. D. Evans.[7] The chamber used in the FOEHN experiment has a sensitivity to gammas of 1200 W/g-A. The FOEHN report does not give a sensitivity to gammas for the glass probes.

2.3.2 Normalization of Tabulated Results

The flux and power data obtained in the FOEHN experiment were reported normalized to an average power density (or flux density) of 1.0 over the core of the reactor. The report did not describe the normalization method in sufficient detail to make it easily reproducible. In this section, the normalization method used in the FOEHN report is explained. A simple and more practical alternative, which is shown to be compatible with that of the experimental report, yet easier to implement, is proposed and described.

2.3.2.1 FOEHN Experiment Normalization Method

The powers reported for the FOEHN experiment are normalized to an average density of 1.0 over the whole reactor core. The procedure followed by the FOEHN experiment authors is described in Sect. 5.1.4 of their report. They used both a "mechanical" (i.e., semigraphical) and a "mathematical"

(i.e., semi-analytical numerical) integration approach to eval[illegible]e total core power for use in normalization. In the mechanical approach, the measured rad[illegible] power distribution is plotted at each value of the axial variable, then graphically integrated. An axial power distribution results that is then integrated to yield a total core power. The normalized power is then determined by multiplying each experimental value by the volume of the core and dividing it by the total power. The resulting distribution has the advantage of consisting of numbers close to 1.0 when the power density measurements are close to the core average power density. The second normalization method used by the authors of the FOEHN experiment differs only in the way the total power integral is obtained. In this second method, the entire set of measurements is fitted by polynomials, and the resulting two-dimensional curve is used in a computational integration procedure. In the next two subsections, an alternative method is introduced that works well when a sufficient number of data points are available.

2.3.2.2 Single Table Normalization

The integration and normalization methods used in the FOEHN experiment should be expected to work well, but they are not fully rigorous from a mathematical point of view. Indeed, the measurements were made with probes of finite dimensions (3 mm × 5 mm × 1.27 mm) that are not negligible with respect to the distance over which the flux changes significantly (in some regions at a rate of 3%/mm). The reported measurement values are actually average values over the probe and not point values. The correct curve fitting procedure taking this fact into account is a complicated one, involving considerations of functional analysis.[8] This method is beyond the scope of this study. A procedure that errs in the opposite direction may be as legitimate as the one used by the authors of the FOEHN experiment, especially when dealing with a large number of experimental points. This procedure is outlined below.

The normalization procedure proposed here differs from those of the FOEHN report only in the use of an *r,H* trapezoidal integration procedure. In this approach, it is assumed that the data from a given probe applies to the domain surrounding it up to the middle of the distance separating it from the center of the closest adjacent probes in the *r* and *H* directions (or up to the edge of the fuel plate if applicable). The integration is then carried out by multiplying the power (or power density) by the volume of the region and summing over all probes. This integration procedure was applied to the data of Table 5.1.5 of the FOEHN report. The average power density is found to be 1.014. The difference of 1.4% between our computations and the expected value of 1.0 shows that the two normalization procedures (FOEHN report and ours) are compatible and confirms the fact that the table in the FOEHN report is normalized to an average density of 1.0.

2.3.2.3 Multiple Tables with Missing Data

It is desirable to obtain an average from multiple tables of similar data (such as Tables 5.3.6, 5.3.7, 5.3.8, and 5.3.9 of the FOEHN report). It is in fact necessary to combine the data from these tables because they cannot be reproduced computationally without precise data on the azimuthal position of the experimental fuel plates that carry the probes. In addition, for the sake of better statistics, the tally cells are actually annuli. The computational results, therefore, correspond to an average of a large number of probes distributed around the core. The averaging of the data from the four experimental plates is the best option available for a comparison.

The construction of a proper average of the experimental data could be achieved in two ways: (1) renormalize the experimental data to 1.0; then form a point-to-point average according to

$$(T_i)_{av} = \frac{1}{N_i} \sum_p (T_i)_p \; ; \tag{4}$$

or (2) perform a point-to-point average according to the formula shown above without first renormalizing the data. In the equation, $(T_i)_{av}$ stands for the average tally for the i-th position (defined by its radial and axial coordinates), $(T_i)_p$ is the i-th position tally in the p-th experimental plate, and N_i is the number of (nonmissing) entries for tallies in the i-th position. These two options should both work well if the number of data points is large in each table (i.e., there are enough data points for the integration procedure to be accurate), and the initial tables are found to be normalized to 1.0 (or very close to 1.0) following the method proposed in Sect. 2.3.2.2. If there are many missing data points, or if the tables are not found to be normalized to an average density close enough to 1.0, then the second procedure must be used. The rationale for this choice is that the reported data are already normalized to an average power density of 1.0 according to the method used in the FOEHN experiment. Such data can then be averaged without further transformation. The resulting combined table should be expected to be more closely approximated by the tallies over annuli that are used in this study. The combined table, having a larger number of points than any of its constituent tables, should also be expected to be normalized to a value closer to 1.0 than (at least some of) the individual tables. The combined data from Tables 5.3.6–5.3.9 of the FOEHN report are shown in Table 2.2. It was verified that the entries of this new table are normalized to an average core power density of ~1.006 according to the procedure in Sect. 2.3.2.2.

2.3.2.4 Normalization of Fluxes

The fluxes in the FOEHN experiment are reported normalized to a total core power of 1.0 W. The MCNP tallies are normalized "per fission neutron." The MCNP tallies must be renormalized to make a direct comparison with experimental values possible. The fluxes are renormalized by multiplying the MCNP tallies by the power normalization factor PN given by[9]

$$PN = P \cdot \nu \cdot \frac{1}{Q} \cdot \frac{1}{k_{eff}} \; , \tag{5}$$

where P is the reactor power, ν is the average number of neutrons per fission, Q is the fission energy, and k_{eff} is the effective multiplication factor from the MCNP run that yielded the flux tallies to be renormalized. The normalization to 1.0 W is achieved by setting P equal to 1.0. In this work, ν is computed within MCNP for each reactor configuration and is reported along with the results that use it. When a value for ν is not reported, the value 2.44175 is assumed. The energy per fission used in this work, Q, is 202.47 MeV/fission, except in the evaluation of the rendement where the value 199.73 MeV was used in order to conform with the practice adopted in the FOEHN report.

Table 2.2. Experimental power production distribution in FOEHN[a]

H/r (mm)	143.5	146.5	149.5	152.5	159.0	167.5	176.0	182.5	185.5	188.5	193.95
2.5	0.5033	0.4701	0.4529	0.4492	0.4462	0.4908	0.5958	0.7363	0.8162	0.9236	1.2140
5.0											1.1739
9.4	0.6978										1.1654
14.5	0.4629					0.4437					1.1657
19.4	0.4880					0.4295					1.1697
28.5	0.4920					0.4270					1.1787
50.0	0.5061	0.4655	0.4540	0.4359	0.4214	0.4560	0.5526	0.6827	0.7796	0.8979	1.2395
75.0	0.5441					0.4965					1.3249
100.0	0.6163					0.5283					1.4047
175.0	0.7386	0.6832	0.6508	0.6328	0.6002	0.6410	0.7650	0.9542	1.0744	1.2272	1.6764
250.0	0.8609					0.7408					1.8965
325.0	0.9626					0.8191					2.0636
400.0	1.0555	0.9788	0.9144	0.8984	0.8473	0.8850	1.0357	1.2898	1.4189	1.6113	2.2120
475.0	1.3656					0.9684					2.2314
550.0	1.4596					0.9621					2.1906
625.0	1.3661	1.2192	1.0878	1.0273	0.9211	0.9003	1.0106	1.2300	1.3538	1.5147	2.0550
700.0	1.2275					0.8055					1.8327
725.0	1.1729					0.7442					1.7600
750.0	1.1257	0.9867	0.8775	0.8289	0.7265	0.7100	0.7993	1.0039	1.0851	1.2325	1.7150
771.5	1.1000					0.6721					1.6685
780.6	1.1352					0.7285					1.6806
785.5	1.1344					0.7188					1.6985
790.6	1.1528										1.7021
795.0											1.7183
797.5	1.2958	1.1534	1.0572	1.0238	0.9171	0.8625	0.9632	1.1537	1.2353	1.3559	1.8193

[a]Combines Tables 5.3.6–5.3.9 of ref. 2.

2.4 ERROR ANALYSIS OF FOEHN RESULTS

2.4.1 Error Reporting in the FOEHN Experiment

The measurement errors on the ratios related to the flux spectrum are reported as 1% for R_{Cd} and $R_{Pu/U}$, and 2% for $R_{Lu/Mn}$ respectively.[2] The errors claimed by the authors of the FOEHN experiment are 2% for the relative thermal flux measurements, 3% for the absolute thermal flux measurements, 4–15% for the relative epithermal fluxes, and 13% for fast flux measurements near the core. They attributed most of the experimental error in the thermal flux measurements to the error in positioning the probes. They claim that the flux varies by 30%/cm on the tank surface at the reactor midplane. The error on the powers is reported to be <1%.[2] In the critical states experiments, the error on the positioning of the control rod is reported as <1 mm, whereas the error on the corresponding boron concentration is not reported. With very little analysis, the errors on the determinations of the rendement are reported in the FOEHN report as ±2, ±2, and ±3%, respectively, for the simple, the intermediate, and the full complexity reactor configurations.

2.4.2 Sources of Errors

2.4.2.1 Geometric Tolerances

The occurrence of geometric inaccuracies leads to errors in the experimentally measured data. Some of the geometric sources of error are the positioning error of foils and probes in the experiment, the error on the dimension of plates and other structures during fabrication, and the tolerance in the positioning of rods. Other geometric sources of error may include the effect of accidental deformation of the fuel plates as well as deformation caused by the actual operation of the reactor.

2.4.2.2 Materials Data

The composition of the various materials used in the FOEHN experiment are not known unequivocally. In particular, no information on the impurity contents was given in the FOEHN report. Another possible (though very likely small) source of error is the undocumented uncertainty on the boron concentration used for criticality experiments. The FOEHN report is ambiguous in its description of the material used for fabrication of the reflector internals. Whereas it is stated that the standard beam tube is made of the AG3-NE aluminum alloy referred to simply as aluminum in the report, the material of other structures is not explicitly described as AG3-NE, but rather only as aluminum.

2.4.2.3 Counting Geometry, Statistics, and Times

The counting statistics and consequent errors of the various measurements were not explicitly reported by the authors of the FOEHN experiment. It is unclear whether the errors they quote relate only to the counting or to the entire experiment. For example, the error of <1% reported for the power measurements is not assigned to any particular aspect of the experimental procedure. It is reasonable to assume that it is related solely to the counting time, geometry, and statistics.

2.4.3 Estimates of the Error on Select Quantities

The errors discussed in the previous section may be viewed as having two types of sources: statistical and systematic. In combining and propagating the two types of errors, care must be taken to use the proper applicable rules. The uncertainty in the measurements of activation associated with the probe positioning constitutes an unknown error of unknown sign. It was estimated by the authors of the experiment at approximately ±3%. This error is random, but since this error is associated to fewer than three measurements for each sample, confidence bounds in the statistical sense cannot be defined for it, and the error cannot be treated like a statistical error. This error also affects all the measurements equally, so it is treated like a systematic error in this work, except that its sign is not known. It is therefore not combined statistically with the other errors. Instead, the corresponding uncertainties are combined conservatively, as if they were known errors. In contrast, the counting errors are of statistical nature. The activities of two probes irradiated at the same location, although under modified conditions, are correlated. It follows that the combination of errors should ideally take the correlation into account. Since the precise way in which the activations are correlated is not known, limiting situations have to be identified. The actual errors would then fall within the range thus determined. Such limiting ranges are defined below for the cadmium ratio, the thermal flux, and the powers. The resulting estimates for the statistical and systematic errors are then combined conservatively in a nonstatistical way.

2.4.3.1 Cadmium Ratio, R_{Cd}

The cadmium ratio, R_{Cd}, is obtained as the ratio of two activities. If a foil is positioned with an error of the order of 1 mm, as claimed in the FOEHN report, the systematic error on its activation would be of the order of 3%. It follows that the error on R_{Cd} would be ~6% from the compounding of the errors on two foils. The contribution of the counting error to the total relative error ranges from 0 to $\sqrt{2}$. These two figures assume the activities to be fully positively correlated and uncorrelated, respectively. The assumption of positive correlation is plausible for activations of foils at the same location in the reactor. If the correlation was negative, the contribution would have been bound by a maximum value of 2%. Other errors, such as the sample-size error, may also be present but are ignored in this analysis. The total error for the cadmium ratio ranges, therefore, between 6 and 7.4%.

2.4.3.2 Thermal Flux

The thermal flux is computed in the FOEHN experiment according to

$$\phi_{th} = B \cdot (v/v_o) \cdot A \cdot (1 - 1/R_{Cd}) , \tag{6}$$

where B is a normalization constant and A is the activation of the thermal probe. It is not clear from the FOEHN report how the cadmium ratio was determined for a given thermal flux measurement. Specifically, it is not clear whether R_{Cd} was measured once at some location in the reflector and used for all thermal flux determinations at that and other locations or if R_{Cd} was reevaluated separately for each location. From the report, it seems that the former approach was adopted. If this is the case, the error on the thermal flux would follow from the error on B, the error on A (comprising at least ~3% for positioning and 1% for counting), and the error on R_{Cd} (comprising the combined errors on two activity measurements, about 6–7.4%). In the present analysis, it is assumed that R_{Cd} was determined

only once, and hence the logic stated at the beginning of Sect. 2.4.3 applies. In the converse, the error on the flux would entail only the errors on the two correlated measurements of the activities under cadmium cover and without cadmium cover.

Contributions to the error on ϕ_{th} arise from each of the factors in the right side of Eq. (6). The first term is the normalization constant B. In the FOEHN report, it is claimed that this normalization is performed using the measured value of the rendement. Such an approach would imply that the factor B would be either proportional or inversely proportional to the rendement and, consequently, that the corresponding relative error would have to be added to the above estimates. In Sect. 2.4.3.4, it is shown that the error on the rendement ranges from 2.2%, when only the error on the ratio v/v_0 is accounted for, to 16.2%, when the positioning errors, the counting errors, and the error on v/v_0 are taken into consideration. The second factor, v/v_0, was shown by Rohrmoser[10] to entail an error of about 2.2%. The last two factors, A and $(1 - 1/R_{Cd})$, contain errors resulting from positioning and counting. If it is assumed that all the statistical errors (i.e., counting errors) and the error on v/v_0 from B and from its explicit occurrence in Eq. (6) cancel out, then the error on ϕ_{th} would be of the order of 15.3% for a value of R_{Cd} of 20. This would decrease toward 15% as R_{Cd} increases and would be reduced to 3.3% if the positioning errors are assumed to cancel out in the evaluation of the rendement. If the errors on v/v_0 do not cancel out, and the cancellation of statistical error is minimal, then the error would be of the order of 22.8%, (10.8% if positioning error is ignored in determination of the rendement). If it is assumed that the error of 2% (to 3%) on the measured rendement claimed in the FOEHN report is correct, then the error on the thermal flux would be between 8.5 and 8.6% (to between 9.5 and 9.6%), depending on the extent of statistical error cancellation.

From the above, it can be seen that estimates of the error on the thermal flux can range from 3.3–22.8%, with a more plausible minimum of the order of 9.6%. If no other sources of error are present, then the error on the thermal flux measurements should be taken to be at least 10%. Since this is unlikely, error bars resulting from the lower estimate based on the claims of the FOEHN experiment report should be regarded as a minimum width for the error, that is, a nonconservative estimate.

2.4.3.3 Powers

In the FOEHN report, the claimed error of 1% on the powers is attributed mainly to the uncertainty in positioning the plates with respect to one another (i.e., distance between adjacent plates). In another part of the report, it is claimed that a positioning error of 1 mm induces an error of up to 3% in the activation (i.e., the flux or the power). It can be expected that the positioning of the fuel plates is known to be about 0.1 mm (the distance between plates is given as 1.8 mm) and hence that the corresponding error would be only as high as 0.3%. To this, the error related to the dimensions of the fission probes proper and the counting must also be accounted for in the calculation. If the counting error (i.e., measurement error) is the same as that for the flux measurements, then it should be taken to be ~1%. The error on the dimensions of the probes cannot be known with any degree of certainty since they are not documented in the report. It can be guessed, however, that they can be related to the errors made on measurements of some of the features of the EOLE reactor. For example, the error on the thickness of the fuel plate is 0.05 mm. If a similar error is made for each of the dimensions of the fission probes, the resulting relative error on the area of a given probe would be ~2.7%. The implied error on the power measurement resulting from this would be the same (i.e., 2.7%). In addition, the error on the dimension of 0.05 mm for each side of the rectangular shapes would induce a positioning error on the flux (or power) similar to that caused by four positioning errors by distances half the dimension error and hence add up to 0.3% for the two sides of the rectangle (or to 0.45% if a thickness positioning error is assumed). The sum of all the errors discussed here ranges from 1–4.15%. The relative error on the thickness of the probes (0.05 mm for a 1.27-mm

thickness) would affect the counting and hence would contribute an additional 3.94% to the power error estimate. A grand total of up to 8% is therefore plausible. Other possible errors resulting from the actual location (i.e., positioning error) of the probes and from deformation (resulting from cutting and use) are not accounted for in this scenario. The upper bound of 4% chosen in the remainder of this work as the error on the power (for use in comparisons to MCNP results) is a lowest estimate and is similar to the estimate of the error on the flux arrived at in Sect. 2.4.3.2 by reanalyzing the FOEHN report data and claims.

2.4.3.4 Rendement

The computation of the rendement in the FOEHN experiment uses four measured activations, an estimate of the energy and core volume averaged fission cross section, an estimate of the ratio v/v_o, and an estimate of the energy released per fission event. Each of these can be known only approximately and, hence, is a source of error. Assuming a relative error on each constituent term in the equation for r, the nonstatistical component of the relative error on r is

$$\frac{\Delta r}{r} = \frac{\Delta A_{Mn,\max}}{A_{Mn,\max}} + \frac{\Delta A_{Mn,R}}{A_{Mn,R}} + \frac{\Delta(v/v_o)}{v/v_o} + \frac{\Delta A_{U,R}}{A_{U,R}} + \frac{\Delta A_{U,C}}{U_{U,C}} + \frac{\Delta \Sigma^U_{f,th}}{\Sigma^U_{f,th}} + \frac{\Delta V_c}{V_c} + \frac{\Delta p}{p} \quad . \tag{7}$$

The statistical error on the activities has to be added. The error on the ratio v/v_o was shown by Rohrmoser to be 2.2%. If the errors on the fission cross section and on the core volume V_c are ignored, and if the error on the activations is taken to be 1% (following the claims in the FOEHN report) to 4% (3% positioning and 1% counting), then the error on r should be between 2.2% (assuming positioning error cancellation, hence ignoring all but the error on v/v_o, and with the counting error contributing 0% for full positive correlation, when maximum cancellation occurs) and 16.2% (positioning errors taken into account and with statistical error contributing 2% in the uncorrelated case). The error sources omitted here may or may not be negligible and might have to be accounted for in the analysis.

2.5 SUMMARY

The FOEHN experiment has been reviewed and its salient features described. The quantities that were measured have been identified. A method for normalizing model data that is compatible with the normalization method used in the FOEHN report has been proposed. The reported estimates of the experimental errors were discussed. It is concluded here that, as given in ref. 2, the error estimates of the FOEHN experiment are significantly underestimated. It is shown, in particular, that the errors on the fluxes should be taken to be at least of the order of 10%, while the errors on the powers should be taken to be at least 4% of the reported values.

3. MCNP MODEL OF THE FOEHN EXPERIMENT

3.1 INTRODUCTION

MCNP models that correspond to the three configurations of the FOEHN experiment have been developed and are described in this chapter. The assumptions and approximations made are outlined in Sect. 3.2. In Sect. 3.3, the geometry and modeled features of the reactor are described. The choice of MCNP tallies and methods for computation of nontally quantities are described in Sect. 3.4. The full MCNP model (i.e., input file) is included as Appendix A.

3.2 MAJOR APPROXIMATIONS AND ASSUMPTIONS

The highest possible degree of geometric fidelity was systematically sought in the modeling of the FOEHN critical experiment. Whenever possible, the exact geometry of the component was used. The reactor core was modeled with some approximations justified in the next section. The reflector internal components were modeled explicitly and in full accordance with the specifications of the FOEHN experiment report. The next two subsections describe geometry and materials approximations made in the development of the MCNP model, respectively.

3.2.1 Homogenous Core, Geometry Details, and Fidelity

The FOEHN core, described in Sect. 2.2.1.1, was modeled as a homogenous hollow cylinder of fuel, cladding and structural materials, and borated heavy water. The dimensions are those specified in the FOEHN report. In the experiment, the power measurements were conducted on individual fuel plates. The highest fidelity description would hence require the explicit modeling of the plates and of the individual fission probes. This is an unpractical option, however, since the fuel plates are shaped as circular involutes, a shape not available in the MCNP geometry modules. In addition, since the fuel plates are much smaller than the mean free path of neutrons in the fuel material, the fuel can be homogenized with no significant loss of accuracy.[11] Another major reason for avoiding explicit treatment of the fission probes is the fact that computing tallies over such small volumes would make obtaining satisfactory statistics prohibitively expensive.

The only other geometric approximations made involve some structural and control materials of the axial end zones separating the core region from the heavy water moderator. In the actual experimental facility, in the simplest reactor configuration, an AG3-NE alloy "plug" plate isolates the borated heavy water in the core region from the surrounding unborated heavy water. It is followed (on the outside) by unborated D_2O and, much farther, by the axial portion of the reactor core barrel. In the intermediate and full complexity configurations, the boron end caps follow the inner AG3-NE alloy plug, replacing some of the D_2O between the axial plug and the axial portion of the core barrel. These boron end caps are constructed as alternate layers of borated and unborated AG3-NE plates in a B/U/B pattern repeated four times (for a total of eight Borated layers and four Unborated ones). In the MCNP model, only the inner AG3-NE seal (plug) is modeled explicitly. The boron end caps are modeled as homogenous regions 30-mm thick. The axial portion of the core barrel (exact location and thickness undocumented), having little neutronic impact, is simply ignored. The modeling of the borated end caps as homogenous regions allows the use of the boron end zone homogenized material description from the FOEHN report. Little effect on global core parameters is anticipated, and only minor perturbations in the core power distribution are expected.

The MCNP model of the radial description of the reactor follows closely the information provided in the FOEHN report. Such information is, however, not complete, and assumptions have to be made. A summary of the description of the core region starting at the reactor centerline and moving outward is given in Sect. 3.3.1.

In some critical states, the control rod top was at a height <1.0 m position in the MCNP coordinate system. In these cases, a portion of the rod was below the bottom of the reflector tank, which is the lower boundary of the MCNP model. In the model, the portion of the rod protruding below the tank floor was neglected. This should not produce any significant problem since the distance of this portion of the rod from the active core is large. In these states, dissolved boron is the primary source of reactivity control, and, hence, the protruding section of the control rod has negligible worth. Further discussion of this phenomenon is included in Sect. 4.2.1.

3.2.2 Assumptions on Materials Data

The materials used in the MCNP model of the FOEHN critical facility mirror as closely as possible the actual materials used in the facility. This was accomplished by using the material compositions given in Table 3.1 of the FOEHN report for the fueled region of the core and for the boron end plates. The atomic contents of all other material compositions (e.g., borated and unborated D_2O, AG3-NE, etc.) were calculated in this work. Where gaps appear in the table, approximations and best guesses had to be used. These are explained below.

Table 3.1. Composition of Zircaloy-4 used in the model[a]

Element	Weight percent
Zr	Balance
Sn	1.5
Fe	0.20
Cr	0.10
Ni	0.007

[a]From S. Glasstone and A. Sesonske, *Nuclear Reactor Engineering*, 3rd Ed., p. 460, Van Nostrand Reinhold, 1981.

The hot source graphite and the cadmium in the safety rods were modeled as elemental graphite and cadmium at full theoretical density with no impurities. This produces an overestimate of the atomic densities for these materials and is expected to produce some local effects, especially in the hot source flux calculations. However, since the safety rods were not included in any of the FOEHN experiments used in these calculations, the cadmium density had no effect on the results.

In several reflector internal components, the zirconium alloy Zircaloy-4 and stainless steel type 304 (SS-304) were used. Compositions for these alloys were not available, so the material composition for SS-304 was taken from a standard handbook,[12] and that of Zircaloy-4 was assumed to be the same as the one used in the MCNP model of the ANS reactor. The composition used for Zircaloy-4 is shown in Table 3.1. Since there is a large range of possible nuclide contents for these alloys, there ensues a consequent degree of uncertainty about the fidelity of the model. This will again produce mainly local effects, with insignificant global consequences. The composition data used for the

AG3-NE aluminum alloy are given in Table 3.2. All heavy water is assumed to be contaminated by 0.25 at. % light water. This value is very close to the values quoted in the FOEHN report.

Table 3.2. Composition of the AG3-NE aluminum alloy

Element	10^{30} atoms/m^3	Element	10^{30} atoms/m^3
Al	0.031673	FE	6.9681×10^{-5}
Co	2.1221×10^{-8}	Ni	6.6513×10^{-7}
Cr	6.493×10^{-5}	Cu	6.3346×10^{-7}
Mn	1.1323×10^{-4}	Ga	4.4342×10^{-6}
Th	4.751×10^{-9}	Ta	3.1673×10^{-6}

3.3 MCNP MODEL DESCRIPTION

The FOEHN experiment incorporates many of the features found in the current design of the ANS reactor. The comparison is illustrated by SABRINA[13] printouts of the MCNP models for the ANS reactor and FOEHN in Figs. 3.1a and 3.1b, respectively. As can be seen from Fig. 3.1b, the MCNP model of the FOEHN critical experiment incorporates a full description of the entire experiment, including all reflector internals and the boron end zones. The cases that did not require either the reflector internals or boron end zones are modeled by substituting heavy water for the actual material in the appropriate zones. The approximations used in developing the model are described in the previous section. The complete model is described below. Additional details of the model can be seen in Figs. 3.1b–3.6. These are SABRINA printouts of six views of the experiment as modeled in MCNP. The views are front, left, right, top, bottom, and rear, respectively.

3.3.1 The Core and Surrounding Structures

The core is modeled as a hollow cylinder 0.8-m tall, with inner and outer radii of 0.14 and 0.195 m, respectively. Figures 3.7a and 3.7b show, respectively, a diagram of an axial and a radial (top view) of the core and the surrounding barrel. The core region is modeled as a homogenous mixture of the uranium fuel, borated heavy water, and aluminum cladding material. The choice of a homogenous core model was justified in Sect. 3.2.1. An additional reason for using a homogenous core model is the fact that the actual plate locations are not documented in the FOEHN report, and their spacings could vary since the fuel plates were not welded to the inner and outer core barrel walls. The core material properties are those of Table 3.1 of the FOEHN report. Dissolved boron in the heavy water was added to the mixture as required for each case, with the appropriate corrections made to the material description and overall atom density. The boron end zones were modeled as homogenous regions at the top and bottom of the core, 30-mm thick, with the same radius as the core.

Figure 3.8 shows an axial diagram of the core region and its surrounding structures. The control rod was modeled as a nickel annulus 5-mm thick and 1-m long. The dimensions for the heavy water regions and surrounding core barrel and isolation cask were derived from detailed figures of these regions (ref. 6). The structures above and below the core were modeled according to Fig. 3.3 in the FOEHN report. Since no exact dimensions were provided, best estimates from the diagram were used.

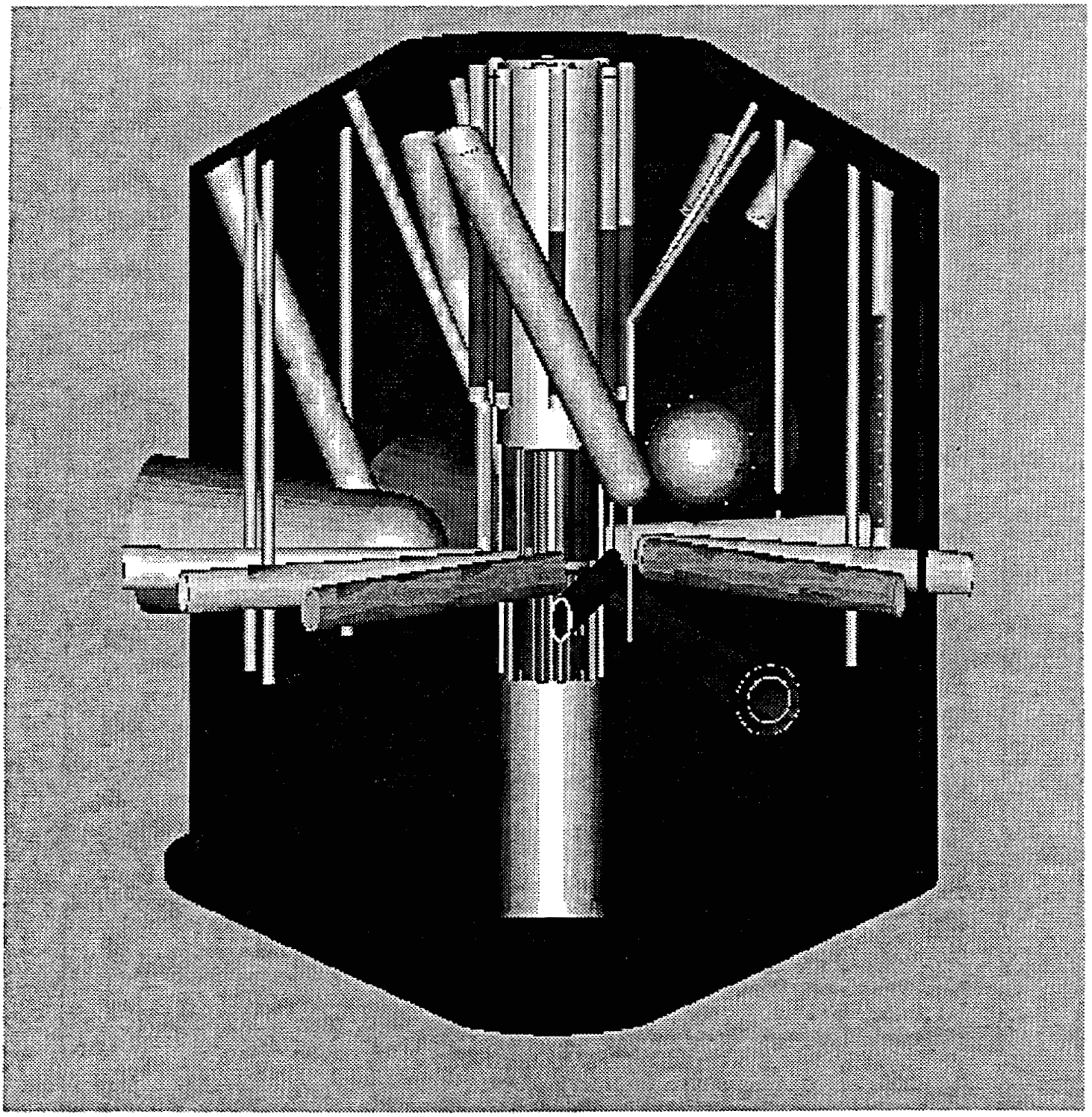

Fig. 3.1a. SABRINA printout of the current ANS reactor design MCNP model.

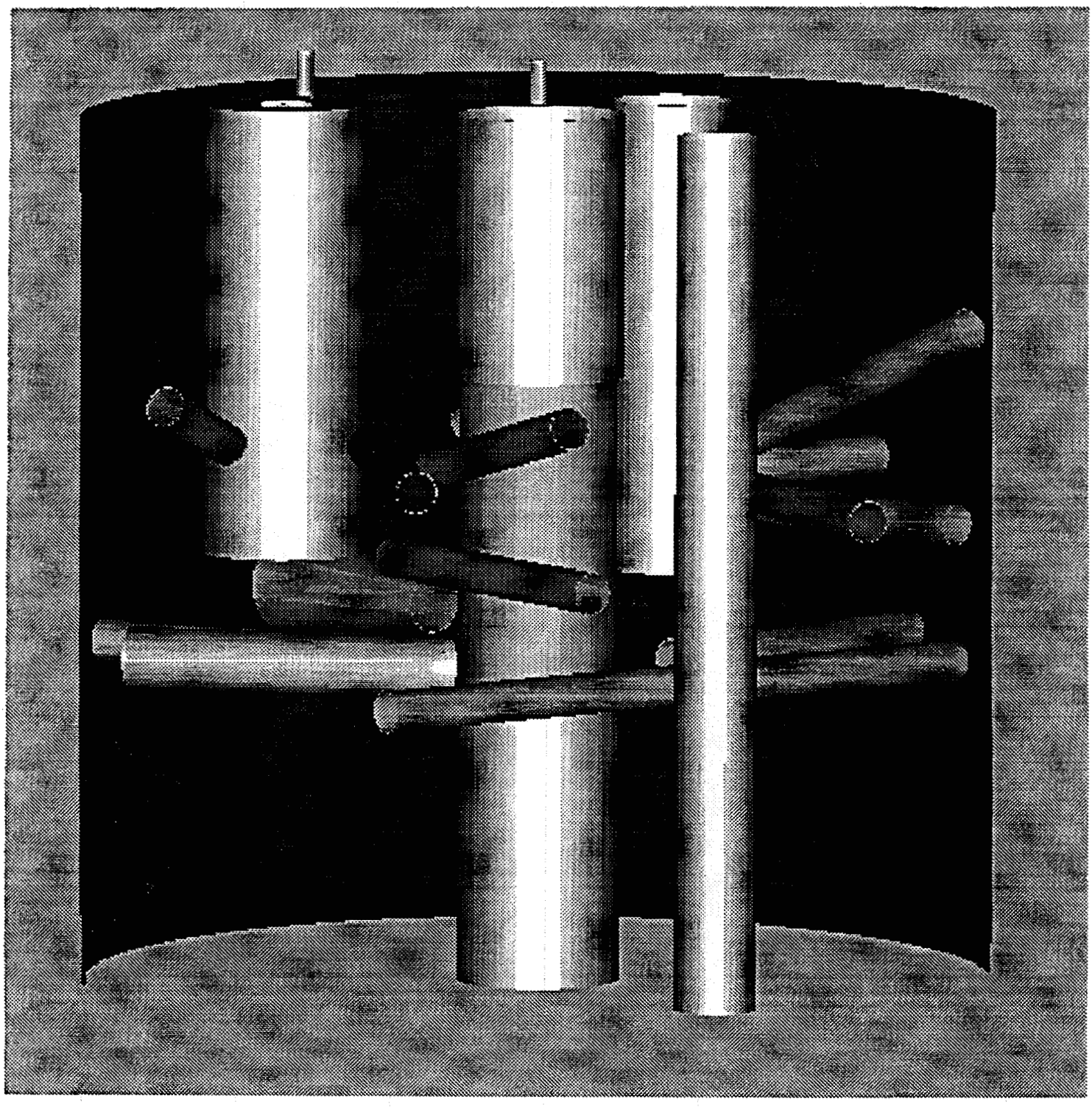

Fig. 3.1b. SABRINA printout of the FOEHN experiment MCNP model (front view).

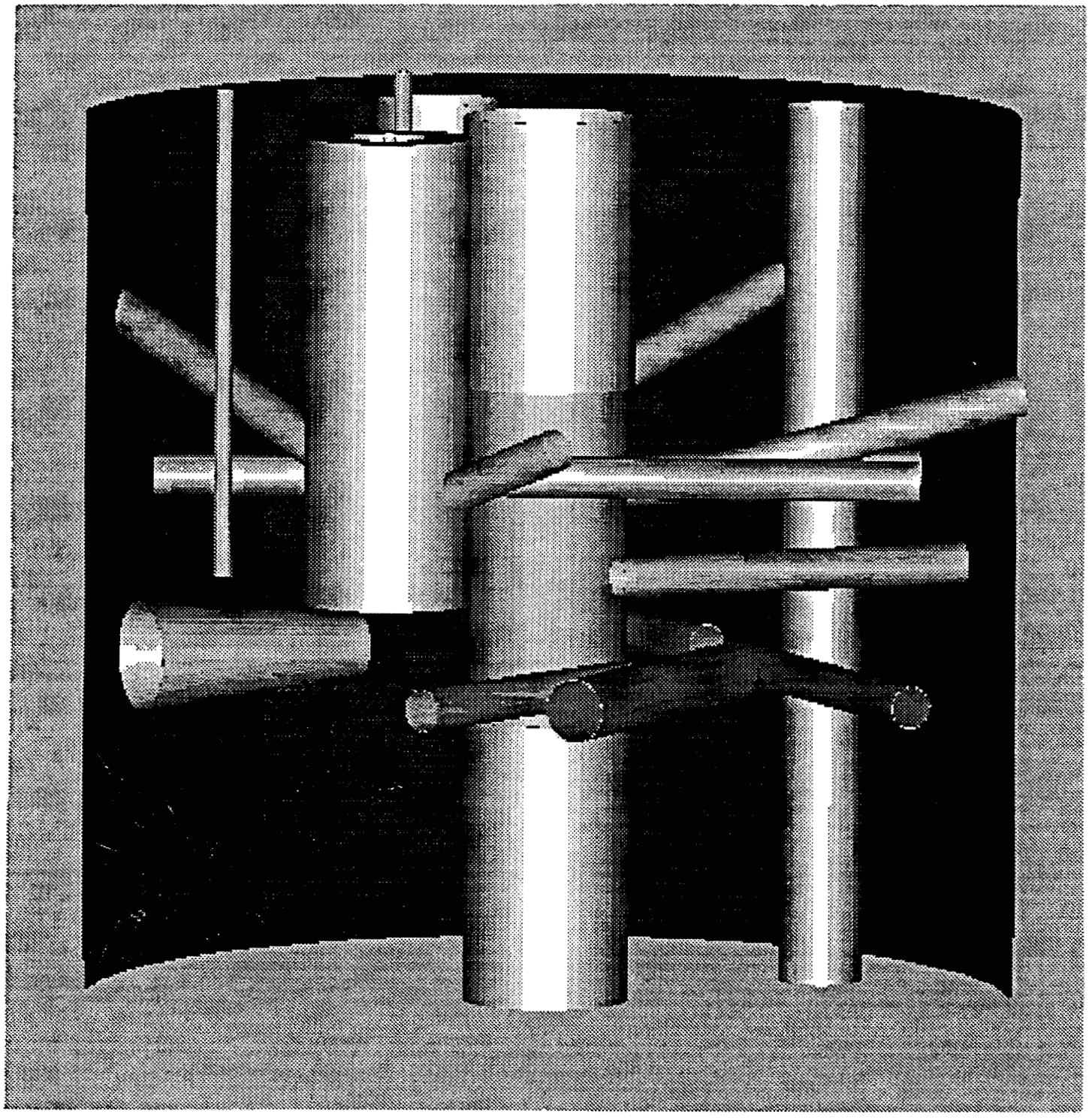

Fig. 3.2. SABRINA printout of the FOEHN experiment MCNP model (left view).

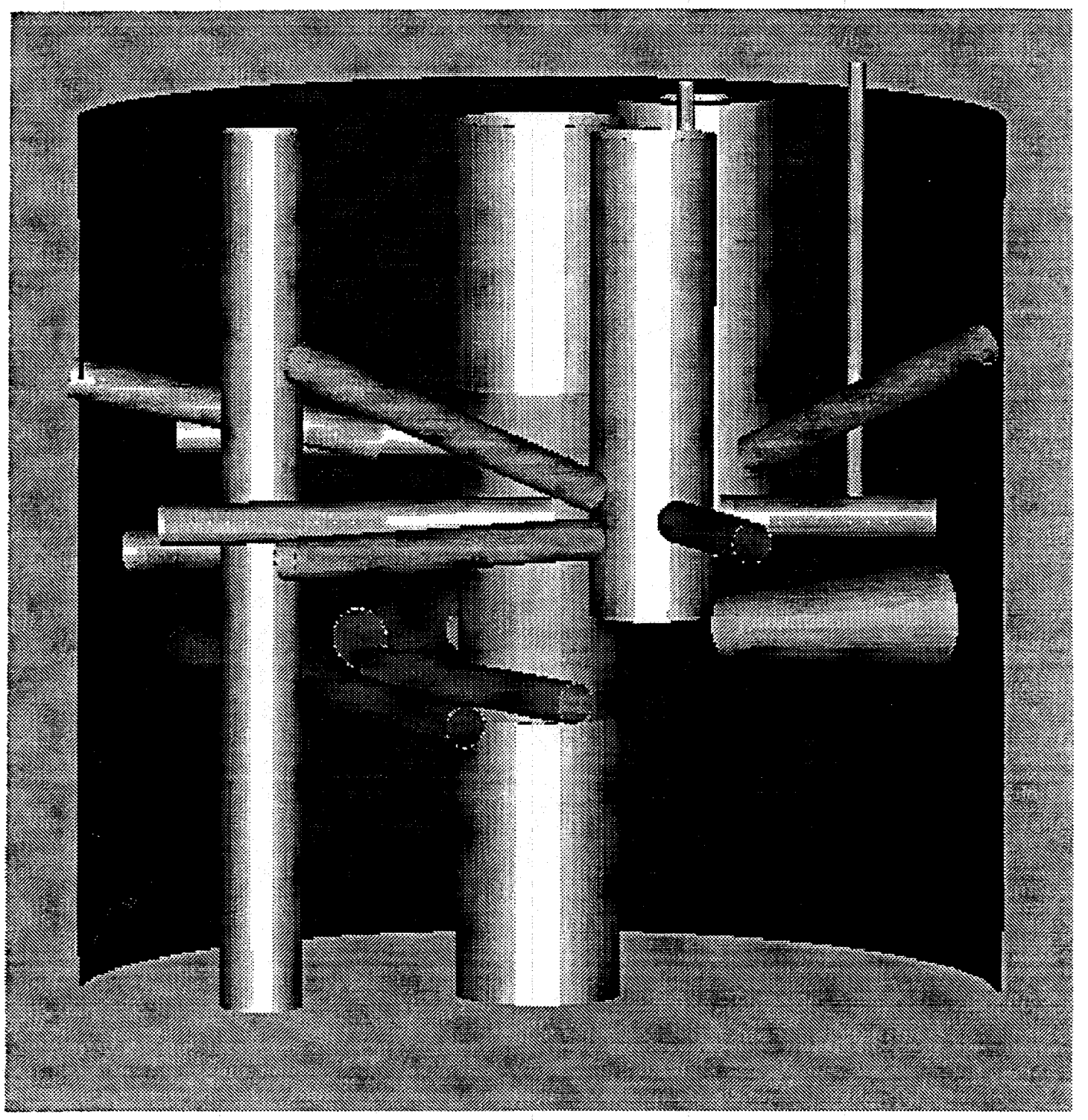

Fig. 3.3. SABRINA printout of the FOEHN experiment MCNP model (right view).

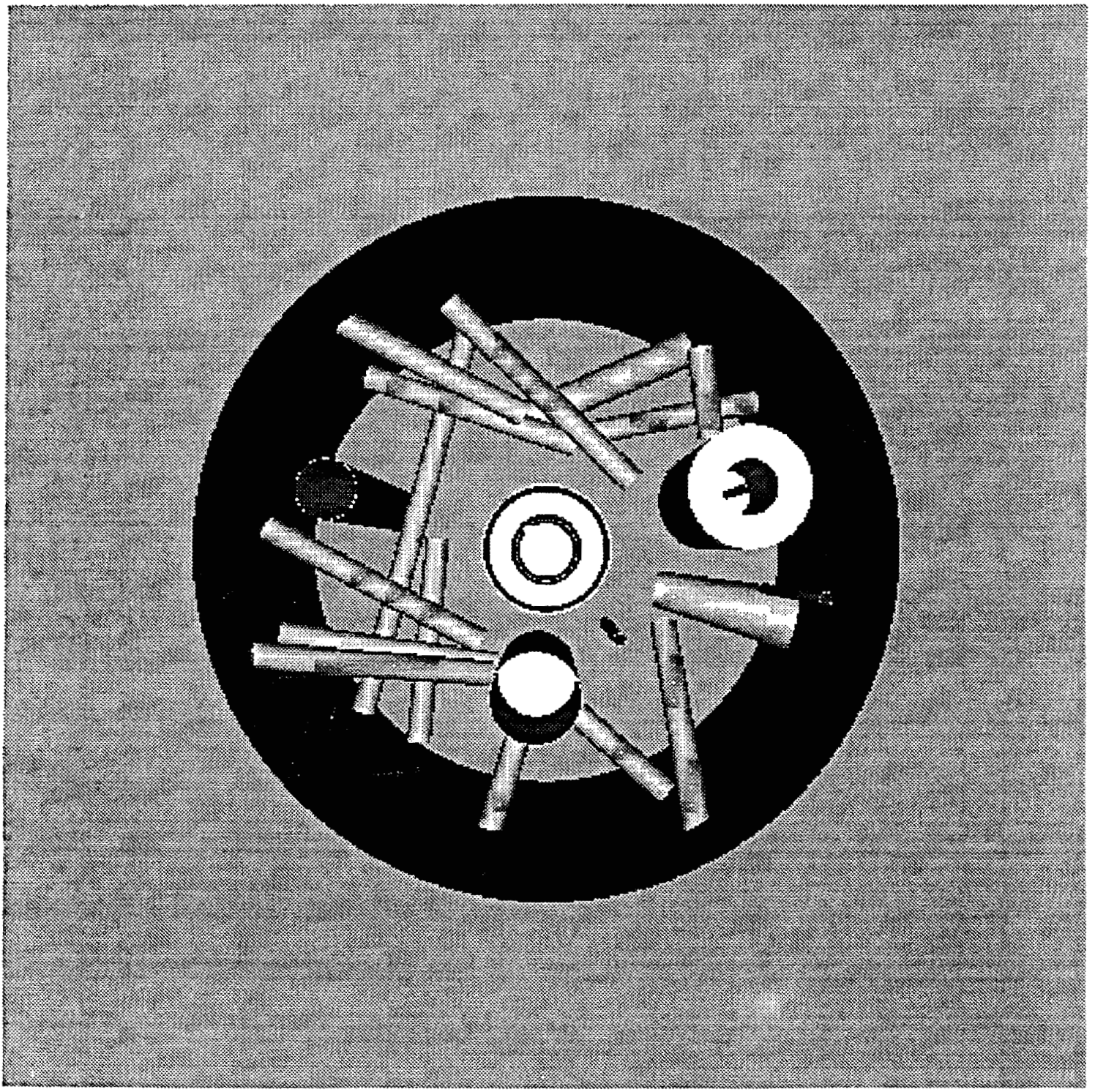

Fig. 3.4. SABRINA printout of the FOEHN experiment MCNP model (top view).

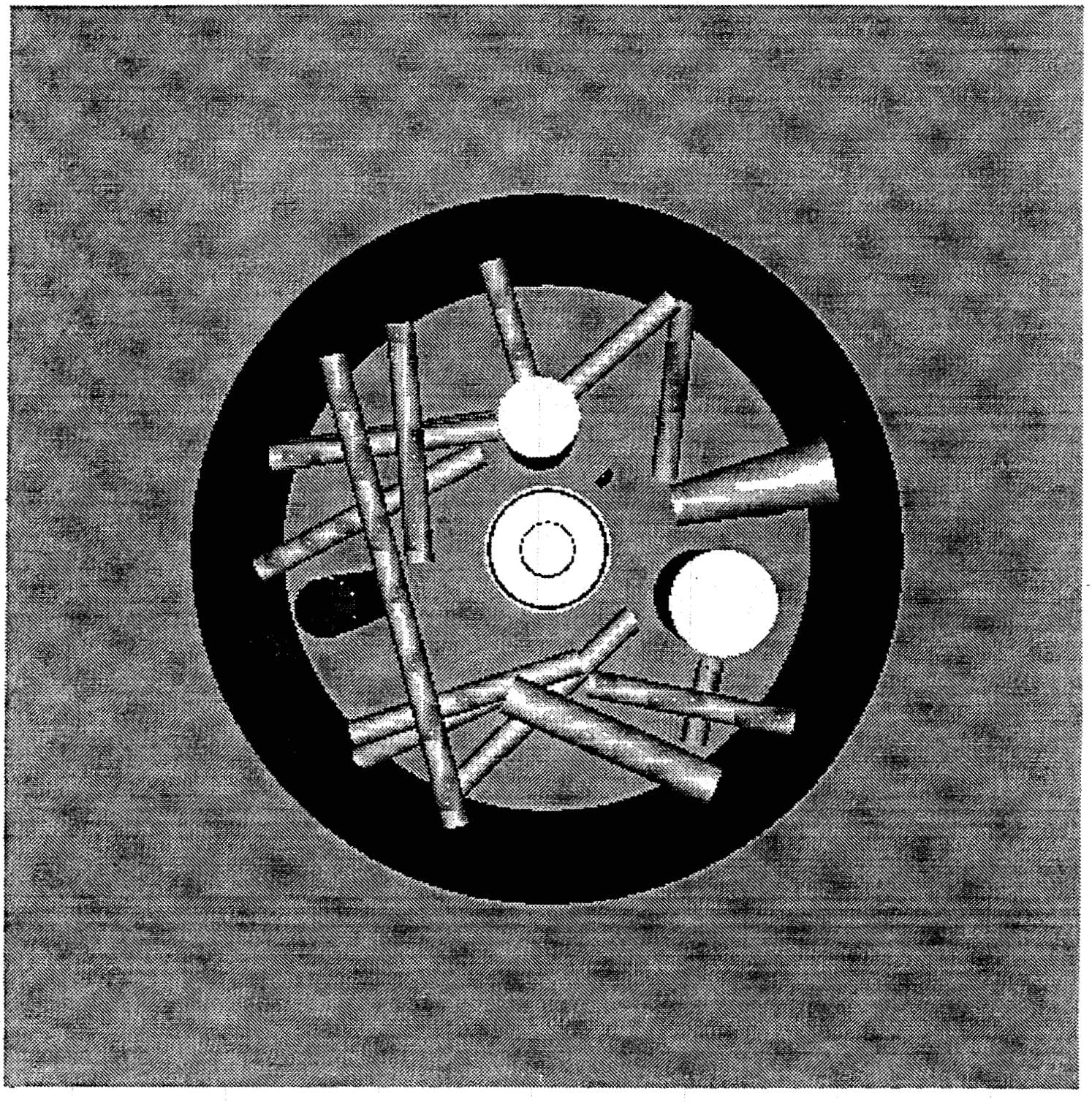

Fig. 3.5. SABRINA printout of the FOEHN experiment MCNP model (lower view).

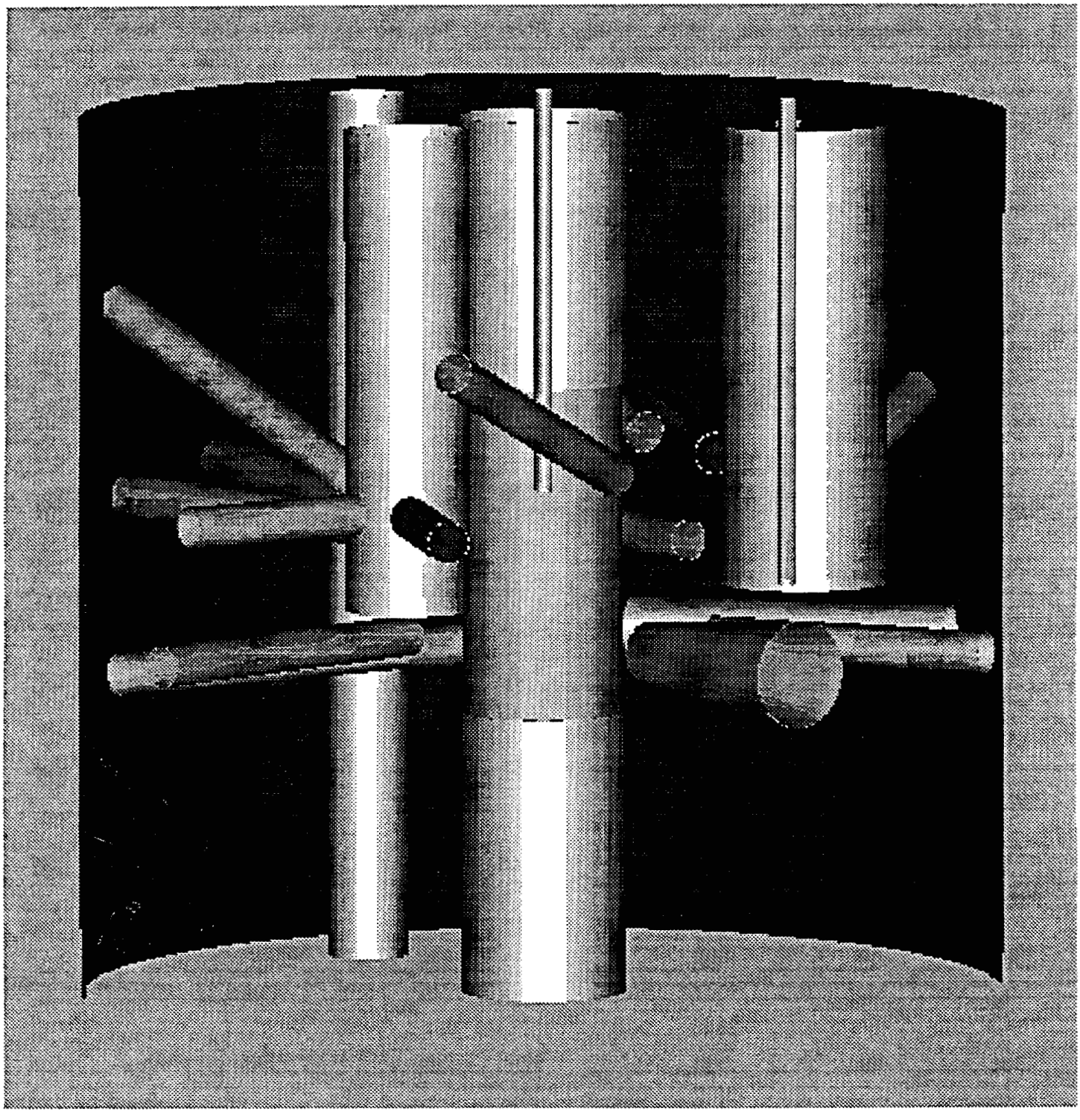

Fig. 3.6. SABRINA printout of the FOEHN experiment MCNP model (back view).

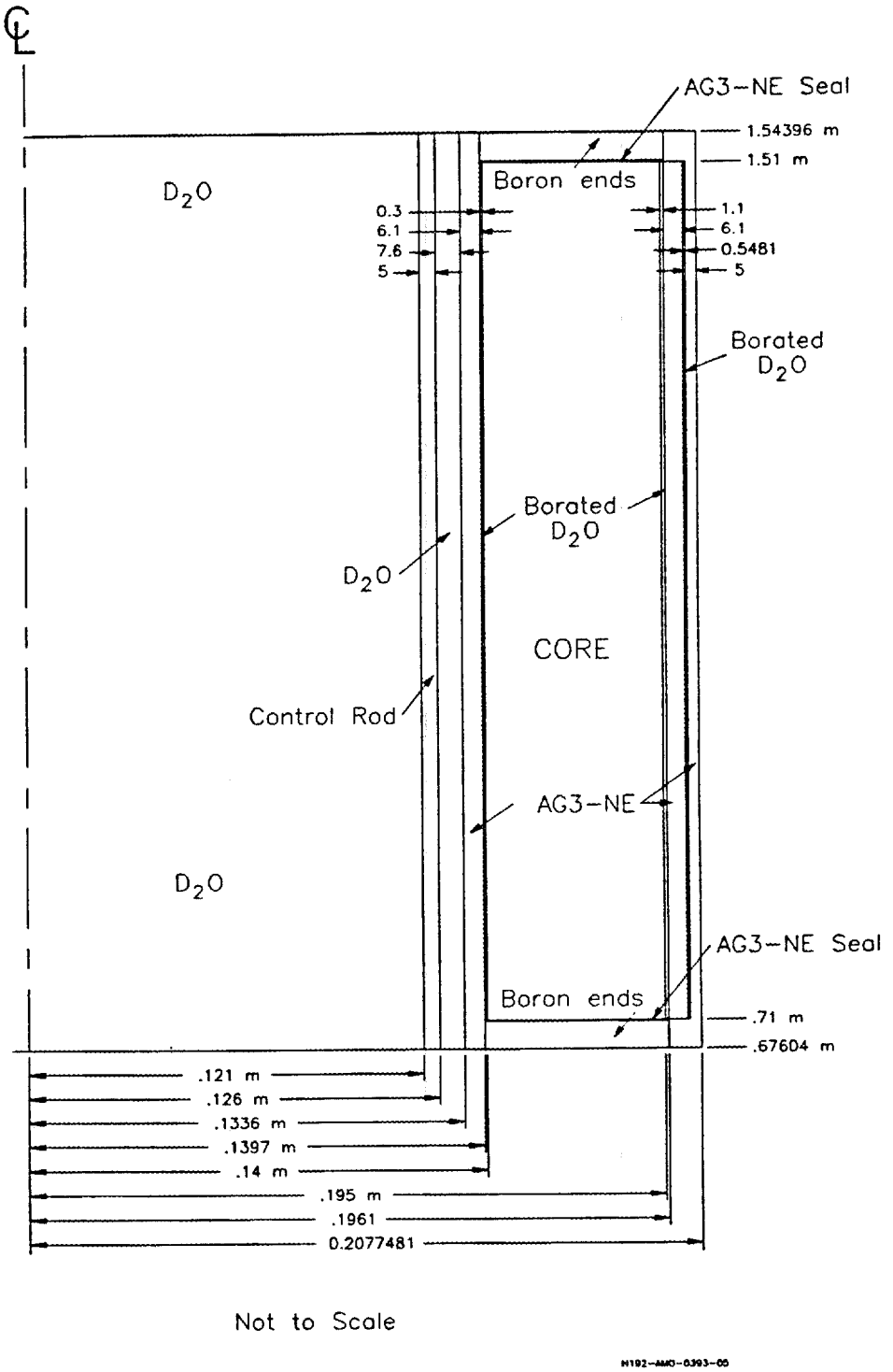

Fig. 3.7a. Axial view of the FOEHN core and its surrounding cask.

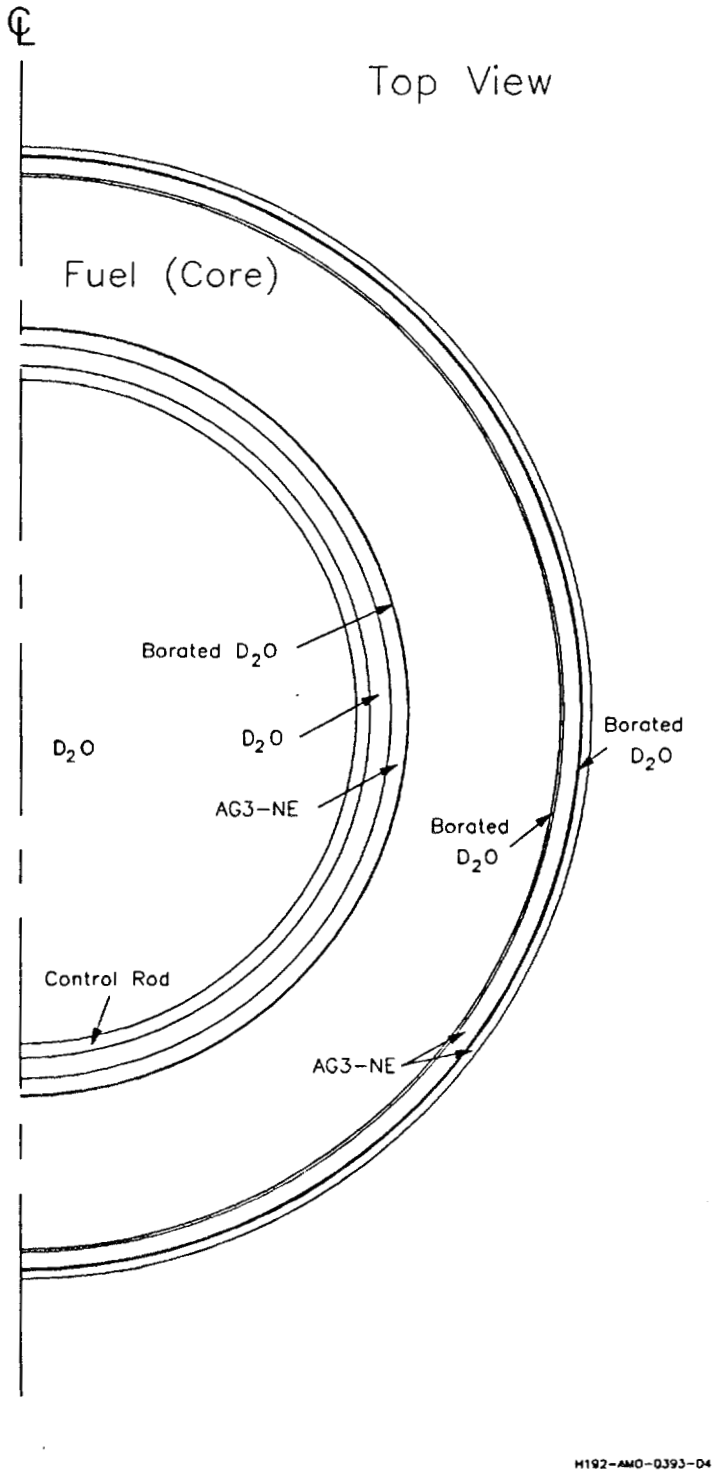

Fig. 3.7b. Radial view of the FOEHN core and its surrounding cask.

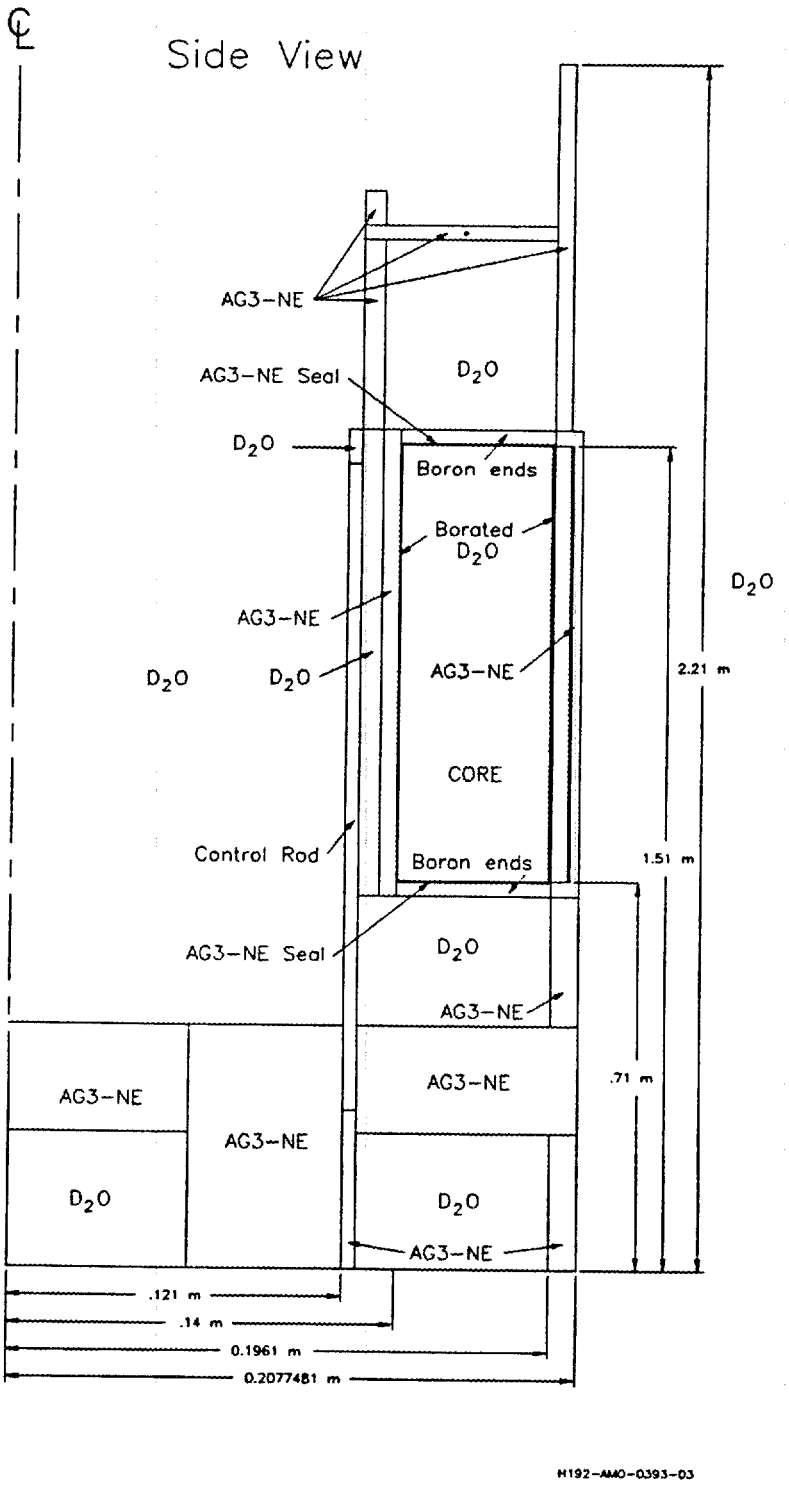

Fig. 3.8. Axial diagram of the FOEHN core and surrounding structures.

In modeling the core, the control cylinder, and the core barrel, a number of assumptions had to be made. Referring to Figs. 3.7a and 3.7b, the core is now described starting from the centerline and moving outward. The central region is occupied by unborated heavy water up to a radius of 121 mm. The following cylindrical shell is the control rod (5-mm thick). Following the control rod is a layer of unborated heavy water extending 7.6 mm. After this heavy water comes the inner wall of the core barrel. The outside surface of this wall, facing the inner reflector and control shell, is smooth. The inside surface, facing the core, is grooved (comb teeth) to hold the fuel plates in place. It is not clear from the FOEHN report whether the inner side combs cover the entire length of the core. In that report, pictures of the external combs show that they do not fully cover the core. The comb region may have gaps containing borated D_2O. In the model, the geometric details of the gaps are ignored; the entire shell (solid portion and comb region) is modeled as a single, solid, 6.1-mm thick AG3-NE shell followed by a 0.3-mm layer of borated D_2O. The fuel lies immediately after this heavy water layer. The thickness of the fuel region is 55.0 mm. This region is assumed to contain a homogenous mixture of borated D_2O, aluminum, and ^{235}U. A borated D_2O-filled gap of 1.1 mm separates the fuel region from the external comb region (also used to hold the fuel plates in place). The remarks made about the inside comb region are applicable to the outside one. The region is also modeled as a solid AG3-NE shell 6.1-mm thick. The water contained in the comb region is modeled as a separate layer of borated D_2O located between the comb shell and the outer wall of the core barrel. This layer also accounts for the fact that the fit between the comb shell and the core barrel wall cannot be exact, and that some tolerance is to be expected. The thickness of the borated D_2O layer is chosen to be 0.5481 mm. This choice accommodates the balance of borated D_2O contained within the core barrel and otherwise not accounted for in the "free" (nonfuel) volume within the core. The outside wall of the core barrel is 5-mm thick. The core barrel is surrounded by the external nonborated D_2O reflector.

The above description contains an assumption pertaining to the distribution of borated heavy water within the core/core barrel region. It is assumed that some of the borated heavy water is not located in the fuel region and instead constitutes a shell within the outer core barrel region. A similar assumption is not made, however, for the inner core barrel region. With these assumptions, the core and core barrel regions are modeled to contain 28.85 L of borated D_2O. This is the measured borated D_2O content of the core/core barrel in FOEHN, and it is different from the design content of 27.0 L.

3.3.2 Reflector Internals

The description and placement of the reflector internals were done according to Fig. 2 and Table 2 of ref. 5. The beam tubes and other assorted channels were modeled as evacuated AG3-NE tubes using material 40 from Table 3.1 of the FOEHN report. The hot and cold sources geometry and materials were modeled exactly as described in Figs. 3 and 4 of ref. 8. The beam tubes were modeled as AG3-NE alloy tubes. The interior of the beam tubes was modeled as a vacuum.

3.3.3 Safety Rods

The safety rods were modeled as described in Sect. 2.2.1.4. Locations for the safety rods were based on Sect. 5.5.2.2 of the FOEHN report with the rod centers located 0.33 m from the core center. The safety rods were not included in any of the experiments modeled. They were replaced, therefore, with heavy water in all model cases.

3.3.4 The Coordinate System

The coordinate system used in the FOEHN model was the same as that used to describe most of the structures in the experiment. The origin was at the core centerline and at the bottom of the reflector tank. The use of this coordinate system allowed direct translation of the core structures and reflector internals to the MCNP geometry model. Figure 3.8 shows the origin and coordinate system used. A different coordinate system was used for the control rod, and, thus, some translation to the MCNP geometry model was required. In the FOEHN report, the origin for the control rod system was 0.1-m above the top of the core, with the positive direction being downward. The top of the control rod was considered to be the zero point on the rod. Thus, when the top of the control rod was 0.1-m above the top of the core, the control rod was said to be inserted to 0.0 m, and downward motion was positive insertion. This system was translated to the MCNP geometry model, which put the zero point at 1.61 m. This created some minor problems when the control rod was at a height of <1.0 m, as the bottom of the rod was then outside the MCNP model. In these cases, the portion of the rod below the tank bottom was neglected.

3.3.5 Materials

The materials used in the model are described in Sect. 3.2.2 of this report. The core and the boron end caps were taken from Table 3.1 of the FOEHN report. The data for graphite, cadmium, Zircaloy-4, and stainless steel 304 (SS-304) were not included in the FOEHN report. The assumptions used in selecting data for these materials are also discussed in Sect. 3.2.2. The actual nuclide concentrations used can be found in Appendix A, which lists the entire input file for the MCNP model. The compositions used for Zircaloy-4 and SS-304 are the same as those previously used in a model of the ANS reactor and a model of the High Flux Reactor of ILL. Figures 3.7 and 3.8 show the MCNP materials used to model the individual core regions. The beam tubes were modeled using the AG3-NE alloy. The core, borated heavy water, and aluminum core structural material compositions were altered as needed to reflect changes in the dissolved boron concentration in the core.

3.4 MCNP TALLIES AND COMPUTATION OF k_{eff} AND RENDEMENT

The choices of MCNP tallies to be used in the comparison between the FOEHN experiment and the computational model are shown, and the reasons for their selection are summarized in this section. In addition, the methods used to compute k_{eff} and the rendement are discussed.

3.4.1 Fluxes

The thermal fluxes reported in the FOEHN experiments are obtained by estimating the activation due to thermal neutrons (the activation is proportional to the flux). They are, therefore, best approximated by a track length estimate of the flux (i.e., a F4:n MCNP tally). The upper energy boundary of the thermal energy group should be chosen as 0.625 eV to conform with the definition of thermal flux chosen in the FOEHN experiment based on the cadmium effective cutoff energy.

3.4.2 Powers

The fission power density or fission power production density is described as power distribution in the FOEHN report. It is measured by evaluating the number of fission events that occurred in a given fission probe. The measurements yield a quantity proportional to the power released in the probe during irradiation. The MCNP tally that most closely represents this physical quantity is a F7:n tally.

3.4.3 Effective Multiplication Factor

The multiplication factor (k_{eff}) is measured via three different methods in the FOEHN experiment (see Sect. 2.3.1.1). In the present work, k_{eff} is computed via the KCODE option of MCNP.

3.4.4 Determination of Rendement

A measure of the neutron efficiency, the rendement, is defined as the ratio of the maximum thermal flux in the reflector to the total recoverable power produced in the reactor. In the MCNP model, the rendement is computed from the maximum value of F4:n tallies in the reflector renormalized using the multiplying factor

$$RN = \nu \cdot \frac{1}{Q} \cdot \frac{1}{k_{eff}} \quad , \tag{8}$$

where ν is the average number of neutrons per fission, Q is the fission energy, and k_{eff} is the effective multiplication factor from the MCNP run that yielded the flux tally to be renormalized. In this work, ν is computed as the ratio of two separate MCNP tallies, and its value is reported whenever pertinent. When a value is not computed for ν, and one is required, the number 2.44175 is used. The energy released per fission event, Q, is taken to be 202.47 MeV/fission unless otherwise specified. In order to obtain a meaningful comparison in the computational determination of the rendement, the same value of Q (199.73 MeV) as that of the FOEHN report is used in this work, but only for "rendement" computations.

3.5 SUMMARY

In this chapter, the MCNP model developed in this work has been presented. The main approximation made was the use of a homogenized fuel region and of homogenized boron axial end covers above and below the core. These approximations were justified by the fact that the neutron mean free path in these regions is much larger than any of the dimensions of the constituting components. The materials used in the model accurately represent the compositions used in the experiment. The only exceptions are the use of full theoretical density graphite (C) and cadmium (Cd) data. When Zircaloy-4 and stainless steel 304 were required, data developed for models of the ANS reactor and of the FGHFR were used. The fluxes and the power production distribution are modeled as F4:n and F7:n tallies, respectively. The rendement is computed as a particular case of a renormalized F4:n tally. The core multiplication factors are obtained via the KCODE option of MCNP.

4. RESULTS

4.1 INTRODUCTION

The results obtained in the course of this study are detailed in this chapter. The FOEHN report is consistently referred to for comparisons. The results are reported by reactor configuration. The core multiplication factor, thermal flux, rendement, and power distribution are addressed in turn. It is shown that the model and the experimental results coincide very well within the computational statistical error and experimental error bounds. The model results are reported normalized as described in the text. The MCNP error estimates (standard deviations σ) are reported as fractions of the tallies they qualify unless otherwise noted to be absolute values.

4.2 SIMPLE REACTOR MODEL

4.2.1 Core Multiplication Factors (k_{eff})

The multiplication factor has been evaluated for 11 critical control rod positions and corresponding boron concentrations for the simple FOEHN configuration (no boron end caps and no reflector internals). These computations used the KCODE option of MCNP with 40 cycles and 3000 histories per cycle. The results are given in Table 4.1 and shown in Fig. 4.1. The cases in Fig. 4.1 are defined in the table as particular combinations of control rod positions and soluble boron concentrations for which the reactor is critical. The case definitions for all reactor configurations are taken from Table 5.1.1 of ref. 2. It can be seen from Fig. 4.1 that the computational results coincide with 1.0 within a tolerance of 2σ for two cases and are very close for five other cases. The miss rate is 9/11 (i.e., nearly 82%). This rate is far greater than the theoretically expected average miss rate of about 5% for 2σ error bars. If the error bars are increased to 3σ, the miss rate drops to five, of which two would be very close misses.

An estimate of the effect of small perturbations in control rod position on the calculated critical states was obtained by moving the control rod up or down 20 mm from the critical position. This was done for each of three different critical states: rod at 1.438 m and 0.2477 g/L of boron in the core; rod at 1.009 m and 0.4509 g/L of boron in the core; and rod at 0.714 m and 0.5386 g/L of boron in the core. The results of these runs are presented in Table 4.2 and Fig. 4.2. These show that for the first critical state (rod initially at 1.438 m and 0.2477 g/L of boron), the rod position perturbation produces the expected behavior—rod withdrawal increases the core multiplication factor, whereas rod insertion reduced it. For the intermediate boron concentration (0.4509 g/L), the same behavior is observed. In the last case, the core multiplication factors of the initial critical state and of the perturbed states are within the 2σ error bars defined by the computational statistics and, thus, are not distinguishable. This can be attributed to the reduced worth of the control rod caused by the high concentration of boron in the core. For this critical state, the boron concentration in the core provides the bulk of the reactivity control, and hence small perturbations in the control rod positions have small effects, and the observed fluctuations have no statistical significance.

4.2.2 Thermal Flux

Calculated MCNP thermal fluxes (F4:n tallies, KCODE, 40 cycles, 10000 histories/cycle) were compared to the results given in Table 5.1.4 of ref. 2. The thermal flux for this comparison was

Table 4.1. MCNP computed core effective multiplication factors (k_{eff}) for various critical states of the simple reactor configuration

Case	Control rod position (m)		Boron conc. (g/L)	MCNP k_{eff}	MCNP error estimate (σ)
	MCNP	FOEHN			
1	1.438	0.172	0.2477	1.0003	0.0019
2	1.253	0.357	0.3349	1.0076	0.0029
3	1.155	0.455	0.3863	1.0092	0.0021
4	1.142	0.4673	0.3855	1.0093	0.0030
5	1.014	0.596	0.4501	1.0127	0.0023
6	1.009	0.601	0.4509	1.0080	0.0031
7	1.008	0.602	0.4536	1.0095	0.0026
8	0.949	0.661	0.4791	1.0069	0.0029
9	0.753	0.857	0.5268	1.0034	0.0033
10	0.720	0.89	0.5386	1.0104	0.0021
11	0.714	0.896	0.5386	1.0069	0.0028

defined as the flux below 0.625 eV. This cutoff energy was chosen to match the cutoff energy used in the FOEHN experiment. The F4:n tally gives the neutron flux averaged over a cell in units of particles/cm^2. Measured thermal fluxes in ref. 2 were reported at specific radii (r) and heights (z), but no specific azimuthal location was given in the report. To model these locations in MCNP, annuli of 0.01-m width and 0.01-m height were used. The center of the annuli were located at the coordinates (r,z) of the detector foils. The control rod height for this case was set at 1.01 m in the MCNP model. The boron-10 (^{10}B) concentration was 0.450 g/L.

The MCNP F4:n tallies were normalized to 1 W total reactor power for a direct comparison with the experimental results. Table 4.3 shows the MCNP-calculated thermal fluxes, and Table 4.4 shows the corresponding computed error estimate (2σ). The entries in these two tables are in units of 10^{11} m^{-2} · s^{-1}. The results in both of these tables use 2.43862 for ν and 202.47 MeV for Q. These results can be directly compared to the thermal fluxes in Table 5.1.4 of ref. 2. In Figs. 4.3, 4.4, and 4.5, experimental and computational axial flux shapes are shown at radii of 0.235 m, 0.355 m, and 0.835 m, respectively, from the center of the reactor. As discussed in Sect. 2.4.3.2, the error bars for the experimental data points are taken as ±12%, a much more realistic figure than the ±2% claim in the FOEHN report. The error bars on the MCNP points are based on a $\pm 2\sigma$ error estimate. These figures show that MCNP-calculated thermal fluxes agree, within statistics and experimental error estimates, with the experimental results. Not seen from the three figures is the total number of points for which the experimental and computational results do not coincide (in the sense that their respective error bars overlap). This total number of misses is six. If the experimental bars are assumed to be

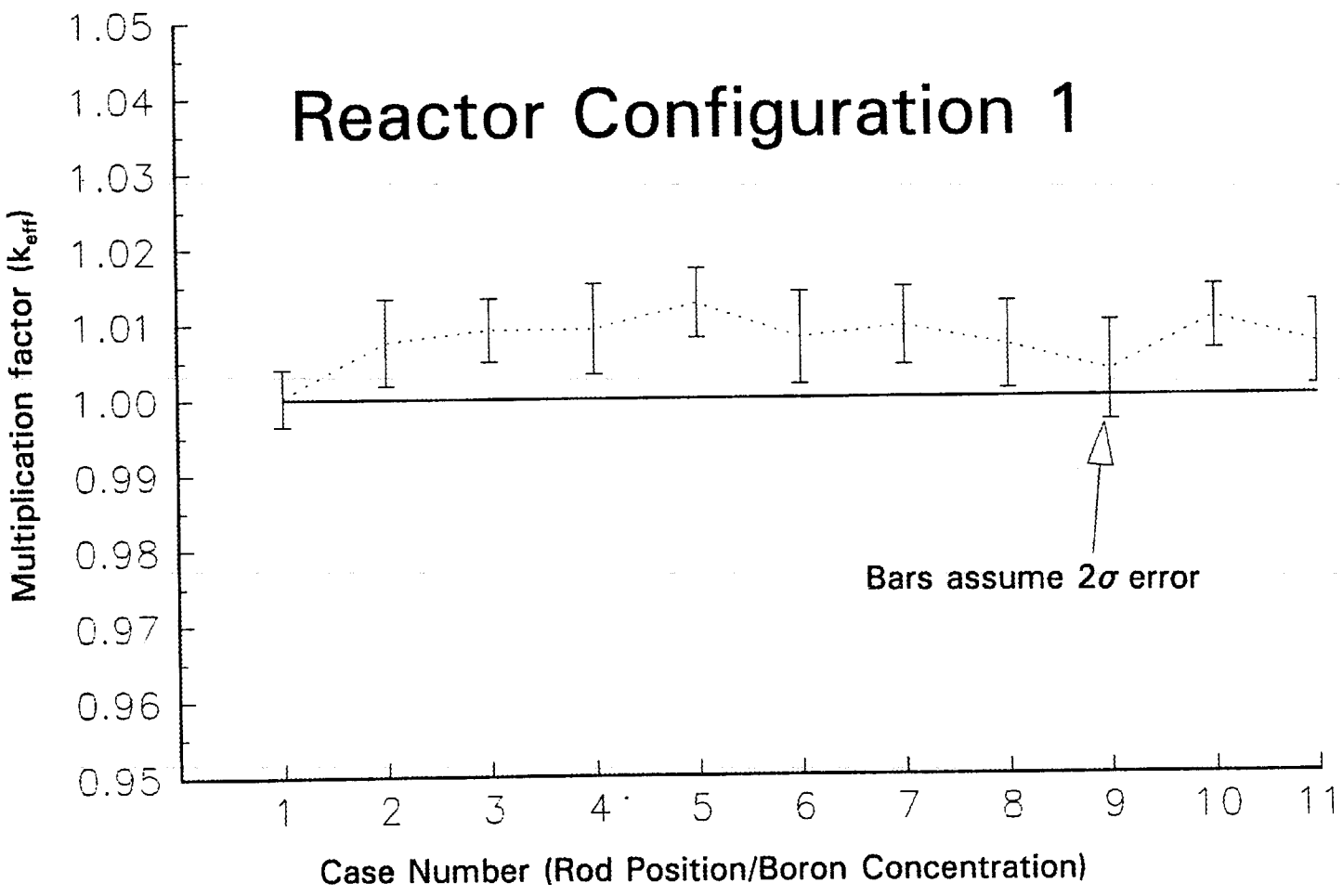

Fig. 4.1. MCNP prediction of k_{eff} for a set of critical states of the simple FOEHN reactor configuration.

Table 4.2. Effect of control rod perturbations on the core effective multiplication factor for three critical states of the simple reactor configuration

Control rod position (m)	Core boron concentration (g/L)	Core multiplication	
		k_{eff}	σ
1.478	0.2477	0.9937	0.0029
1.438 (base)	0.2477	1.0003	0.0019
1.398	0.2477	1.0068	0.0030
1.049	0.4509	1.0016	0.0025
1.009 (base)	0.4509	1.0080	0.0031
0.969	0.4509	1.0165	0.0029
0.760	0.5386	1.0030	0.0031
0.720 (base)	0.5386	1.0104	0.0021
0.680	0.5386	1.0054	0.0027

more narrow, the number of misses increases to 15 for 10% experimental error and to 38 for 8% experimental error. Since there are 158 experimental points, these misses represent miss rates of 3.8, 9.5, and 24% respectively. The 12% experimental error assumption yields results that are compatible with the statistical interpretation of the 2σ computational bars.

4.2.3 Rendement

For the simple reactor configuration, the measured rendement (r_{meas}) is 2.480×10^{11} neutrons/$m^2 \cdot s \cdot W$. The error on this quantity ranges from at least ±2.2% to possibly as much as 16.2% as estimated in Sect. 2.4.3.4 (vs the FOEHN report claim of ±2%). In the remainder, it is assumed that the error is the same as that on the flux—about 12%.

The MCNP computed rendement, r_{calc}, is found to be 2.777×10^{11} neutrons/$m^2 \cdot s \cdot W$, with a standard deviation (σ) of 0.94% (assuming Q is 199.73 MeV, the same as the one used in the FOEHN report, and ν is 2.43862). The computed value of the rendement is ~12% higher than the experimental one. A similar result (14% higher) was found independently by Rohrmoser.[10] The two error bands (experimental and computational—2σ) overlap significantly. They would overlap slightly even if the experimental error was taken to be as low as ~10%. The two estimates of the rendement can be considered to be coinciding.

4.2.4 Power

The MCNP model of the FOEHN critical experiment has been used to obtain F7:n tallies. The tallies have been normalized to the same constant (1.014239) as the data of the corresponding Table 5.1.5 of the FOEHN report, according to the procedure summarized in Sect. 2.3.2.2. The

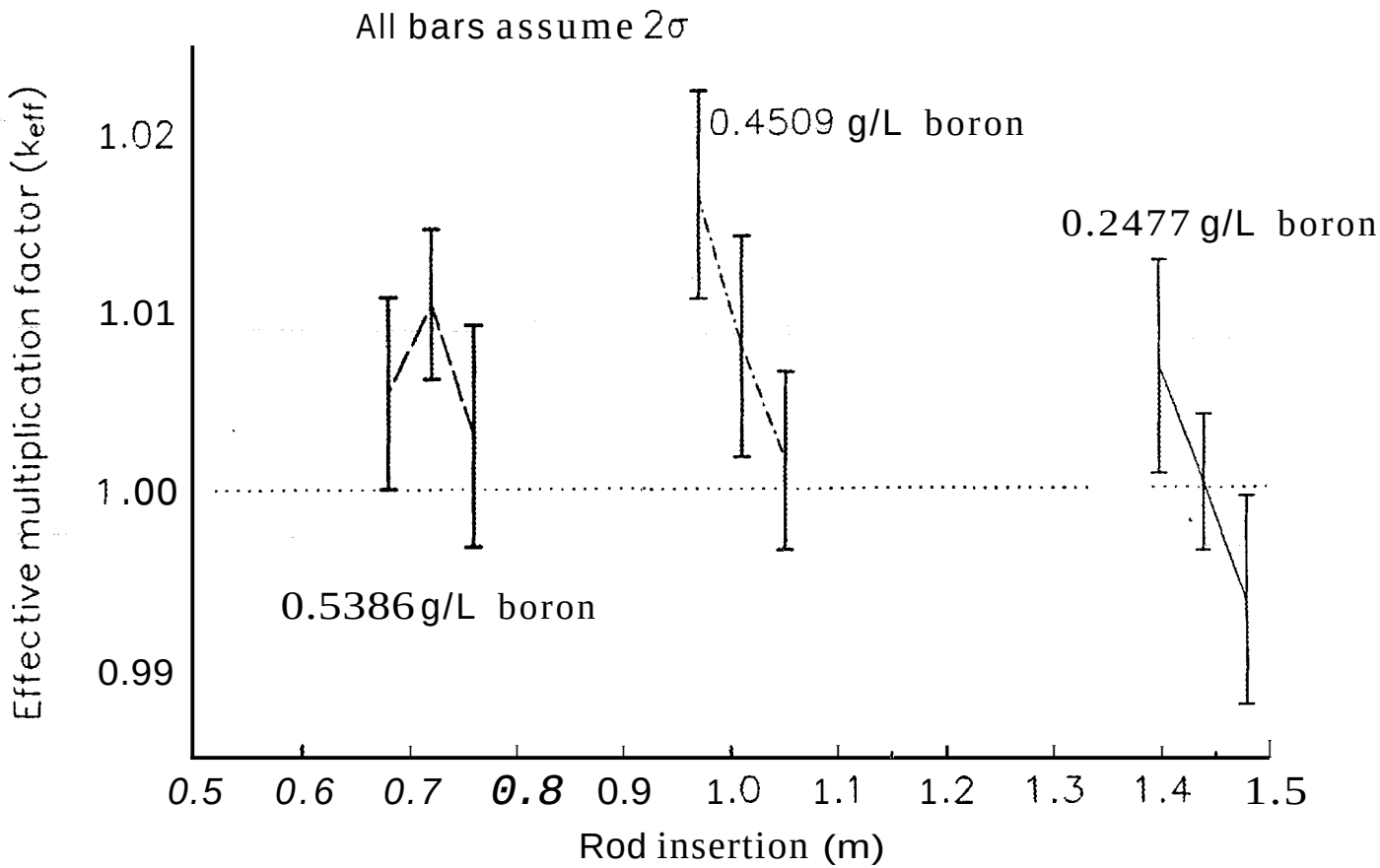

Fig. 43. Control rod position perturbation effect on k_{eff} in the simple FOEHN reactor configuration.

Table 4.3. Computed thermal fluxes for the simple reactor configuration (MCNP F4:n tallies; 0.625 eV cutoff; 1 W reactor power; units: 10^{11} $m^{-2} \cdot s^{-1}$)

H/r (mm)	235	255	275	295	315	335	355	395	435	515	635	755	835
525	0.6062	0.6828	0.7652	0.7298	0.7819	0.7997	0.8147	0.7878	0.7916	0.6971	0.5548	0.4008	0.3043
625	0.9433	1.0015	1.0857	1.0532	1.1355	1.1259	1.1325	1.0841	1.0632	0.9136	0.7038	0.4942	0.3714
725	0.9636	1.1321	1.3528	1.3327	1.4048	1.4777	1.4824	1.4568	1.3779	1.1713	0.8622	0.5972	0.4579
825	1.1441	1.4061	1.7076	1.5790	1.7676	1.8411	1.8447	1.8072	1.6965	1.4314	1.0106	0.7069	0.5353
925	1.3566	1.6437	2.0492	1.8655	2.1158	2.1648	2.1489	2.1101	1.9917	1.6737	1.1570	0.8019	0.6018
975	1.4740	1.7678	2.1728	2.0135	2.2842	2.3366	2.3357	2.2271	2.1308	1.7431	1.2169	0.8280	0.6295
1075	1.6401	1.9841	2.3830	2.2314	2.5320	2.5096	2.5115	2.4646	2.2986	1.8900	1.3199	0.8768	0.6564
1125	1.7087	2.0244	2.5312	2.2904	2.5933	2.6569	2.6205	2.5339	2.3806	1.9510	1.3422	0.9029	0.6707
1225	1.7296	2.1213	2.5841	2.3716	2.6410	2.6807	2.6773	2.5733	2.4249	1.9489	1.3576	0.9011	0.6574
1275	1.6828	2.1096	2.5514	2.3458	2.6393	2.6709	2.7046	2.5457	2.3463	1.8856	1.3205	0.8724	0.6429
1325	1.6915	2.0312	2.4320	2.3055	2.5459	2.5847	2.5897	2.4973	2.3164	1.8541	1.2858	0.8580	0.6446
1375	1.5896	1.9342	2.3635	2.2044	2.4702	2.4866	2.4523	2.3535	2.1798	1.7959	1.2447	0.8239	0.6251
1425	1.5401	1.8585	2.2559	2.1000	2.2881	2.3401	2.3536	2.3021	2.0707	1.7082	1.1965	0.8102	0.5820
1525	1.6926	1.8797	2.0065	1.9877	2.0685	2.0725	2.0369	1.9349	1.8237	1.5049	1.0570	0.7181	0.5280
1675	1.6369	1.6406	1.6205	1.6262	1.5828	1.5827	1.5395	1.4569	1.3349	1.1077	0.8017	0.5635	0.4370
1825	1.0853	1.0584	1.0410	1.0707	1.0461	1.0075	0.9953	0.9314	0.8624	0.7334	0.5652	0.4316	0.3054

Table 4.4. MCNP error estimate (2σ, absolute) for the thermal fluxes for the simple reactor configuration (units: 10^{11} $m^{-2} \cdot s^{-1}$)

H/r (mm)	235	255	275	295	315	335	355	395	435	515	635	755	835
525	0.0258	0.0270	0.0282	0.0279	0.0281	0.0277	0.0272	0.0255	0.0249	0.0215	0.0173	0.0135	0.0180
625	0.0341	0.0341	0.0337	0.0345	0.0341	0.0331	0.0324	0.0301	0.0293	0.0249	0.0194	0.0147	0.0121
725	0.0335	0.0355	0.0376	0.0384	0.0374	0.0384	0.0371	0.0358	0.0331	0.0281	0.0216	0.0164	0.0136
825	0.0368	0.0405	0.0423	0.0417	0.0428	0.0427	0.0417	0.0394	0.0370	0.0312	0.0234	0.0180	0.0145
925	0.0404	0.0434	0.0467	0.0451	0.0461	0.0463	0.0447	0.0426	0.0398	0.0338	0.0250	0.0192	0.0155
975	0.0419	0.0449	0.0482	0.0471	0.0484	0.0477	0.0467	0.0441	0.0409	0.0345	0.0258	0.0194	0.0161
1075	0.0440	0.0476	0.0500	0.0495	0.0511	0.0497	0.0482	0.0458	0.0428	0.0355	0.0267	0.0198	0.0163
1125	0.0444	0.0478	0.0521	0.0499	0.0513	0.0510	0.0493	0.0466	0.0438	0.0363	0.0274	0.0202	0.0165
1225	0.0453	0.0496	0.0527	0.0512	0.0518	0.0509	0.0503	0.0473	0.0441	0.0366	0.0272	0.0204	0.0162
1275	0.0441	0.0494	0.0520	0.0511	0.0523	0.0507	0.0508	0.0468	0.0427	0.0354	0.0267	0.0197	0.0161
1325	0.0450	0.0483	0.0506	0.0507	0.0509	0.0501	0.0492	0.0464	0.0431	0.0352	0.0265	0.0196	0.0162
1375	0.0436	0.0468	0.0501	0.0498	0.0509	0.0497	0.0481	0.0447	0.0414	0.0352	0.0259	0.0190	0.0158
1425	0.0422	0.0461	0.0496	0.0483	0.0485	0.0482	0.0471	0.0447	0.0402	0.0342	0.0256	0.0190	0.0150
1525	0.0454	0.0481	0.0466	0.0473	0.0459	0.0456	0.0436	0.0410	0.0383	0.0319	0.0241	0.0181	0.0144
1675	0.0465	0.0453	0.0418	0.0436	0.0405	0.0399	0.0382	0.0358	0.0326	0.0272	0.0205	0.0159	0.0133
1825	0.0380	0.0354	0.0335	0.0351	0.0333	0.0316	0.0307	0.0279	0.0257	0.0219	0.0172	0.0035	0.0109

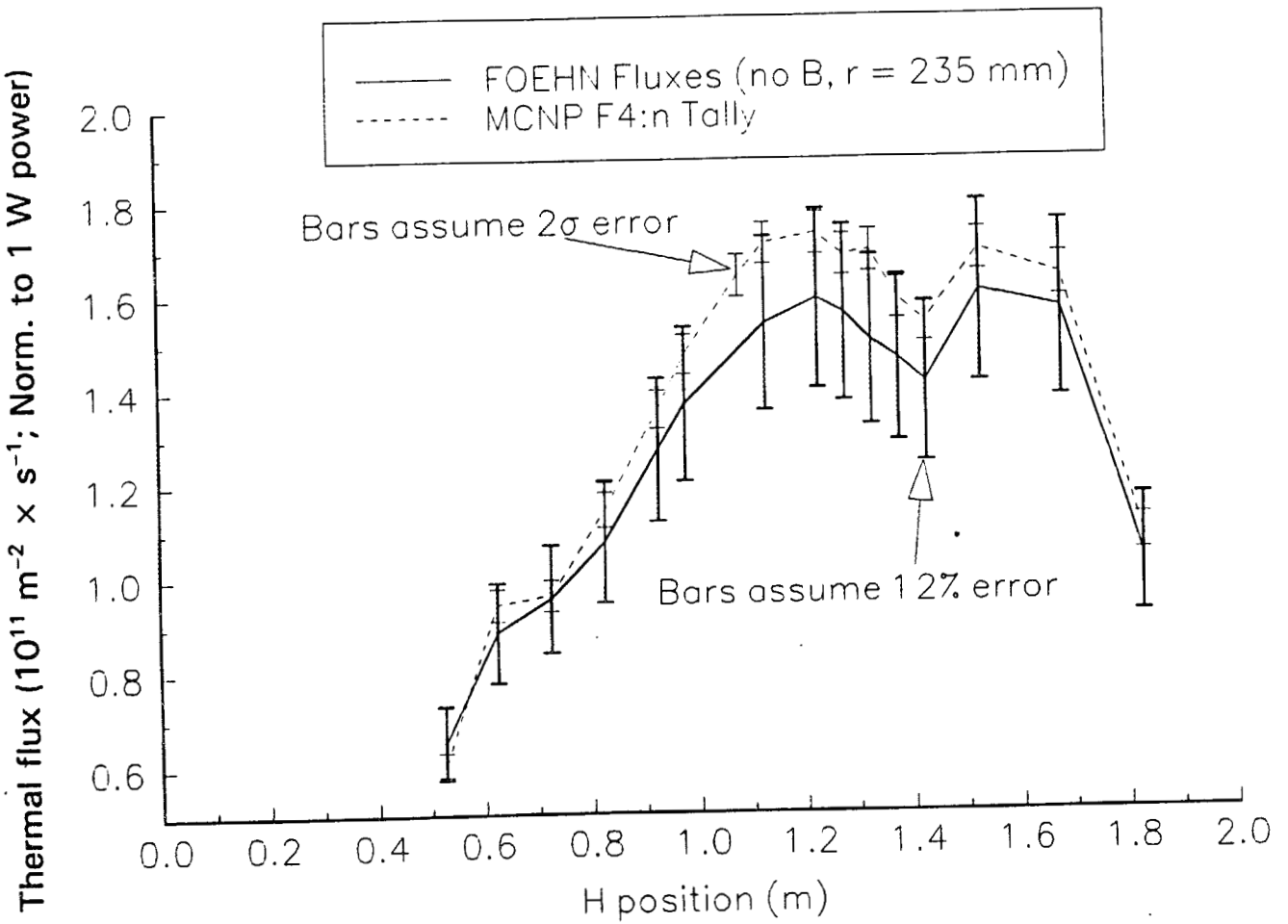

Fig. 4.3. Comparison of experimental and computed axial flux shapes at r = 235 mm in the simple FOEHN configuration.

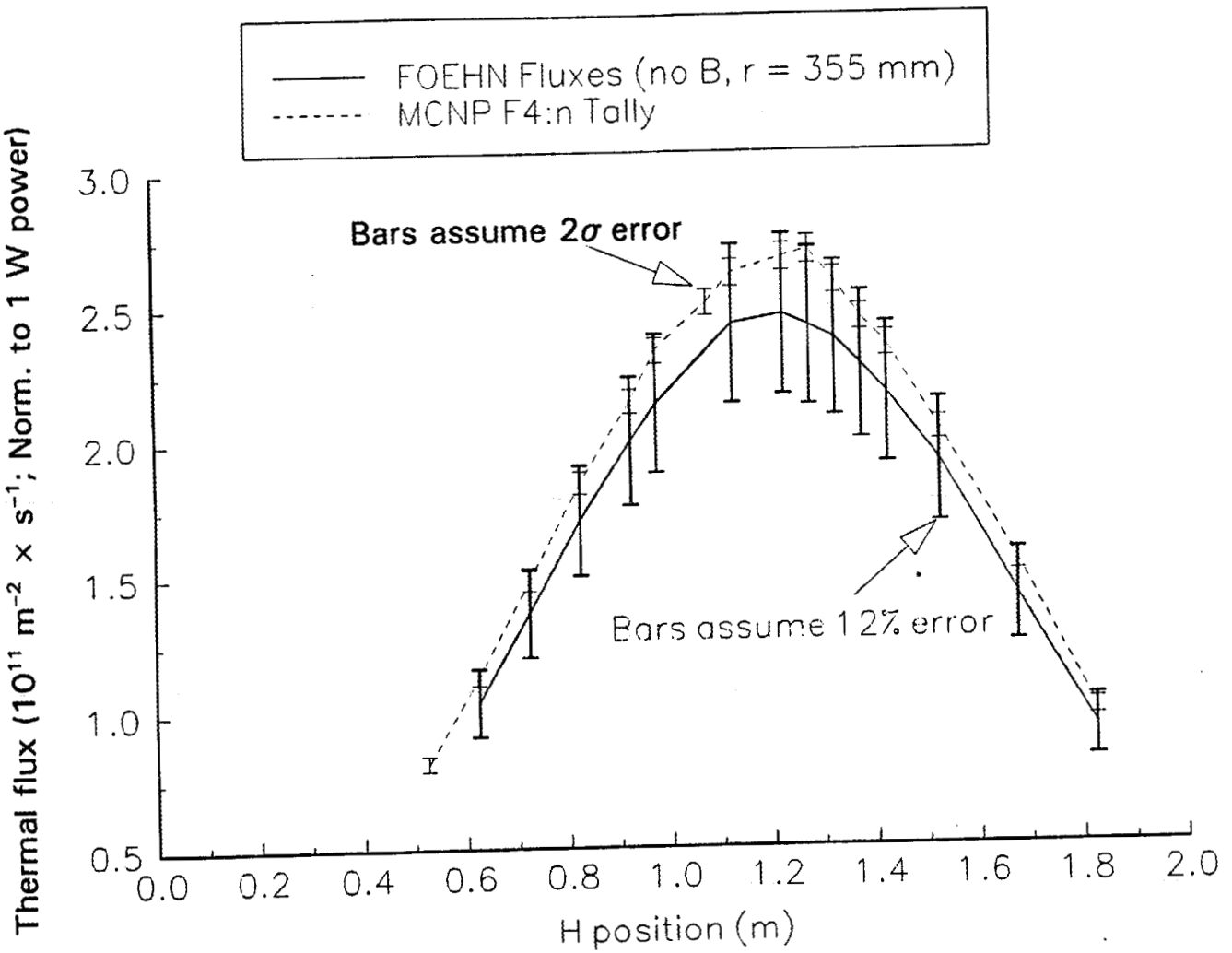

Fig. 4.4. Comparison of experimental and computed axial flux shapes at r = 355 mm in the simple FOEHN configuration.

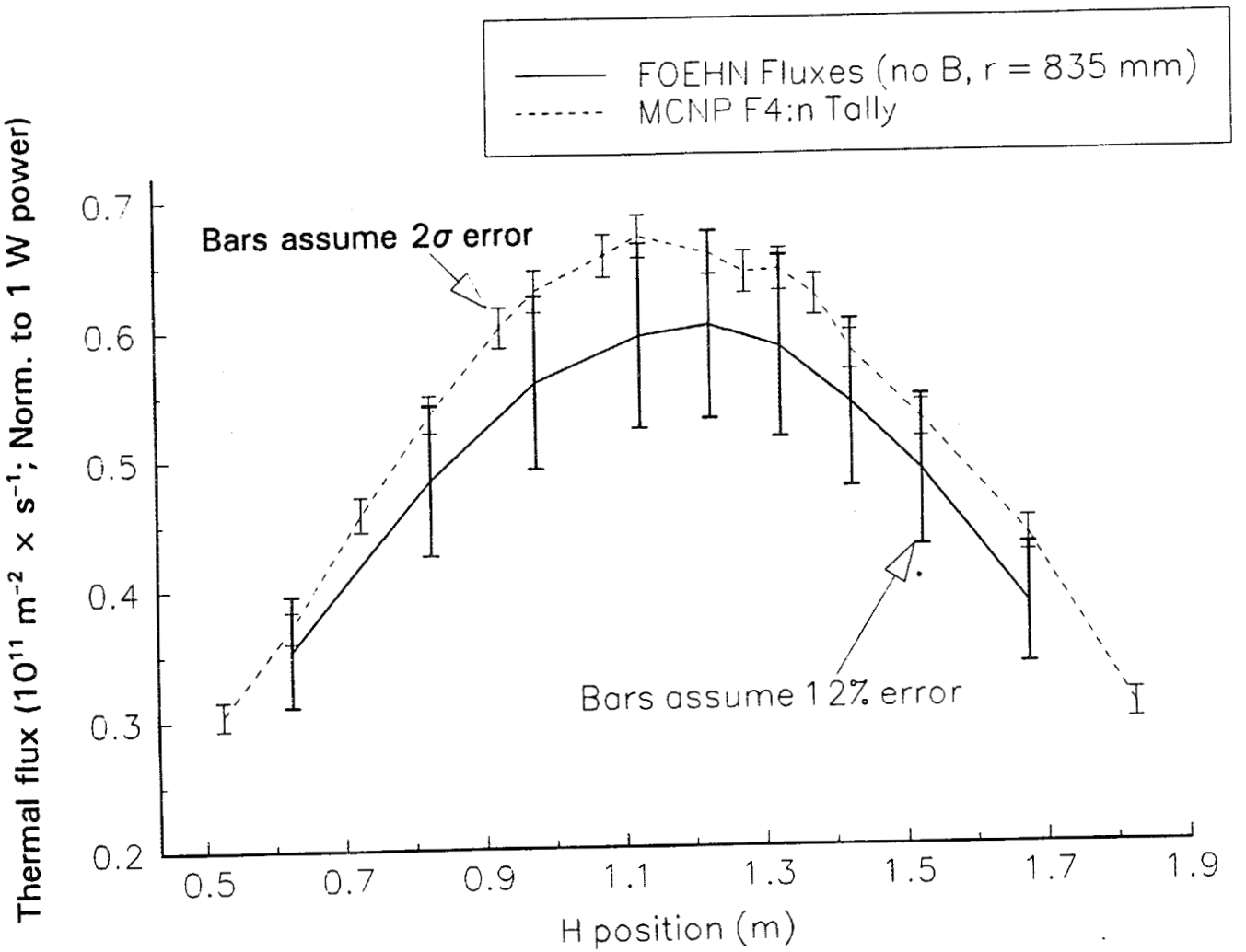

Fig. 4.5. Comparison of experimental and computed axial flux shapes at r = 835 mm in the simple FOEHN configuration.

normalized results are shown in Table 4.5. In Table 4.6, the corresponding MCNP error estimates (2σ, i.e., two times the standard deviation from the normalized entries of Table 4.5) are shown.

The tallies (from Table 4.5) and the experimental data from Table 5.1.5 of the FOEHN report are compared in Figs. 4.5–4.15. The error bars shown for the computed results correspond to the 2σ values tabulated in Table 4.6. The error bars for the experimental points correspond to the 4% estimate for the error discussed in Chap. 2.

In Figs. 4.6, 4.7, and 4.8, the power distribution is plotted as a function of the axial coordinate H for the radii of 143.5 mm, 167.5 mm, and 193.95 mm, respectively. In Figs. 4.9–4.15, the power density is plotted as a function of the radius, r, for the axial planes at 2.5, 50, 175, 400, 625, 750, and 797.5 mm, respectively. In this way, every data point featured in Table 5.1.5 of the FOEHN report is plotted at least once. It can be seen from the figures that, for most points, there is at least partial overlap of the error bars from the computational predictions and the experiment. In most cases, the overlap is significant, with the experimental point actually falling within the computational error bar (or vice versa). The only points that do not show any overlap are those given by the r,H coordinate pairs in mm (143.5, 325.0) and (143.5, 400.0).

These two points correspond to slightly <1.64% of the total number (122) of experimental points. This result is in remarkably high agreement with the statistical interpretation of the computational error bars. The bars are 2σ in width. It follows that there is a 95% probability that the physically correct value of the computed quantity lie within the band defined by such error bars. The 1.64% of the points lying outside the error band is compatible with the corresponding 5% probability that points lie outside the band. In an independent study, using the discrete ordinate transport code DOT, Rohrmoser[10] obtained similar results—the same two experimental points were not reproduced by his model. The difference between models and experiment are in the same direction. The agreement between the two independent modeling efforts suggests that the experimental points might be incorrect. The difference (~3%) is not significant. The use of a homogenized representation for the fuel is known to be capable of producing local power variations as high as 5% in MCNP computations.[11] This effect appears not to be significant in the present case.

4.3 INTERMEDIATE COMPLEXITY REACTOR MODEL

4.3.1 Core Multiplication Factor (k_{eff})

The results of KCODE calculations (40 cycles, 3000 histories/cycle) for the intermediate complexity reactor configuration are tabulated in Table 4.7 and shown in Fig. 4.16. The cases referred to in the figure are defined in Table 4.7. For this reactor configuration, the k_{eff} predictions coincide (within 2σ) with the expected experimental value of 1.0 in four cases out of six. The two misses are within the 3σ band. These results can be interpreted as 0–33% misses.

4.3.2 Thermal Flux

Calculated MCNP thermal fluxes were compared to the results given in Table 5.2.5 of ref. 2. As stated previously, thermal fluxes for this benchmarking analysis were computed as F4:n tallies for neutron energies below 0.625 eV in a KCODE calculation using 40 cycles of 10000 particles each. Modeling of the detectors was done in the same way as described in Sect. 4.2.2. The control rod height for this case was set at 1.163 m in MCNP (corresponding to the experimental control rod height of 0.447 m given in ref. 2). The boron (^{10}B) concentration was set to 0.258 g/L.

Table 4.5. Normalized MCNP power production (F7:n tallies) for the simple reactor configuration

H/r (mm)	143.5	146.5	149.5	152.5	159.0	167.5	176.0	182.5	185.5	188.5	193.95
02.5	0.9140	0.9214	0.8688	0.8321	0.8763	0.9120	1.0486	1.1412	1.1877	1.3026	1.6102
09.4	0.7367										1.3728
14.5	0.6567					0.5302					
19.4	0.6551					0.5064					1.2527
28.5	0.5374					0.4774					1.2152
50.0	0.5492	0.4938	0.4541	0.4255	0.3944	0.4528	0.5227	0.6585	0.7909	0.8983	1.2714
75.0	0.5344					0.4611					1.2705
100.0	0.5565					0.4441					1.3406
175.0	0.6676	0.6066	0.5734	0.5360	0.4921	0.5390	0.6686	0.7855	0.8908	1.0792	1.4619
250.0	0.7621					0.6617					1.7424
325.0	1.1703					0.7913					2.0383
400.0	1.3068	1.1060	0.9866	0.9477	0.8592	0.8242	0.9336	1.1980	1.3518	1.5135	2.1311
475.0	1.3052					0.8577					2.1121
550.0	1.3527					0.8606					2.1074
625.0	1.3112	1.2016	1.0356	0.9174	0.8360	0.8374	0.9156	1.0927	1.2429	1.4430	2.0251
700.0	1.2340					0.7771					1.9788
725.0	1.2306					0.7680					1.9595
750.0	1.3354	1.1567	1.0637	0.9207	0.8023	0.7971	0.9368	1.1539	1.2480	1.4645	2.0040
771.5	1.6154					0.9039					2.0945
780.6	1.7211					1.0737					2.2735
785.5	1.8351					1.1864					2.4136
790.6	2.0209										2.5324
797.5	2.5715	2.3638	2.2892	2.2125	2.0568	2.0743	2.1973	2.2845	2.4287	2.5611	2.9713

Table 4.6. MCNP error estimate (2σ, absolute) for the normalized MCNP power production for the simple reactor configuration

H/r (mm)	143.5	146.5	149.5	152.5	159.0	167.5	176.0	182.5	185.5	188.5	193.95
02.5	0.0590	0.0617	0.0553	0.0536	0.0535	0.0529	0.0581	0.0600	0.0615	0.0659	0.0776
09.4	0.0497										0.0659
14.5	0.0475					0.0346					
19.4	0.0455					0.0351					0.0609
28.5	0.0361					0.0334					0.0593
50.0	0.0379	0.0337	0.0330	0.0328	0.0280	0.0353	0.0343	0.0412	0.0478	0.0512	0.0651
75.0	0.0340					0.0319					0.0653
100.0	0.0365					0.0283					0.0660
175.0	0.0403	0.0385	0.0346	0.0331	0.0312	0.0320	0.0397	0.0426	0.0499	0.0546	0.0699
250.0	0.0407					0.0379					0.0725
325.0	0.0620					0.0416					0.0828
400.0	0.0674	0.0551	0.0493	0.0476	0.0450	0.0425	0.0463	0.0568	0.0611	0.0657	0.0831
475.0	0.0637					0.0444					0.0828
550.0	0.0666					0.0432					0.0830
625.0	0.0645	0.0627	0.0551	0.0490	0.0426	0.0467	0.0449	0.0538	0.0562	0.0638	0.0814
700.0	0.0647					0.0401					0.0815
725.0	0.0655					0.0424					0.0815
750.0	0.0686	0.0620	0.0589	0.0516	0.0440	0.0454	0.0482	0.0554	0.0569	0.0624	0.0814
771.5	0.0821					0.0483					0.0825
780.5	0.0840					0.0543					0.0873
785.5	0.0921					0.0603					0.0932
790.6	0.0922										0.0942
797.5	0.1080	0.1040	0.1016	0.0938	0.0872	0.0888	0.0875	0.0896	0.0923	0.0942	0.1046

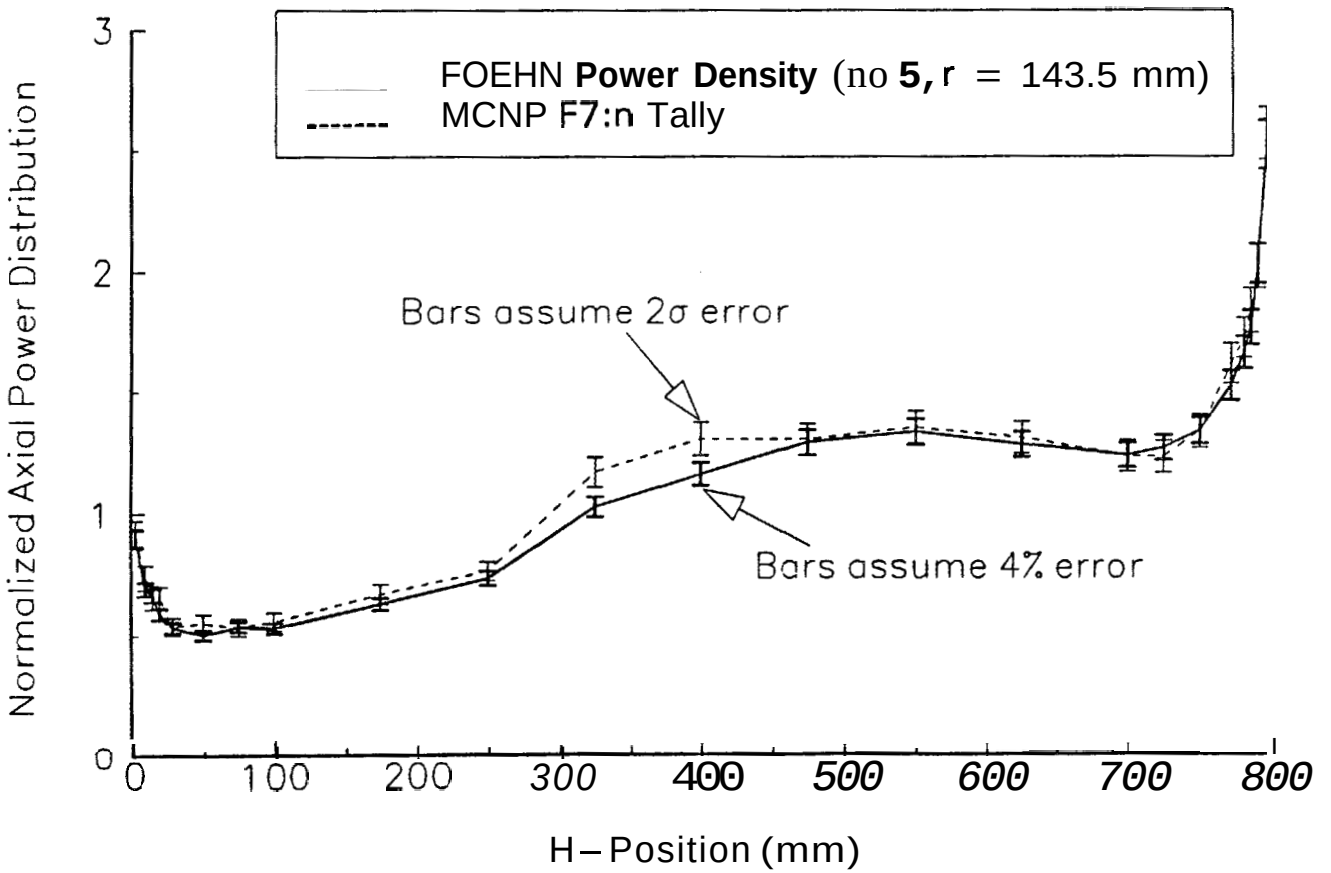

Fig. 4.6. Comparison of normalized experimental and computed axial power distribution in the simple FOEHN configuration at r = 1435 mm.

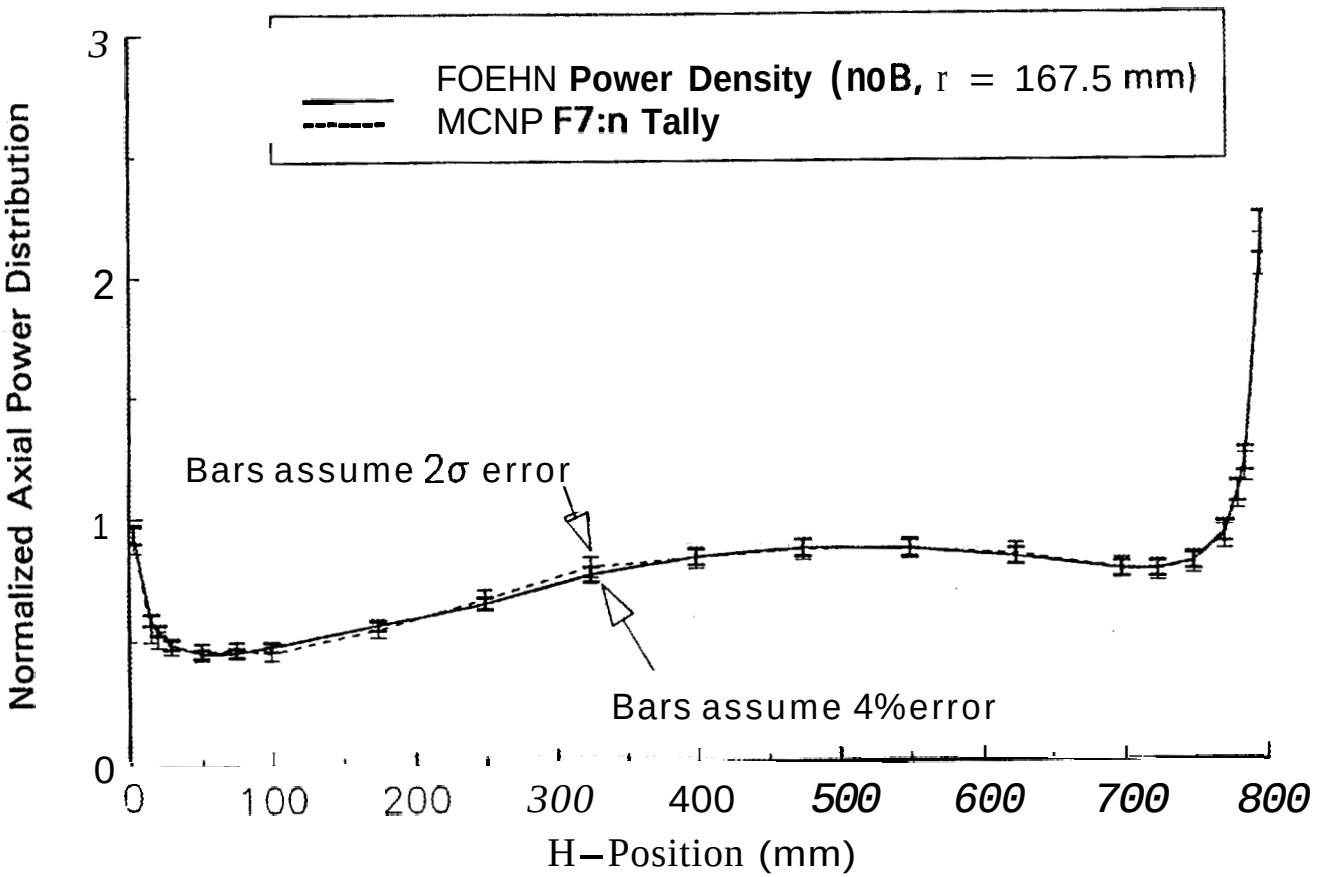

Fig. 4.7. Comparison of normalized experimental and computed axial power distribution in the simple FOEHN configuration at r = 167.5 mm.

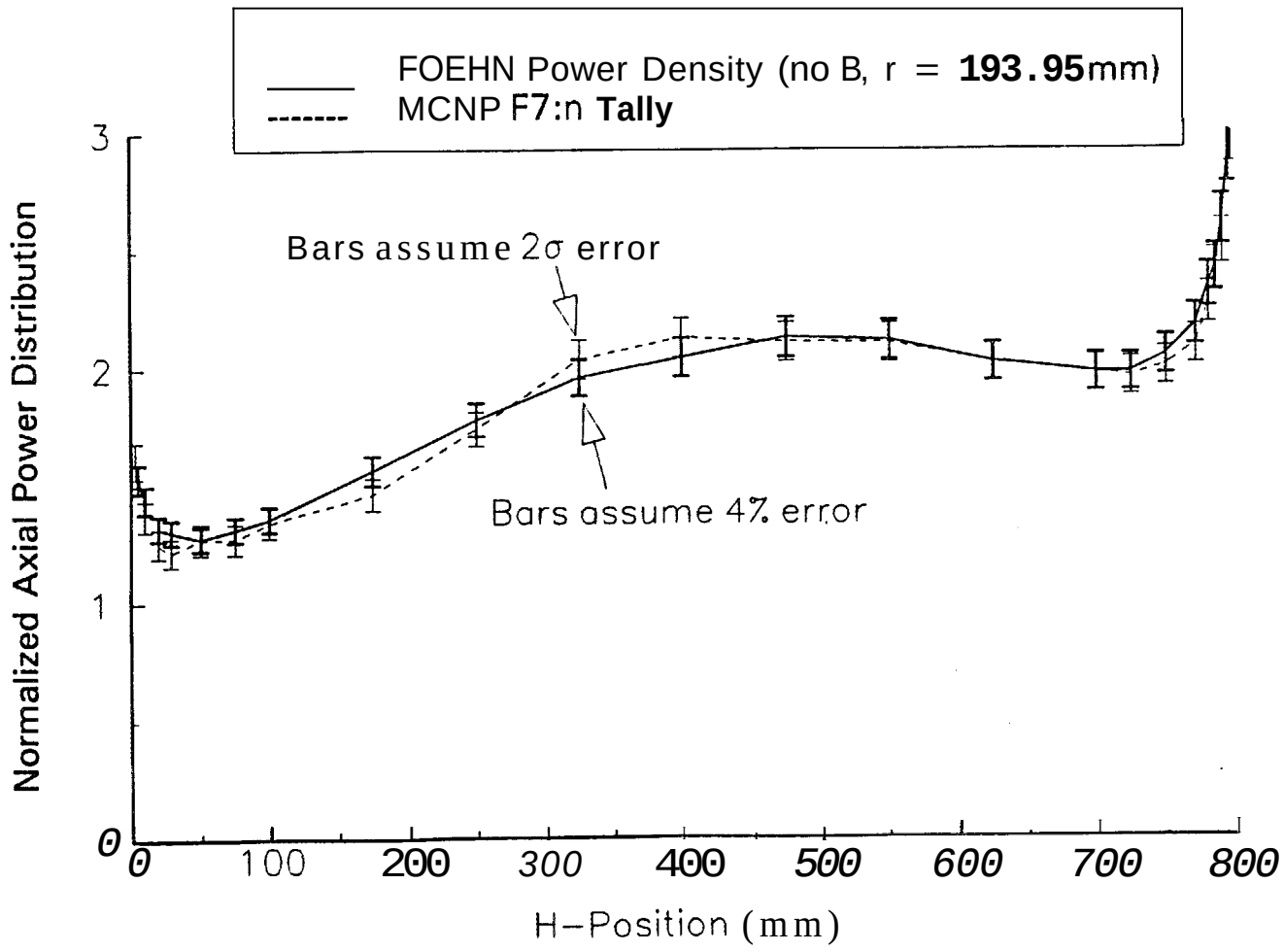

Fig. 4.8. Comparison of normalized experimental and computed axial power distribution in the simple FOEHN configuration at r = 193.95 mm.

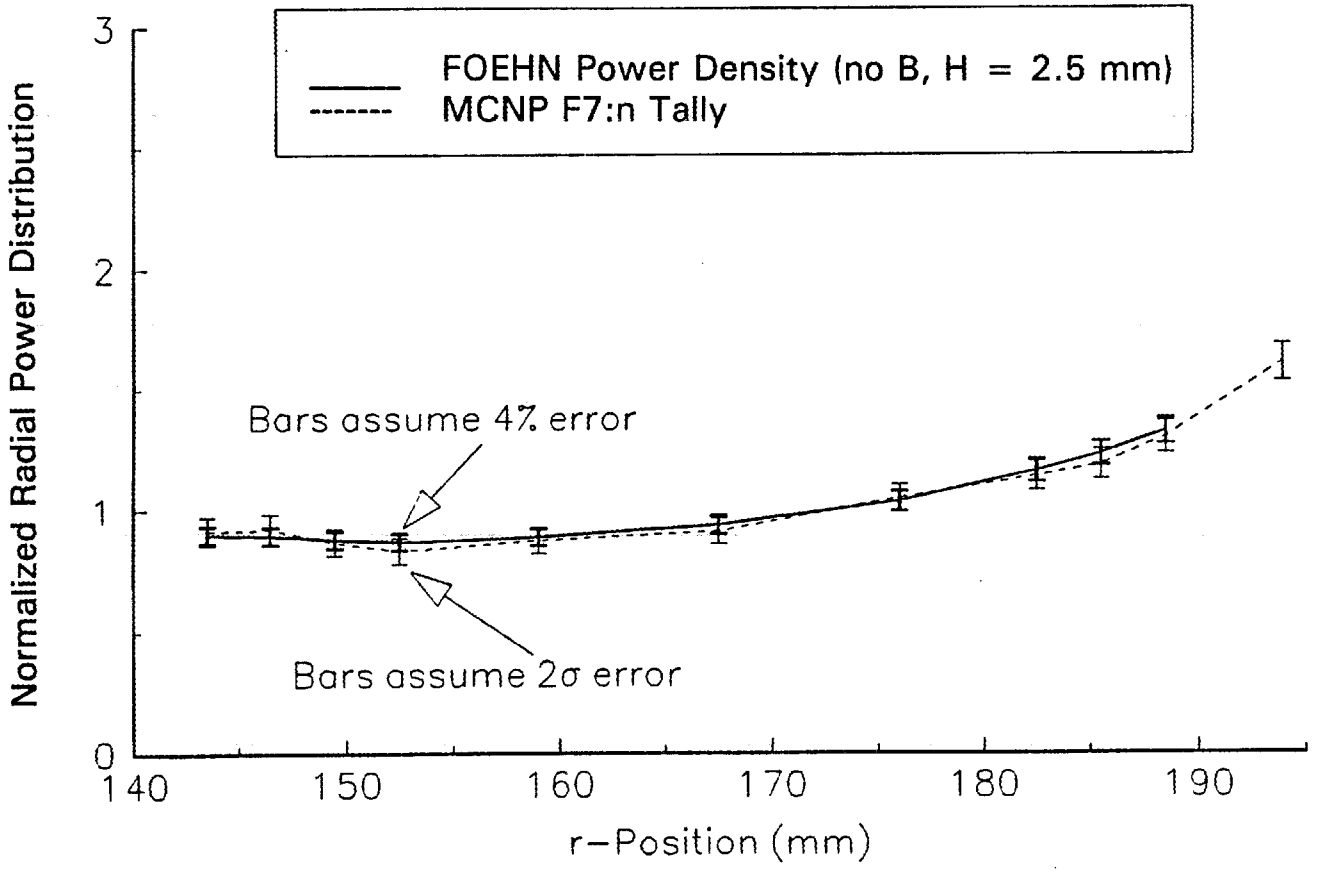

Fig. 4.9. Comparison of normalized experimental and computed axial power distribution in the simple FOEHN configuration at H = 2.5 mm.

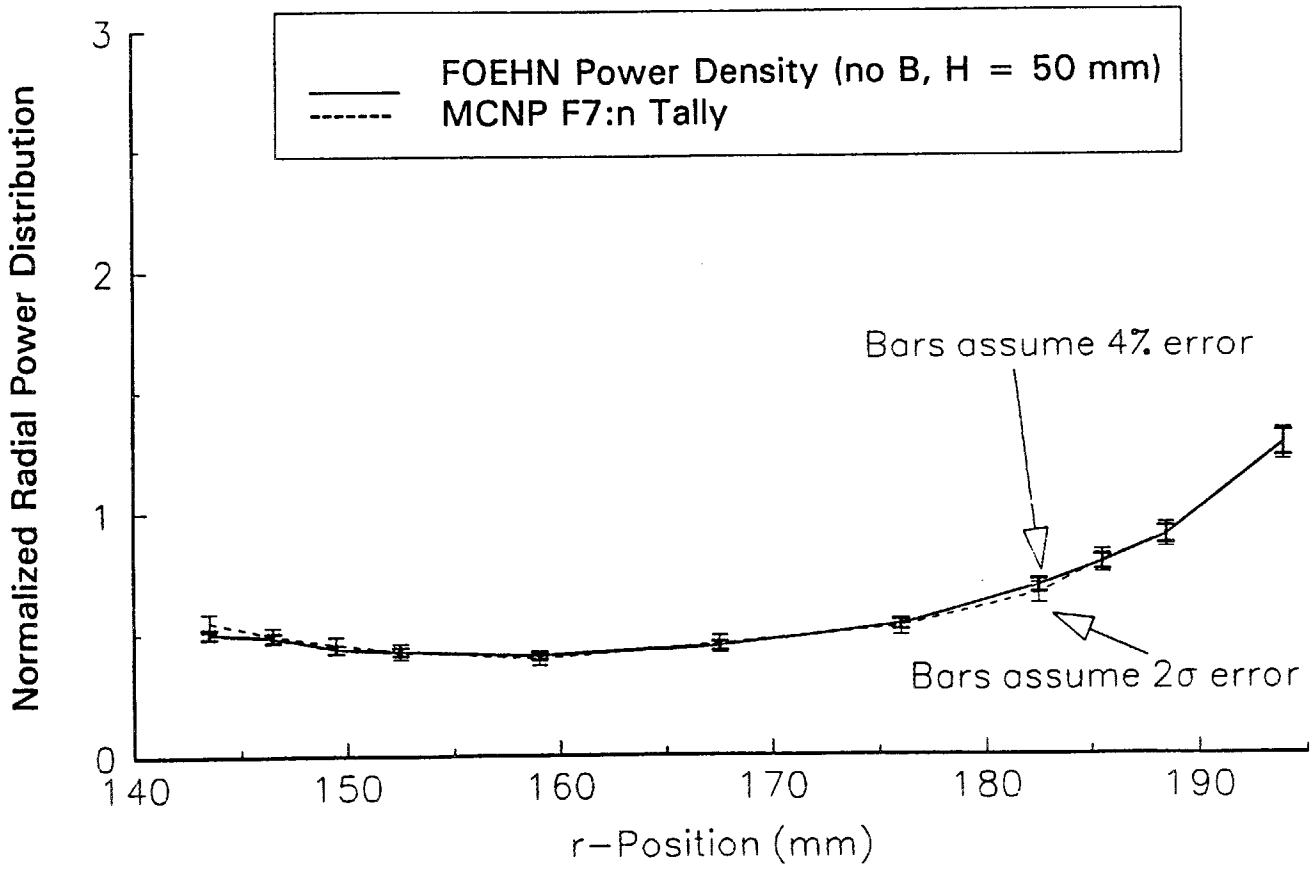

Fig. 4.10. Comparison of normalized experimental and computed radial power distribution in the simple FOEHN configuration at H = 50 mm.

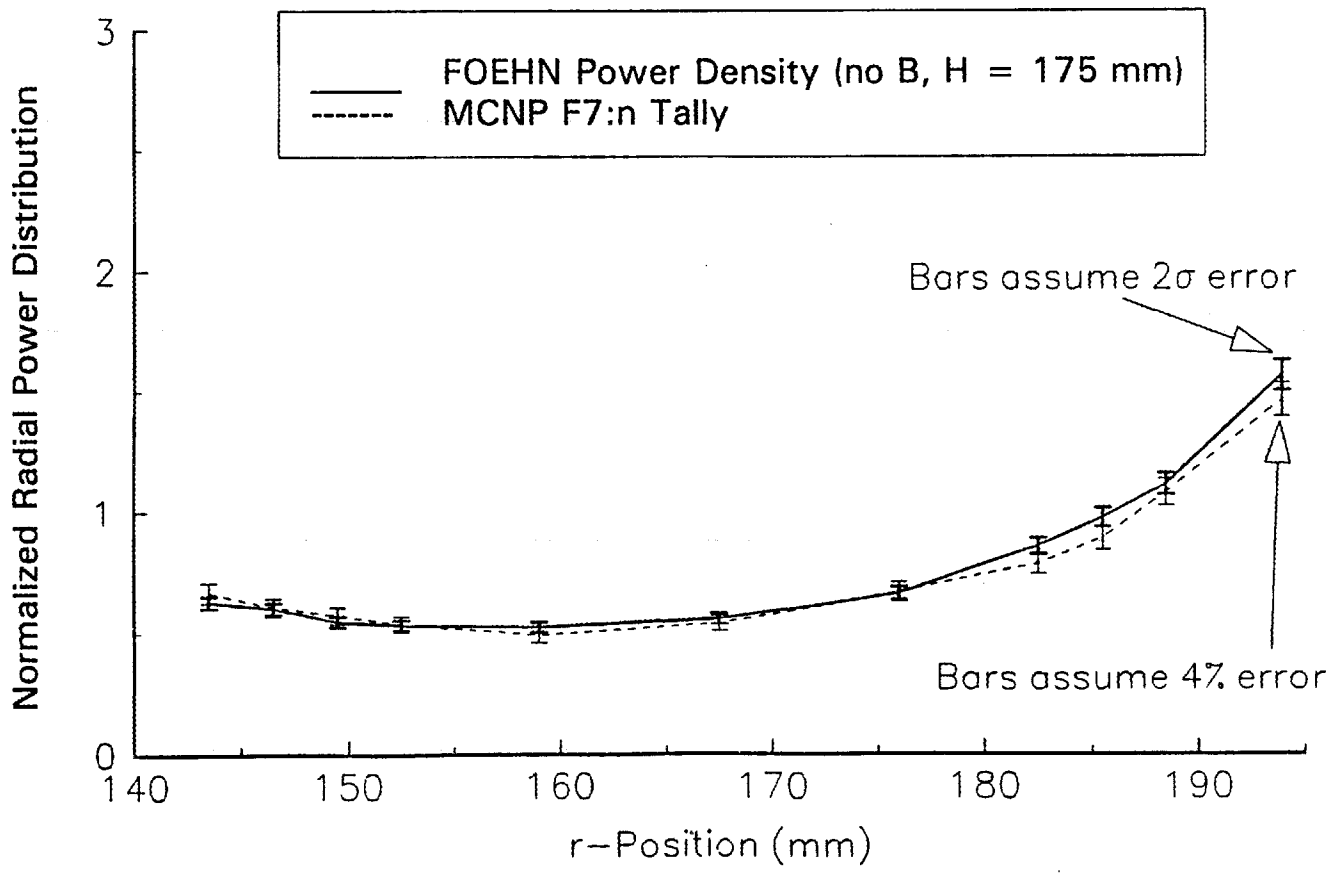

Fig. 4.11. Comparison of normalized experimental and computed radial power distribution in the simple FOEHN configuration at H = 175 mm.

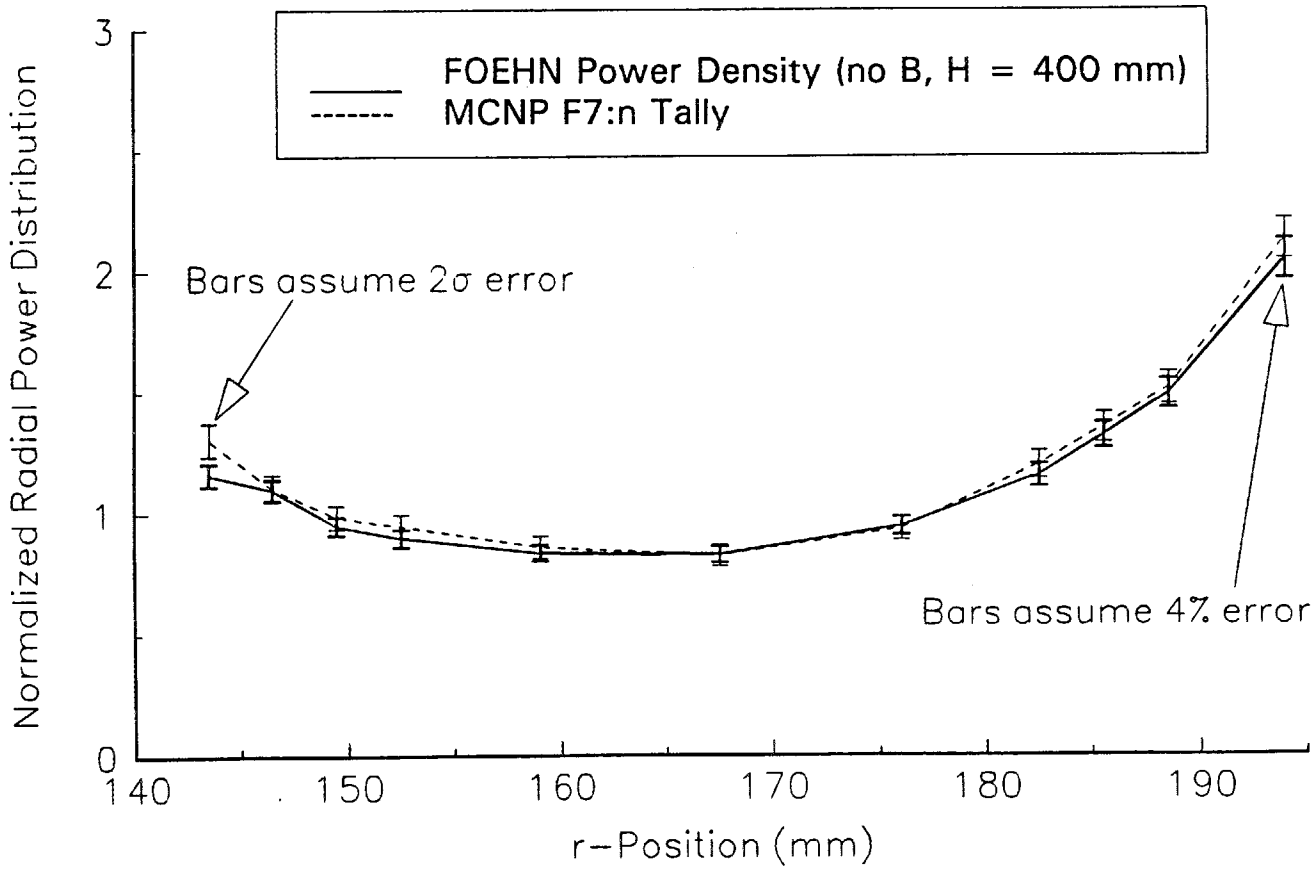

Fig. 4.12. Comparison of normalized experimental and computed radial power distribution in the simple FOEHN configuration at H = 400 mm.

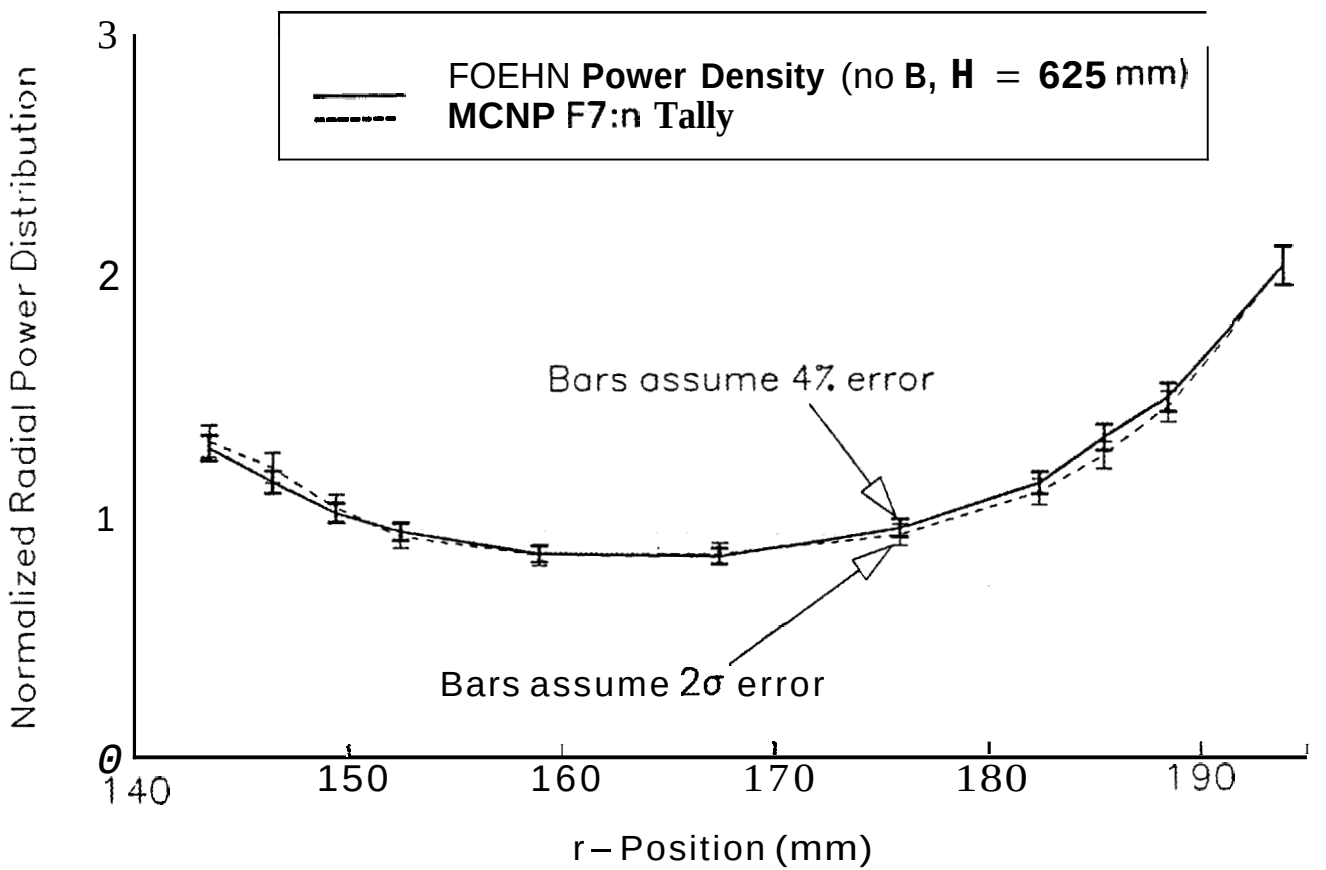

Fig. 4.13. Comparison of normalized experimental and computed radial power distribution in the simple FOEHN configuration at H = 625 mm.

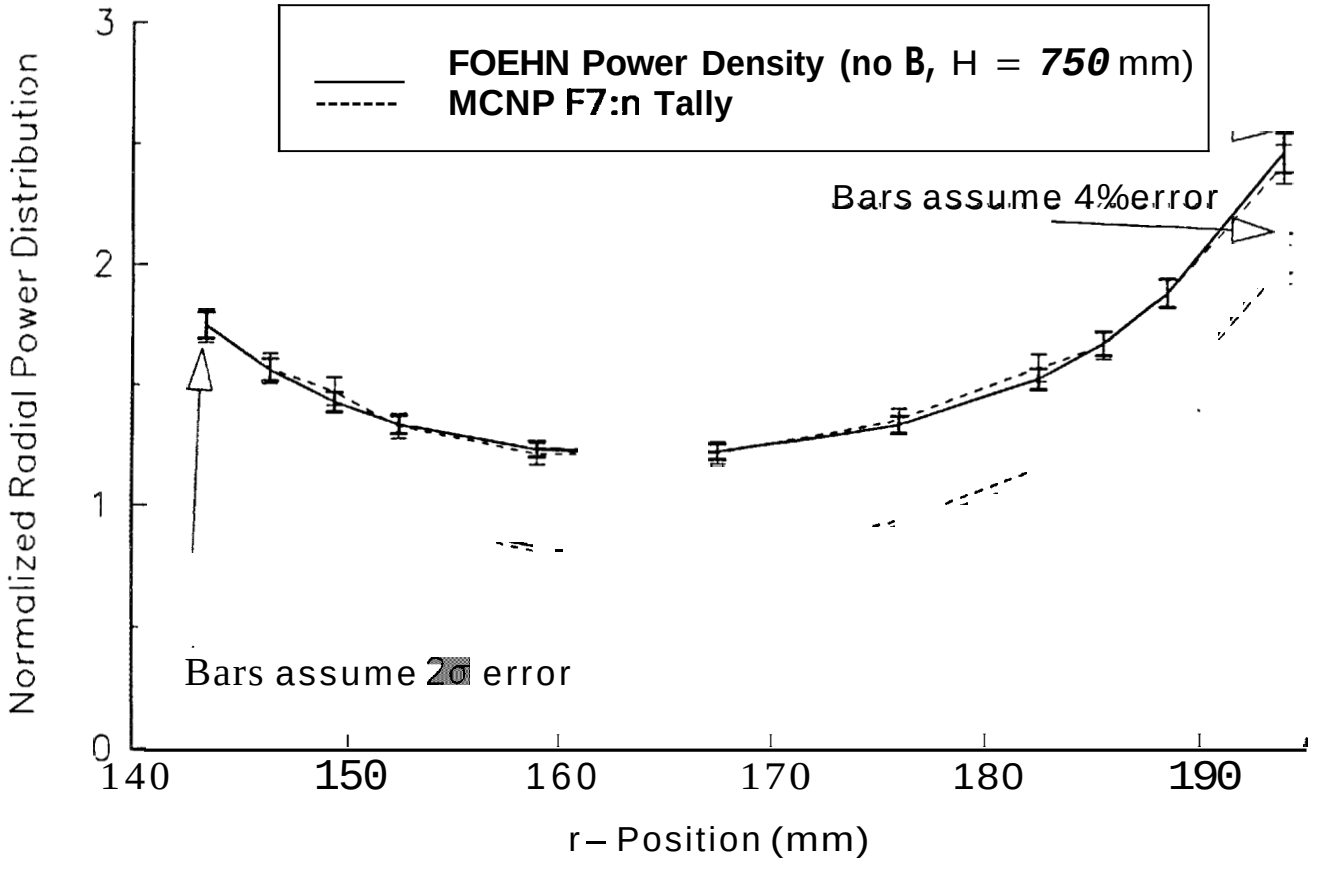

Fig. 4.14. Comparison of normalized experimental and computed radial power distribution in the simple FOEHN configuration at *H* = 750 mm.

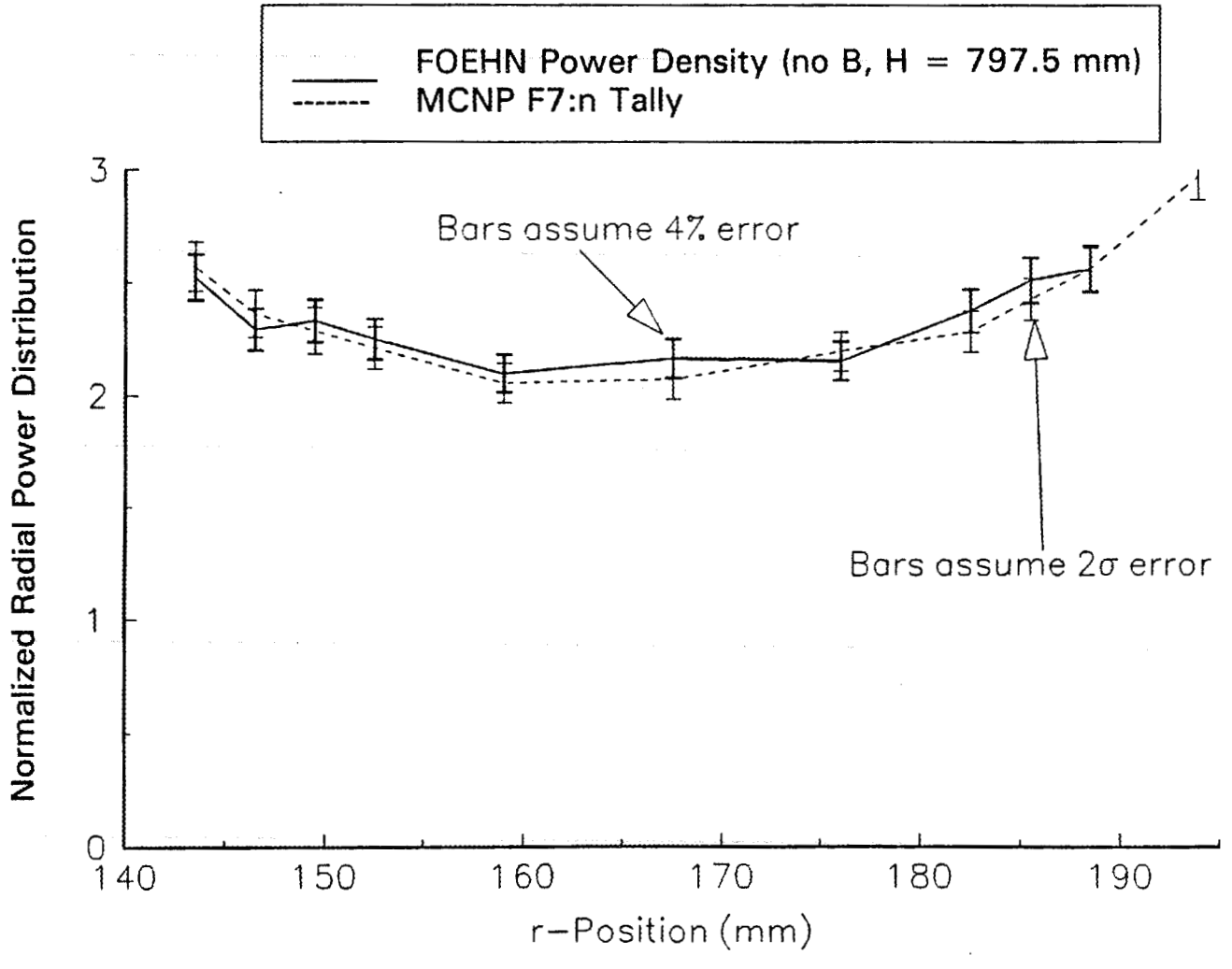

Fig. 4.15. Comparison of normalized experimental and computed radial power distribution in the simple FOEHN configuration at H = 797.5 mm.

Table 4.7. MCNP computed core effective multiplication factors (k_{eff}) for various critical states of the intermediate complexity reactor configuration

Case	Control rod position (m)		Boron conc. (g/L)	MCNP k_{eff}	MCNP error estimate (σ)
	MCNP	FOEHN			
1	1.2578	0.3522	0.210	1.0017	0.0028
2	1.163	0.447	0.258	1.0090	0.0030
3	1.153	0.457	0.270	1.0004	0.0026
4	1.001	0.609	0.350	1.0025	0.0036
5	0.946	0.664	0.371	1.0081	0.0025
6	0.795	0.815	0.419	1.0054	0.0026

The MCNP F4:n tallies were normalized to 1 W total reactor power to allow a direct comparison to the experimental thermal fluxes of Table 5.2.5 in ref. 2. Table 4.8 shows the MCNP-calculated thermal fluxes, and Table 4.9 shows their respective relative errors (2σ). The entries in these two tables are in units of 10^{11} $m^{-2} \cdot s^{-1}$. In this case, the computed value of 2.43871 was used for ν. The value of Q was 202.47 MeV, except for the estimate of the rendement for which the value 199.73 MeV was used. Figures 4.17, 4.18, and 4.19 show a comparison of the MCNP-calculated and the experimental results at the radii of 0.235 m, 0.355 m, and 0.835 m. The error bars assume $\pm 2\sigma$ for the computational points and ±4, ±8, ±8% for the experimental points in the three figures, respectively (vs the ±2% claimed in the FOEHN report). These figures show that MCNP-calculated thermal fluxes and the experimental fluxes are in agreement within the bands defined by the experimental error and the statistical limits.

4.3.3 Rendement

The rendement calculated by MCNP, r_{calc}, is 2.8529×10^{11} neutrons/$m^2 \cdot s \cdot W$ with a standard deviation, σ, of 0.94%. The measured rendement, reported in ref. 2, r_{meas}, is 2.56×10^{11} neutrons/$m^2 \cdot s \cdot W$. As discussed in Sect. 2.4.3.4, an error of between 2.2 and 16.2% should be associated with the measured value (vs the ±2% claimed in ref. 2). In the following, it is assumed that the experimental error is of the order of 12% (same as for the fluxes). The difference between the computational and the experimental results is approximately +11.5%. Rohrmoser independently computed a value 13% larger than the experimental one. As in the previous case (simplest reactor configuration), the two estimates of the rendement can be considered to be coinciding since the error bands associated with them (±12% and $\pm 2\sigma$) overlap significantly. It is noteworthy that the two estimates overlap even if the experimental error band is decreased to ~10%.

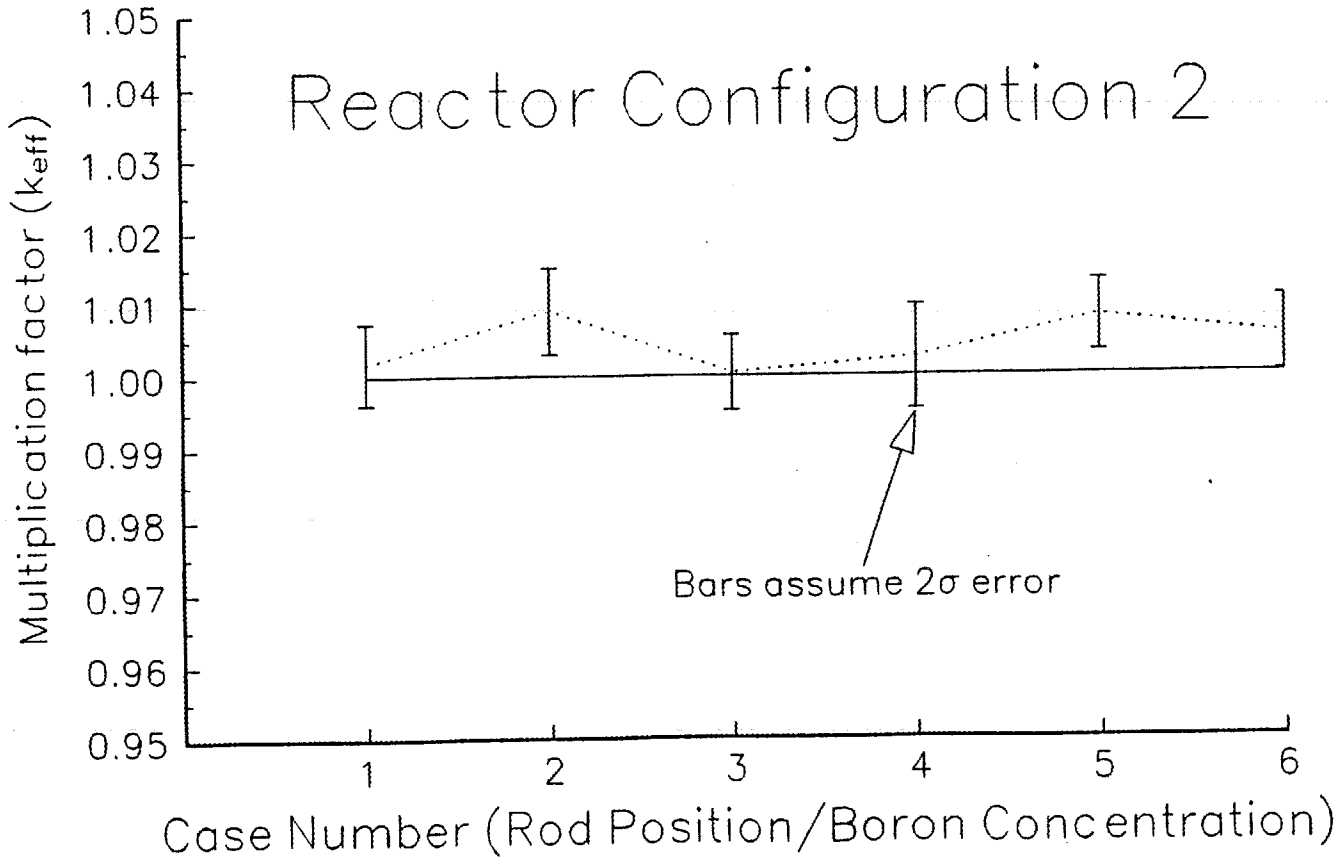

Fig. 4.16. MCNP prediction of k_{eff} for a set of critical states of the intermediate FOEHN reactor configuration.

Table 4.8. Computed thermal fluxes for the intermediate reactor configuration[a]

H/r (mm)	235	275	315	335	355	375	395	435	515	675	755	835	915	955
510	0.5603	0.6461	0.7398	0.7621	0.7548	0.7485	0.7479	0.7136	0.6620	0.4824	0.3943	0.3082	0.2156	0.1813
610	0.8278	0.9498	1.0481	1.0725	1.0791	1.0900	1.0517	1.0041	0.9047	0.6014	0.4917	0.3746	0.2696	0.2242
710	0.8786	1.1951	1.3845	1.4176	1.4361	1.4378	1.3973	1.3660	1.1741	0.7774	0.5935	0.4518	0.3303	0.2672
810	1.1505	1.5598	1.7764	1.8310	1.8264	1.8080	1.7878	1.6916	1.4122	0.9175	0.7098	0.5300	0.3712	0.3052
910	1.4072	1.9431	2.2152	2.2280	2.2166	2.1946	2.1763	2.0602	1.6964	1.0593	0.8042	0.5922	0.4212	0.3498
1010	1.6225	2.2402	2.4869	2.5653	2.5538	2.4961	2.4833	2.2784	1.8769	1.1445	0.8766	0.6404	0.4602	0.3673
1060	1.7193	2.3355	2.6097	2.6120	2.6530	2.6175	2.5585	2.3745	1.9351	1.1672	0.8880	0.6599	0.4614	0.3788
1110	1.7867	2.4579	2.6938	2.7880	2.7620	2.7043	2.6319	2.4422	2.0041	1.1935	0.8841	0.6701	0.4598	0.3818
1160	1.7484	2.4750	2.7342	2.7930	2.7921	2.7693	2.6698	2.4847	1.9970	1.1929	0.9148	0.6738	0.4719	0.3804
1210	1.8122	2.4653	2.7421	2.8143	2.8009	2.7308	2.7065	2.4567	2.0027	1.2021	0.9094	0.6711	0.4709	0.3825
1260	1.7670	2.4378	2.6935	2.7644	2.7510	2.6683	2.6162	2.4439	1.9291	1.1699	0.8877	0.6622	0.4621	0.3773
1310	1.7220	2.3228	2.6046	2.6796	2.6408	2.5680	2.5494	2.3327	1.8961	1.1377	0.8500	0.6453	0.4491	0.3651
1410	1.5132	2.0385	2.2988	2.3106	2.3220	2.2738	2.2254	2.0807	1.7147	1.0423	0.8020	0.5976	0.4177	0.3389
1510	1.3235	1.7094	1.8858	1.9349	1.9423	1.8933	1.8538	1.7593	1.4920	0.9171	0.7079	0.5392	0.3868	0.3139
1610	1.4131	1.5393	1.5722	1.5757	1.5798	1.5135	1.4815	1.4285	1.2118	0.7973	0.6172	0.4595	0.3239	0.2781
1710	1.2452	1.2212	1.2136	1.2185	1.2026	1.1993	1.1537	1.0896	0.9507	0.6216	0.4965	0.3804	0.2812	0.2232
1810	0.9437	0.9385	0.9127	0.8981	0.8985	0.8724	0.8627	0.8218	0.7003	0.4915	0.4290	0.2994	0.2212	0.1867

[a]MCNP F4:n tallies; 0.625 eV cutoff; 1 W reactor power; units: 10^{11} $m^{-2} \cdot s^{-1}$.

Table 4.9. MCNP error estimate (2σ, absolute) for the thermal fluxes for the intermediate reactor configuration (units: 10^{11} $m^{-2} \cdot s^{-1}$)

H/r (mm)	235	275	315	335	355	375	395	435	515	675	755	835	915	955
510	0.0252	0.0264	0.0275	0.0271	0.0261	0.0254	0.0250	0.0233	0.0211	0.0157	0.0133	0.0111	0.0087	0.0077
610	0.0320	0.0325	0.0329	0.0326	0.0319	0.0314	0.0297	0.0277	0.0246	0.0173	0.0148	0.0121	0.0097	0.0087
710	0.0320	0.0366	0.0377	0.0371	0.0365	0.0362	0.0347	0.0333	0.0282	0.0199	0.0164	0.0134	0.0109	0.0092
810	0.0364	0.0415	0.0426	0.0425	0.0413	0.0401	0.0390	0.0365	0.0308	0.0217	0.0179	0.0146	0.0115	0.0101
910	0.0405	0.0466	0.0478	0.0468	0.0457	0.0448	0.0435	0.0408	0.0343	0.0235	0.0193	0.0154	0.0123	0.0109
1010	0.0438	0.0497	0.0502	0.0503	0.0490	0.0474	0.0467	0.0428	0.0360	0.0245	0.0200	0.0163	0.0130	0.0111
1060	0.0454	0.0514	0.0517	0.0502	0.0499	0.0487	0.0471	0.0473	0.0364	0.0245	0.0202	0.0165	0.0128	0.0114
1110	0.0457	0.0526	0.0523	0.0524	0.0508	0.0498	0.0474	0.0440	0.0373	0.0251	0.0200	0.0166	0.0129	0.0113
1160	0.0451	0.0525	0.0530	0.0520	0.0508	0.0498	0.0481	0.0447	0.0367	0.0246	0.0203	0.0166	0.0130	0.0113
1210	0.0464	0.0523	0.0532	0.0529	0.0510	0.0497	0.0482	0.0442	0.0368	0.0252	0.0206	0.0166	0.0131	0.0115
1260	0.0456	0.0531	0.0528	0.0525	0.0506	0.0486	0.0471	0.0445	0.0363	0.0246	0.0202	0.0164	0.0130	0.0113
1310	0.0451	0.0506	0.0516	0.0514	0.0496	0.0478	0.0474	0.0429	0.0360	0.0241	0.0196	0.0163	0.0127	0.0110
1410	0.0430	0.0473	0.0487	0.0481	0.0474	0.0450	0.0436	0.0408	0.0343	0.0231	0.0191	0.0155	0.0123	0.0107
1510	0.0400	0.0438	0.0445	0.0441	0.0435	0.0417	0.0404	0.0376	0.0319	0.0216	0.0177	0.0149	0.0118	0.0102
1610	0.0421	0.0428	0.409	0.0400	0.0392	0.0369	0.0359	0.0343	0.0288	0.0204	0.0169	0.0136	0.0106	0.0098
1710	0.0408	0.0379	0.0357	0.0351	0.0339	0.0336	0.0316	0.0292	0.0255	0.0177	0.0150	0.0122	0.0101	0.0086
1810	0.0347	0.0332	0.0307	0.0300	0.0291	0.0279	0.0274	0.0253	0.0214	0.0157	0.0034	0.0108	0.0089	0.0079

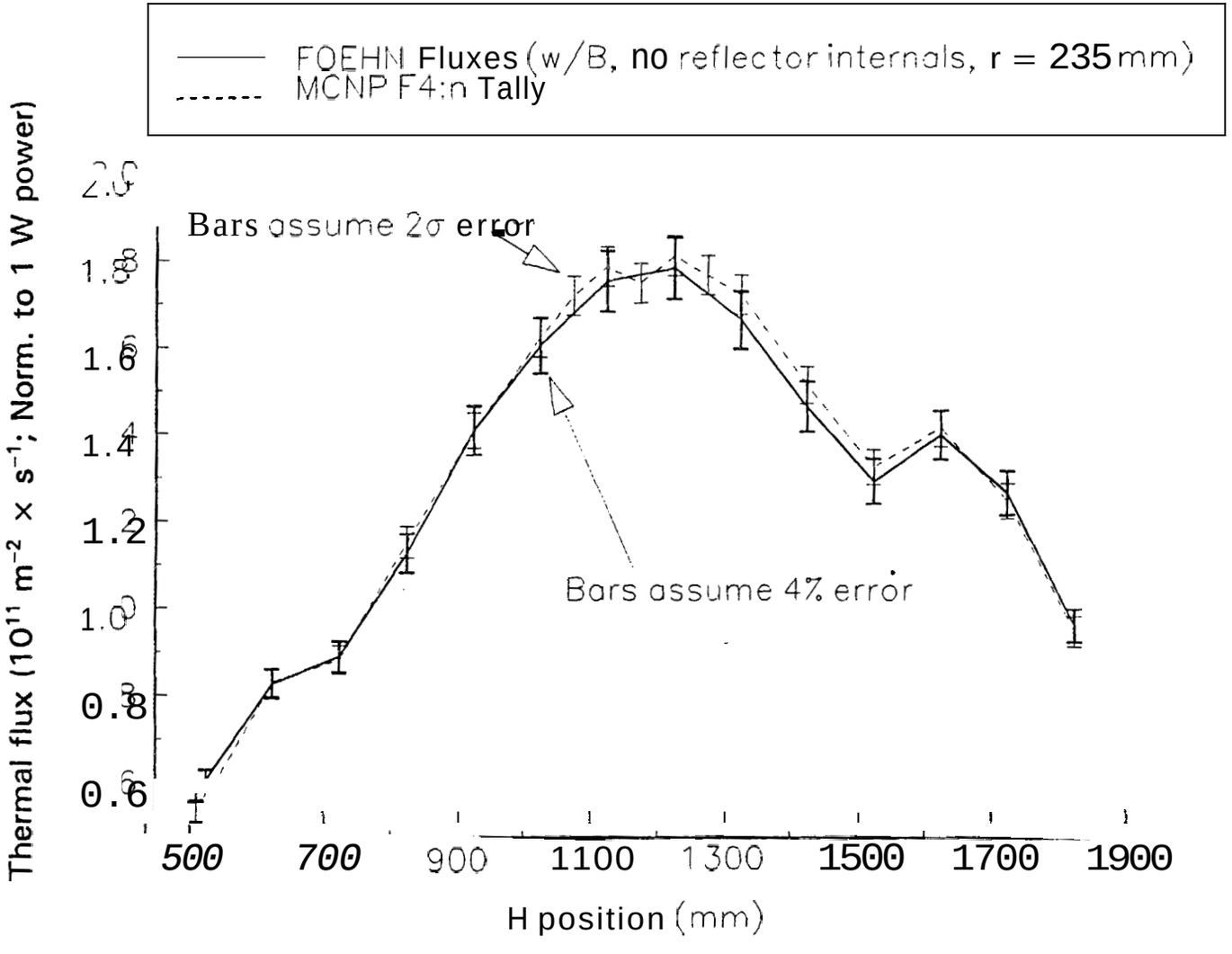

Fig. 4.17. Comparison of experimental and computed axial flux shapes at r = 235 mm in the intermediate FOEHN configuration.

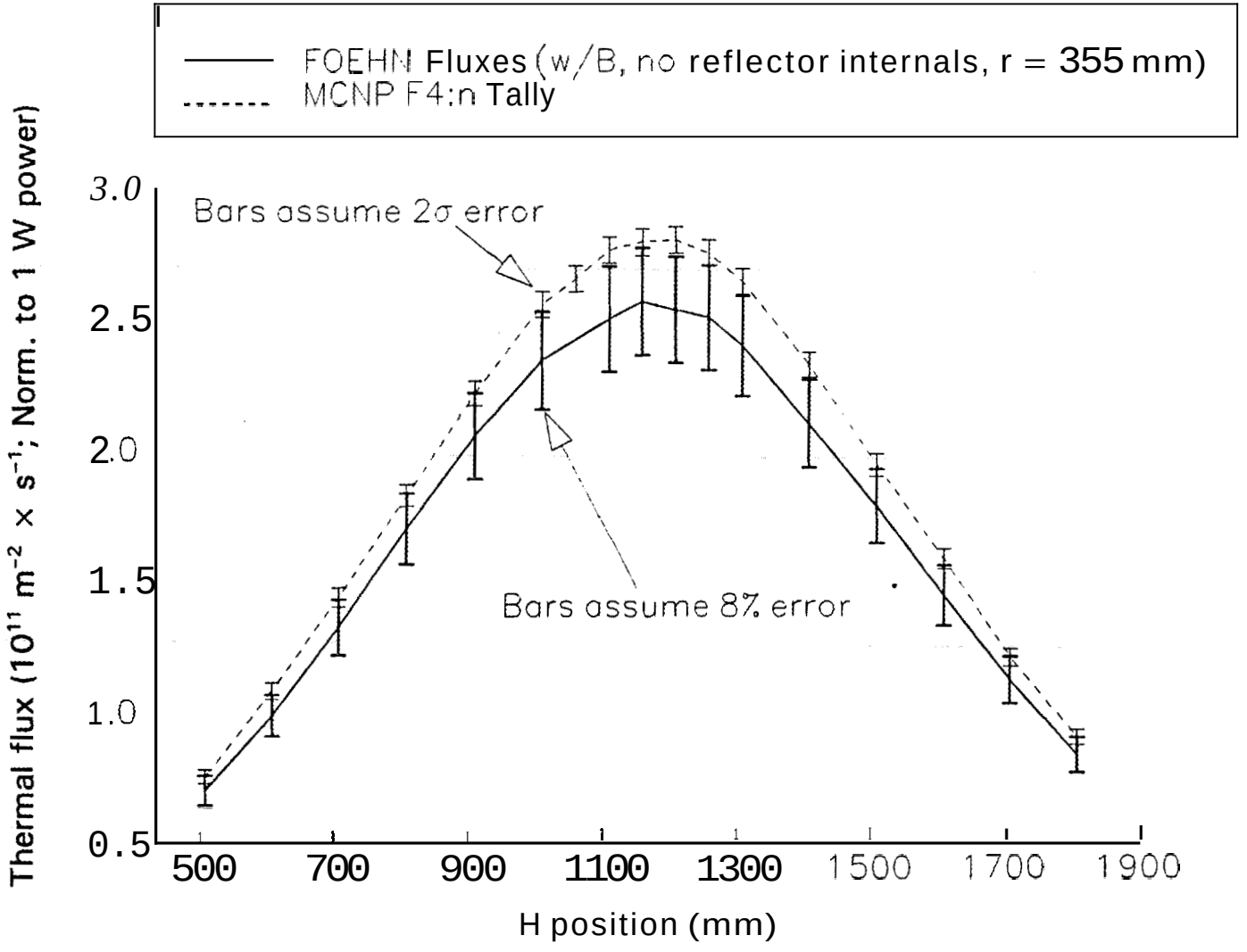

Fig. 4.18. Comparison of experimental and computed axial flux shapes at *r* = 355 mm in the intermediate FOEHN configuration.

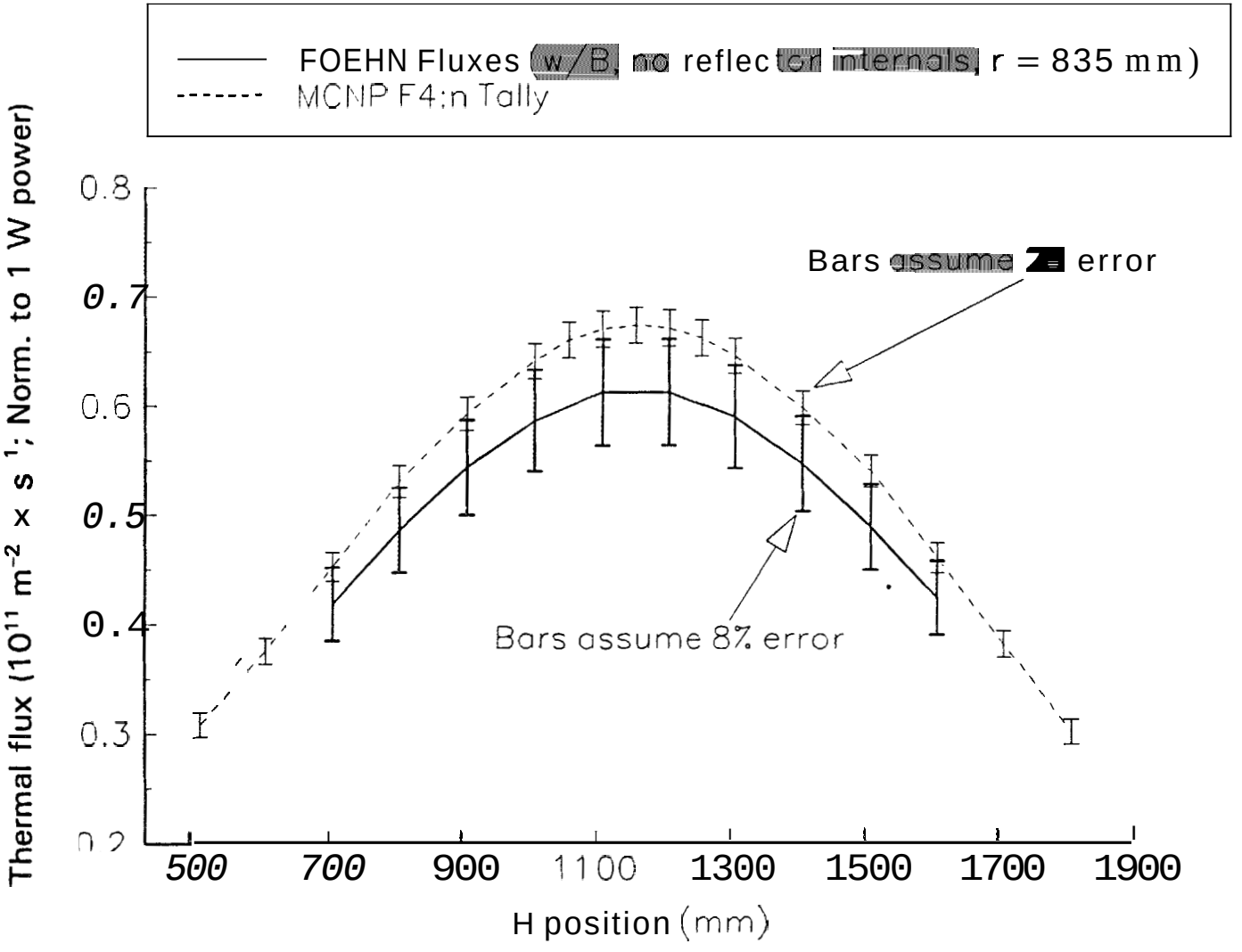

Fig. 4.19. Comparison of experimental and computed axial flux shapes at r = 835 mm in the intermediate FOEHN configuration.

4.3.4 Power

The intermediate complexity MCNP model of the FOEHN critical experiment has been used to obtain F7:n tallies (KCODE option, 80 cycles, 10000 particles/cycle). The tallies have been normalized to the same constant (0.99781) as the data of the corresponding table of the FOEHN report (Table 5.2.6), according to the procedure summarized in Sect. 2.3.2.2. The normalized MCNP results are shown in Table 4.10. In Table 4.11, the corresponding MCNP error estimates (2σ) are shown. For the sake of completeness, the experimental data (Table 5.2.6 of ref. 2) are shown in Table 4.12.

The tallies from Table 4.10 and the experimental data from Table 5.2.6 of the FOEHN report are compared in Figs. 4.20–4.22. The error bars shown for the computed results correspond to the 2σ values tabulated in Table 4.11. The error bars for the experimental points correspond to the 4% estimate for the error discussed in Chap. 2.

In Figs. 4.20–4.22, the power distribution is plotted as a function of the axial coordinate H for the radii of 143.5, 167.5, and 193.95 mm, respectively. It can be seen from the figures that for most points in the reactor interior, there is at least partial (and most of the time significant) overlap of the error bars from the computational predictions and the experiment. In Table 4.13, all the experimental and computational results are compared in the sense of overlap of their respective error bands. In the table, an entry of 0 indicates overlap, whereas an entry of 1 indicates no overlap. There are 12 nonoverlapping points out of a total of 123 data points. This implies a nonmatching rate of 9.76%. The table shows that overlap occurs for most points internal to the reactor and that nearly all points at the top and bottom of the core show no overlap. This can be attributed to a lack of precise information about the location of the boron end caps and their modeling as homogenous rather than heterogenous regions. In addition, a possible, though probably negligible, effect might be the impact of the absence of an external AG3-NE end cover. These external covers (axial portion of the reactor tank, beyond the inner AG3-NE seals and the boron end caps) were not modeled because their size is not known, and they are expected to have little neutronic relevance, if any. If the nonmatching end points (9 points—2 at top and 7 at bottom of core) are excluded from the nonmatching count, the nonmatching rate drops to 2.44%, well within the expected nonoverlap rate of 5% predictable from the use of the $\pm 2\sigma$ error bands.

4.4 FULL COMPLEXITY REACTOR MODEL

4.4.1 Core Multiplication Factor (k_{eff})

The multiplication factor for the FOEHN experiment in the full complexity reactor configuration has been computed for several control rod positions and corresponding critical soluble boron concentrations (defined in Table 5.3.2 of ref. 2). The KCODE estimates (40 cycles, 3000 histories/cycle) of k_{eff} for the full-featured reactor configuration are tabulated in Table 4.14 and are shown in Fig. 4.23. They display three close misses and one miss by about 1σ. In three cases, the estimate of k_{eff} overlaps with the expected value of 1.0 (within 2σ). In these three cases, however, the overlap is by a very small margin. As in the previous two configurations, the small number of cases limits the statistical significance of the results.

4.4.2 Thermal Flux

For the full-complexity FOEHN configuration, the thermal flux was measured at the noses of several beam tubes, radially and axially through the hot source, axially through the cold source, and

Table 4.10. Normalized MCNP power production (F7:n tallies) for the intermediate reactor configuration

H/r (mm)	143.5	146.5	149.5	152.5	159.0	167.5	176.0	182.5	185.5	188.5	193.95
2.5	0.4918	0.4541	0.4300	0.4241	0.3590	0.4224	0.5387	0.6491	0.7339	0.8520	1.1667
9.4	0.4905										1.1733
14.5	0.4708					0.4285					1.1304
19.4	0.4607					0.4342					1.2063
28.5	0.4858					0.4325					1.1563
50.0	0.5447	0.4788	0.4491	0.4717	0.4044	0.4271	0.5349	0.6463	0.7655	0.8724	1.2390
75.0	0.5334					0.4732					1.3318
100.0	0.6005					0.5259					1.4222
175.0	0.7687	0.7013	0.6651	0.6403	0.5809	0.6249	0.7231	0.9331	1.0298	1.1228	1.5690
250.0	0.8994					0.7783					1.9762
325.0	0.9600					0.8230					2.0875
400.0	1.0411	0.9761	0.9307	0.8933	0.8266	0.8588	1.0681	1.2665	1.4233	1.6231	2.2295
475.0	1.4025					0.9759					2.2987
550.0	1.4749					0.9592					2.2911
625.0	1.3238	1.2077	1.0794	1.0092	0.8876	0.8658	0.9922	1.1805	1.3557	1.6413	2.1978
700.0	1.1736					0.7781					1.8758
725.0	1.1740					0.7317					1.7848
750.0	1.1131	0.9953	0.8451	0.7881	0.7397	0.6913	0.7818	1.0226	1.1521	1.2781	1.7095
771.5	1.0583					0.6549					1.7299
780.6	1.1249					0.6785					1.7121
785.5	1.0787					0.6380					1.7523
790.6	1.1233										1.7326
797.5	1.1574	1.0260	0.9053	0.8431	0.7667	0.7043	0.8371	1.0455	1.1916	1.2919	1.7957

Table 4.11. MCNP error estimate (2σ, absolute) for the normalized MCNP power production for the intermediate reactor configuration

H/r (mm)	143.5	146.5	149.5	152.5	159.0	167.5	176.0	182.5	185.5	188.5	193.95
2.5	0.0409	0.0343	0.0315	0.0327	0.0279	0.0307	0.0373	0.0439	0.0483	0.0491	0.0653
9.4	0.0344										0.0615
14.5	0.0347					0.0308					0.0619
19.4	0.0334					0.0309					0.0644
28.5	0.0345					0.0309					0.0624
50.0	0.0395	0.0338	0.0322	0.0362	0.0289	0.0296	0.0342	0.0401	0.0452	0.0508	0.0619
75.0	0.0366					0.0311					0.0666
100.0	0.0364					0.0351					0.0697
175.0	0.0423	0.0390	0.0372	0.0365	0.0345	0.0376	0.0419	0.0504	0.0505	0.0546	0.0715
250.0	0.0455					0.0405					0.0806
325.0	0.0511					0.0430					0.0843
400.0	0.0498	0.0472	0.0477	0.0481	0.0428	0.0419	0.0536	0.0580	0.0615	0.0665	0.0843
475.0	0.0679					0.0472					0.0910
550.0	0.0711					0.0468					0.0894
625.0	0.0675	0.0623	0.0555	0.0557	0.0447	0.0448	0.0488	0.0548	0.0594	0.0702	0.0870
700.0	0.0638					0.0426					0.0773
725.0	0.0664					0.0414					0.0778
750.0	0.0634	0.0569	0.0507	0.0476	0.0493	0.0411	0.0439	0.0515	0.0583	0.0649	0.0773
771.5	0.0622					0.0411					0.0758
780.6	0.0637					0.0419					0.0774
785.5	0.0613					0.0389					0.0785
790.6	0.0660					0.0000					0.0807
797.5	0.0681	0.0630	0.0581	0.0528	0.0486	0.0421	0.0487	0.0533	0.0617	0.0641	0.0787

Table 4.12. Experimental power production distribution in the intermediate reactor configuration[a]

H/r (mm)	143.5	146.5	149.5	152.5	159.0	167.5	176.0	182.5	185.5	188.5	193.95
2.5	0.5018	0.4759	0.4512	0.4397	0.4338	0.4766	0.5805	0.7211	0.8090	0.9171	
4.5											1.1850
9.4	0.4839										1.1990
14.5	0.4794					0.4238					1.2000
19.4	0.4794					0.4167					1.1911
28.5	0.4847					0.4245					1.2224
50.0	0.5110	0.4742	0.4459	0.4239	0.4093	0.4420	0.5392	0.6769	0.7785	0.8976	1.2601
75.0	0.5567					0.4770					1.3421
100.0	0.5930					0.5121					1.4317
175.0	0.7313	0.6753	0.6400	0.6051	0.5872	0.6257	0.7491	0.9407	1.0623	1.2310	1.7123
250.0	0.8502					0.7224					1.9383
325.0	0.9511					0.8000					2.1266
400.0	1.0142	0.9537	0.8855	0.8438	0.8084	0.8560	1.1200	1.2612	1.4062	1.6161	2.2504
475.0	1.3118					0.9275					2.3172
550.0	1.3564					0.9315					2.2620
625.0	1.3150	1.1794	1.0616	0.9743	0.8880	0.8800	0.9931	1.2161	1.3458	1.5414	2.1313
700.0	1.1813					0.7740					1.9097
725.0	1.1423					0.7301					1.8183
750.0	1.0947	0.9687	0.8770	0.7968	0.7082	0.6966	0.8015	0.9889	1.1146	1.2653	1.7799
771.5	1.0978					0.6885					1.7620
780.6	1.0300					0.7054					1.7518
785.5	1.1152					0.7138					1.7609
790.6	1.1577										1.7956
797.5	1.2617	1.1367	1.0807	0.9924	0.9023	0.8946	0.9708	1.1586	1.2664	1.4038	1.8400

[a]Table 5.2.6 of ref. 2.

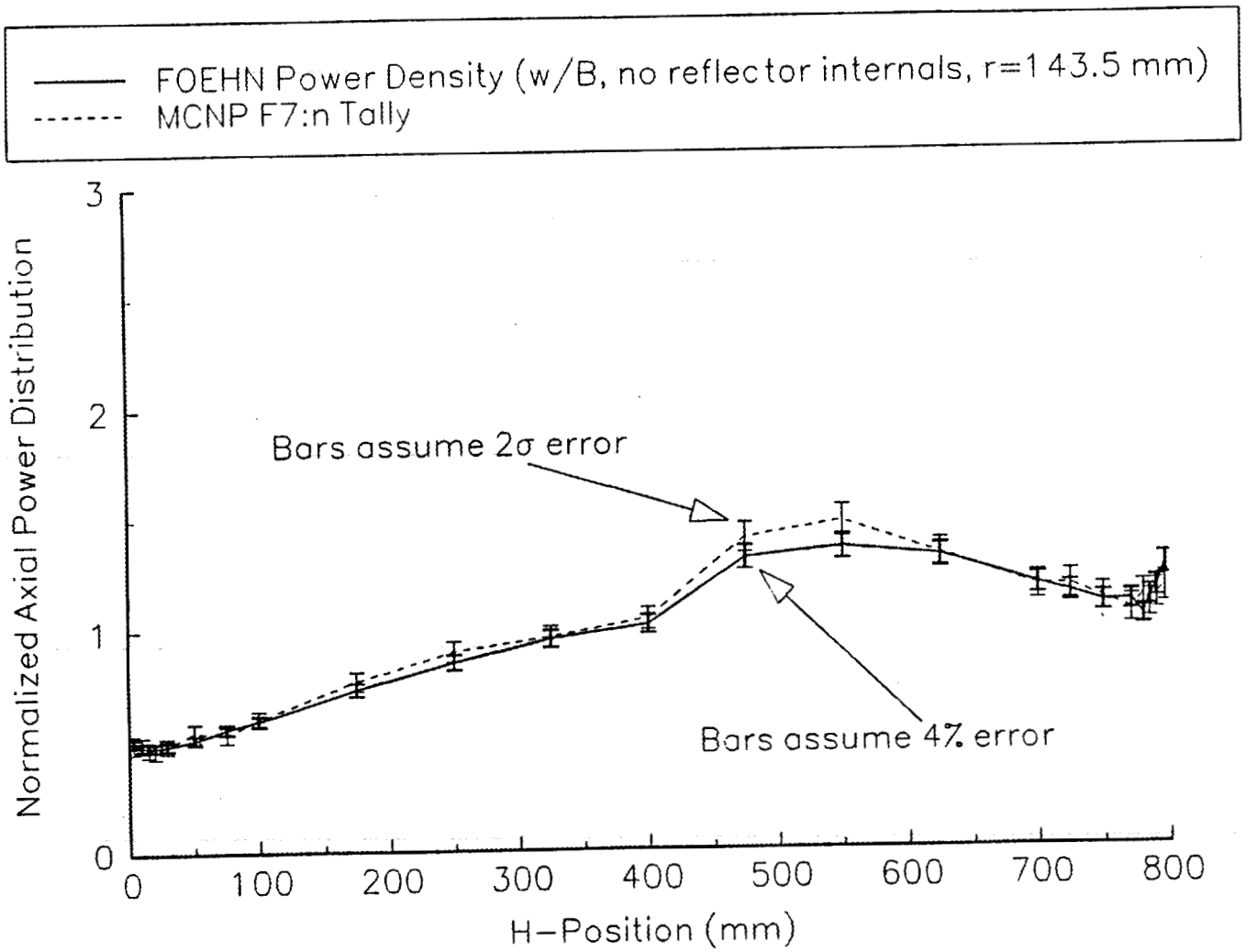

Fig. 4.20. Comparison of normalized experimental and computed axial power distribution in the intermediate FOEHN configuration at r = 143.5 mm.

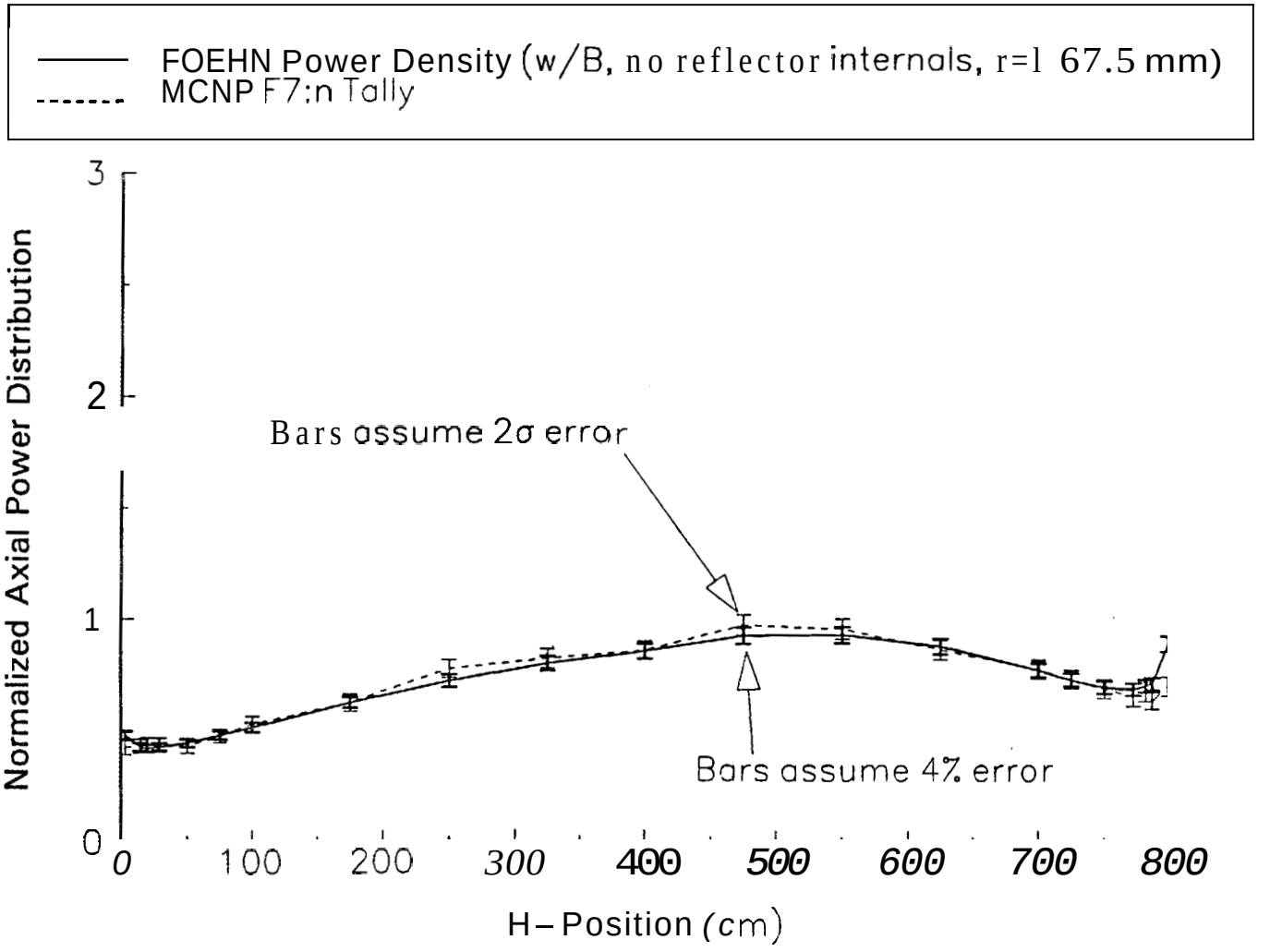

Fig. 4.21. Comparison of normalized experimental and computed axial power distribution in the intermediate FOEHN configuration at r = 167.5 mm.

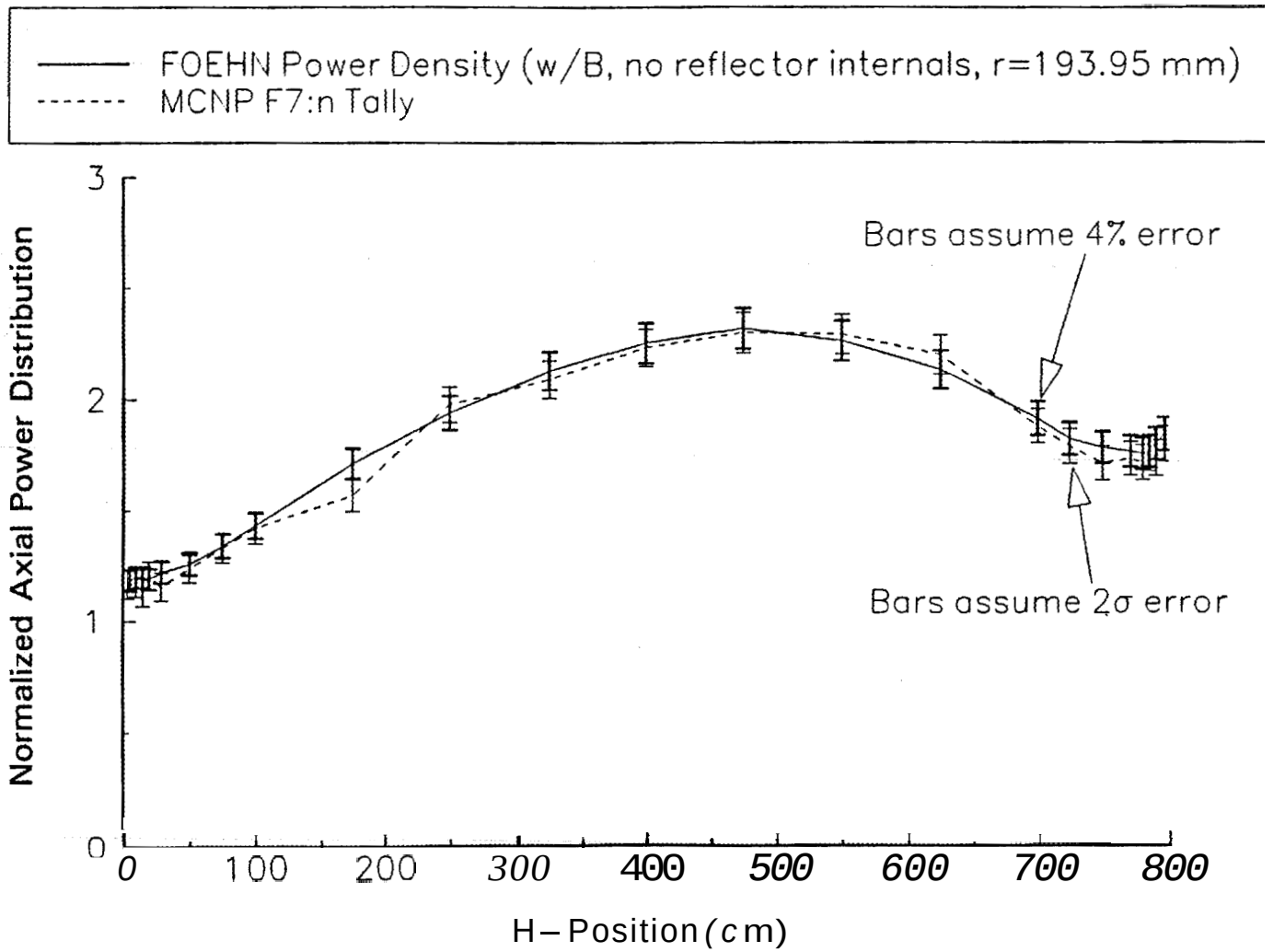

Fig. 4.22. Comparison of normalized experimental and computed axial power distribution in the intermediate FOEHN configuration at r = 193.95 mm.

Table 4.13. Points of nonmatching power production density in the intermediate reactor configuration

H/r (mm)	143.5	146.5	149.5	152.5	159.0	167.5	176.0	182.5	185.5	188.5	193.95
2.5	0	0	0	0	1	1	0	0	0	0	0
4.5											
9.4	0										0
14.5	0					0					0
19.4	0					0					0
28.5	0					0					0
50.0	0	0	0	0	0	0	0	0	0	0	0
75.0	0					0					0
100.0	0					0					0
175.0	0	0	0	0	0	0	0	0	0	1	1
250.0	0					0					0
325.0	0					0					0
400.0	0	0	0	0	0	0	0	0	0	0	0
475.0	0					0					0
550.0	0					0					0
625.0	0	0	0	0	0	0	0	0	0	0	0
700.0	0					0					0
725.0	0					0					0
750.0	0	0	0	0	0	0	0	0	0	0	0
771.5	0					0					0
780.6	0					0					0
785.5	0					1					0
790.6	0										0
797.5	0	1	1	1	1	1	1	1	0	0	0

Table 4.14. MCNP-computed core effective multiplication factors (k_{eff}) for various critical states of the full complexity reactor configuration

Case	Control rod position (mm)		Boron conc. (g/L)	MCNP k_{eff}	MCNP error estimate (σ)
	MCNP	FOEHN			
1	0.806	0.804	0.347	0.9935	0.0027
2	0.899	0.711	0.311	0.9981	0.0024
3	1.014	0.596	0.260	0.9973	0.0027
4	1.031	0.579	0.248	0.9935	0.0027
5	1.107	0.503	0.210	0.9931	0.0027
6	1.225	0.385	0.143	0.9943	0.0028
7	1.361	0.249	0.078	0.9890	0.0028

axially on the surface of Channel 17. In an attempt to accurately model these measurements, point detector tallies (i.e., next collision estimator, MCNP F5 tallies) were used. These allowed the flux at exact locations to be calculated with better statistics than the track length tallies (F4 tally) with small volume elements. The beam tube fluxes were calculated with the control rod position set to 1.139 m and a core boron concentration of 0.177 g/L. The other flux calculations were performed with the control rod set at 1.016 m and a core boron concentration of 0.255 g/L. The results obtained displayed a very large number of significant discrepancies between the experimental and the MCNP-computed fluxes, with many points showing no overlap between the computational and experimental error bands by a large margin. These large discrepancies result mainly from the inability of MCNP point detector tallies to incorporate histories involving $S(\alpha,\beta)$ interactions with moderating materials. The computational results have no value from a benchmarking point of view and, hence, are omitted from this report. The $S(\alpha,\beta)$ effect is explained below.

The $S(\alpha,\beta)$ cross-section data correspond to the coherent and incoherent elastic and incoherent inelastic scattering cross sections for materials with significant crystalline or other lattice-dependent scattering effects. These cross-section data, incorporated in the MCNP cross-section libraries and utilized in the FOEHN MCNP models, have a large effect on the behavior of heavy-water-moderated reactors and also influence the performance of other materials, such as liquid deuterium in cold sources and graphite in hot sources.

The large quantity of heavy water in the FOEHN experiment induces nearly all thermal neutrons to undergo at least one lattice-influenced thermal interaction before reaching the reflector components. These $S(\alpha,\beta)$ interactions are not accounted for by MCNP point detector tallies. This can result in a significant discrepancy between the computed tallies and the measured values. This was made very apparent in the initial analysis of the reflector thermal fluxes for the full complexity configuration, when inclusion of the $S(\alpha,\beta)$ data produced flux results that were a factor of two to four below the experimental values. The alternative to this method is to compute the fluxes without using the $S(\alpha,\beta)$ cross-section data. This would produce global inaccuracies in the flux energy distribution since fewer

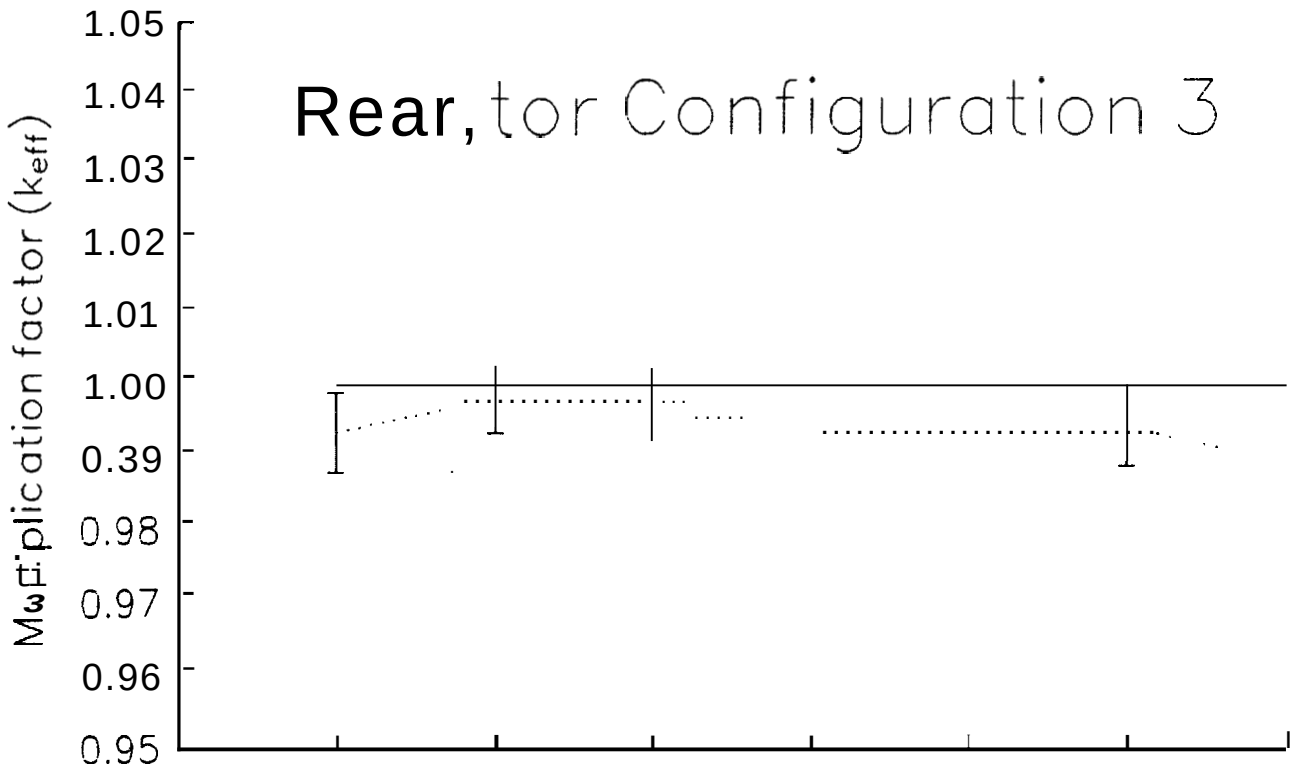

Fig. 4.23. MCNP prediction of k_{eff} for a set of critical states of the full-featured FOEHN reactor configuration.

neutrons would be scattered into the lower thermal energy ranges (<0.625 eV). However, this would allow all neutron histories to interact with the point detector tallies. This method was tried and produced a systematic underestimation of the thermal fluxes calculated. These results are also omitted from this report.

An additional effect of the lack of $S(\alpha,\beta)$ cross-section data is seen in the results for the hot source. The presence of hot (~2000 K) graphite in the hot source introduces another set of $S(\alpha,\beta)$ cross-section data into the calculation. These have a different effect on the flux energy distribution, as there is significantly more upscattering from interactions with hot graphite than from interactions with room-temperature heavy water. The result is a tendency to lower the thermal flux (<0.625 eV) with increasing penetration into the hot source. Since the $S(\alpha,\beta)$ treatment is absent from the simulation, there ensues a large overestimation of the radial and axial thermal flux distributions in the hot source.

4.4.3 Rendement

The MCNP computed rendement, r_{calc}, is 2.4114×10^{11} neutrons/m^2 · s · W. The error estimate on this, 2σ, is 4.968×10^9 neutrons/m^2 · s · W. The measured rendement reported in ref. 2, r_{meas}, is 2.30×10^{11} neutrons/m^2 · s · W. The error reported in ref. 2 is $\sim 0.05 \times 10^{11}$ neutrons/m^2 · s · W (i.e., ~3%). This error may be underestimated and could be as large as ~16.2% (see Sect. 2.4.3.4). With a difference of only 4.84% between the center values, the two estimates of the rendement agree within statistics (even with the lowest error estimates).

4.4.4 Power

The full complexity MCNP model of the FOEHN critical experiment has been used to obtain F7:n tallies (KCODE option, 80 cycles, 10000 particles/cycle). The tallies have been normalized to the same value (1.006) as the data of Table 2.2 obtained in Sect. 2.3.2.3 by combining the results of Tables 5.3.6–5.3.9 of the FOEHN report. The normalized MCNP results are shown in Table 4.15 of this report. In Table 4.16, the corresponding MCNP error estimates (2σ) are shown. The tallies from Table 4.15 and the combined experimental data from Table 2.2 are compared in Figs. 4.24–4.26. The error bars shown for the computed results are the 2σ values tabulated in Table 4.16. The error bars for the experimental points correspond to the 4% estimate for the error discussed in Chap. 2.

In Figs. 4.24–4.26 the power distribution is plotted as a function of the axial coordinate H for the radii of 143.5, 167.5, and 193.95 mm, respectively. As in the intermediate complexity case, it can be seen from the figures that for most points in the reactor interior, there is at least partial (and, in most instances, significant) overlap of the error bars from the computational predictions and the experiment. In Table 4.17, all the experimental and computational results are compared in the sense of overlap of their respective error bands. In the table, an entry of 0 indicates overlap, whereas an entry of 1 indicates no overlap. There are 18 nonoverlapping points out of a total of 125 data points. This implies a nonmatching rate of 14.4%. The table shows that overlap occurs for most points internal to the reactor and that nearly all points at the bottom and almost half the points at the top of the core show no overlap. As in the previous configuration, this can be attributed to the lack of precise information about the location of the borated end caps, the omission of the AG3-NE end covers in the model, and possibly to the modeling of the boron end caps as homogenous rather than heterogenous regions. If the end points (14 points, top and bottom of core) are excluded from the nonmatching count, the nonmatching rate drops to 3.20%, well within the expected nonoverlap rate of 5% predictable from the use of the $\pm 2\sigma$ error bands. Aside from the axial end points, two of the remaining four nonoverlap points occur at the inner radius of the core near the tip of the inserted control rod, where flux gradients are sharp and the discrepancy between MCNP F7:n tallies and the measured power

Table 4.15. Normalized MCNP power production (F7:n tallies) for the full complexity reactor configuration

H/r (mm)	143.5	146.5	149.5	152.5	159.0	167.5	176.0	182.5	185.5	188.5	193.95
2.5	0.5044	0.4600	0.4189	0.4090	0.4294	0.4340	0.5167	0.6771	0.7065	0.7916	1.1002
9.4	0.4881										1.1871
14.5	0.4829					0.4092					
19.4	0.4854					0.4351					1.2219
28.5	0.5392					0.4283					1.1927
50.0	0.5305	0.4931	0.4392	0.4430	0.4566	0.4293	0.5406	0.6496	0.7680	0.9189	1.2167
75.0	0.5806					0.5034					1.3222
100.0	0.6347					0.5598					1.3701
175.0	0.7294	0.6678	0.6653	0.6339	0.6275	0.6528	0.7472	0.9301	1.0398	1.2076	1.5916
250.0	0.9000					0.7454					1.9029
325.0	0.9773					0.8130					2.0977
400.0	1.0904	1.0323	0.9687	0.9121	0.8414	0.8904	1.0201	1.2561	1.4289	1.6747	2.2091
475.0	1.5061					1.0533					2.2745
550.0	1.6064					0.9873					2.1995
625.0	1.3510	1.2273	1.1075	1.0047	0.8925	0.9016	1.0031	1.2251	1.3244	1.5141	2.0027
700.0	1.3155					0.8339					1.8211
725.0	1.1976					0.7740					1.7019
750.0	1.1100	0.9172	0.8365	0.7941	0.7155	0.7349	0.8652	1.0136	1.1565	1.2903	1.7236
771.5	1.0874					0.6835					1.6379
780.6	1.1191					0.7063					1.6754
785.5	1.1037					0.6727					1.5936
790.6	1.1370										1.6444
797.5	1.2027	1.0695	0.9411	0.8474	0.7471	0.7574	0.8243	0.0116	1.0783	1.2262	1.6124

Table 4.16. MCNP error estimate (2σ, absolute) for the normalized MCNP power production for the full complexity reactor configuration

H/r (mm)	143.5	146.5	149.5	152.5	159.0	167.5	176.0	182.5	185.5	188.5	193.95
2.5	0.0377	0.0353	0.0318	0.0316	0.0327	0.0317	0.0372	0.0437	0.0455	0.0477	0.0607
9.4	0.0344										0.0651
14.5	0.0356					0.0300					
19.4	0.0335					0.0329					0.0689
28.5	0.0418					0.0322					0.0656
50.0	0.0383	0.0346	0.0299	0.0327	0.0383	0.0288	0.0375	0.0433	0.0501	0.0535	0.0638
75.0	0.0383					0.0342					0.0677
100.0	0.0410					0.0366					0.0680
175.0	0.0398	0.0369	0.0379	0.0350	0.0438	0.0377	0.0427	0.0484	0.0526	0.0599	0.0754
250.0	0.0468					0.0404					0.0784
325.0	0.0481					0.0429					0.0856
400.0	0.0497	0.0508	0.0469	0.0440	0.0406	0.0459	0.0492	0.0575	0.0634	0.0693	0.0844
475.0	0.0723					0.0518					0.0873
550.0	0.0774					0.0486					0.0845
625.0	0.0676	0.0631	0.0571	0.0508	0.0469	0.0445	0.0488	0.0590	0.0615	0.0669	0.0793
700.0	0.0687					0.0484					0.0772
725.0	0.0651					0.0430					0.0735
750.0	0.0666	0.0532	0.0478	0.0483	0.0454	0.0428	0.0495	0.0545	0.0601	0.0614	0.0782
771.5	0.0642					0.0421					0.0737
780.6	0.0642					0.0436					0.0754
785.5	0.0640					0.0398					0.0739
790.6	0.0664										0.0779
797.5	0.0702	0.0640	0.0574	0.0534	0.0466	0.0457	0.0465	0.0542	0.0552	0.0601	0.0735

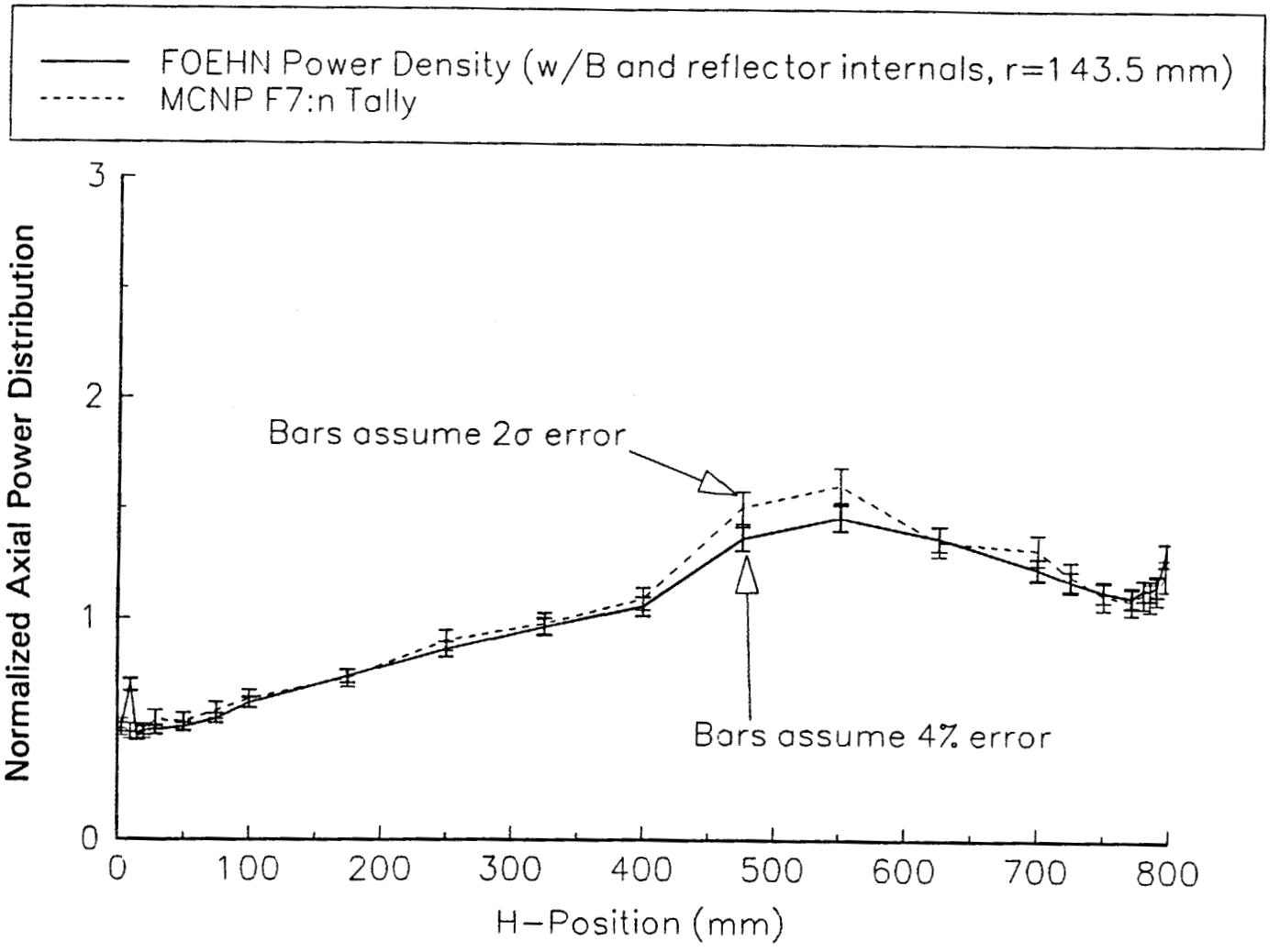

Fig. 4.24. Comparison of normalized experimental and computed axial power distribution in the full-featured FOEHN configuration at r = 143.5 mm.

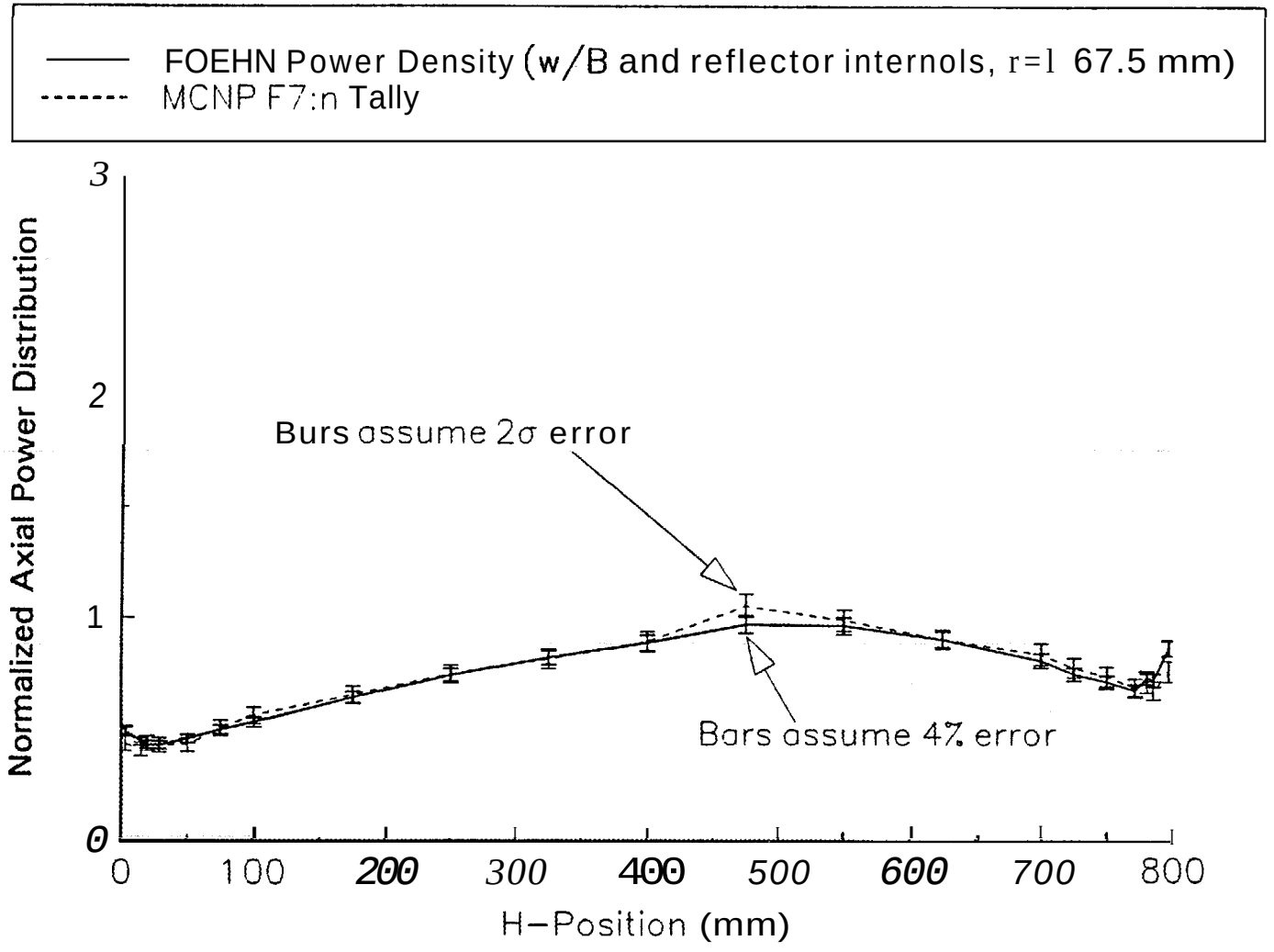

Fig. 4.25. Comparison of normalized experimental and computed axial power distribution in the full-featured FOEHN configuration at r = 167.5 mm.

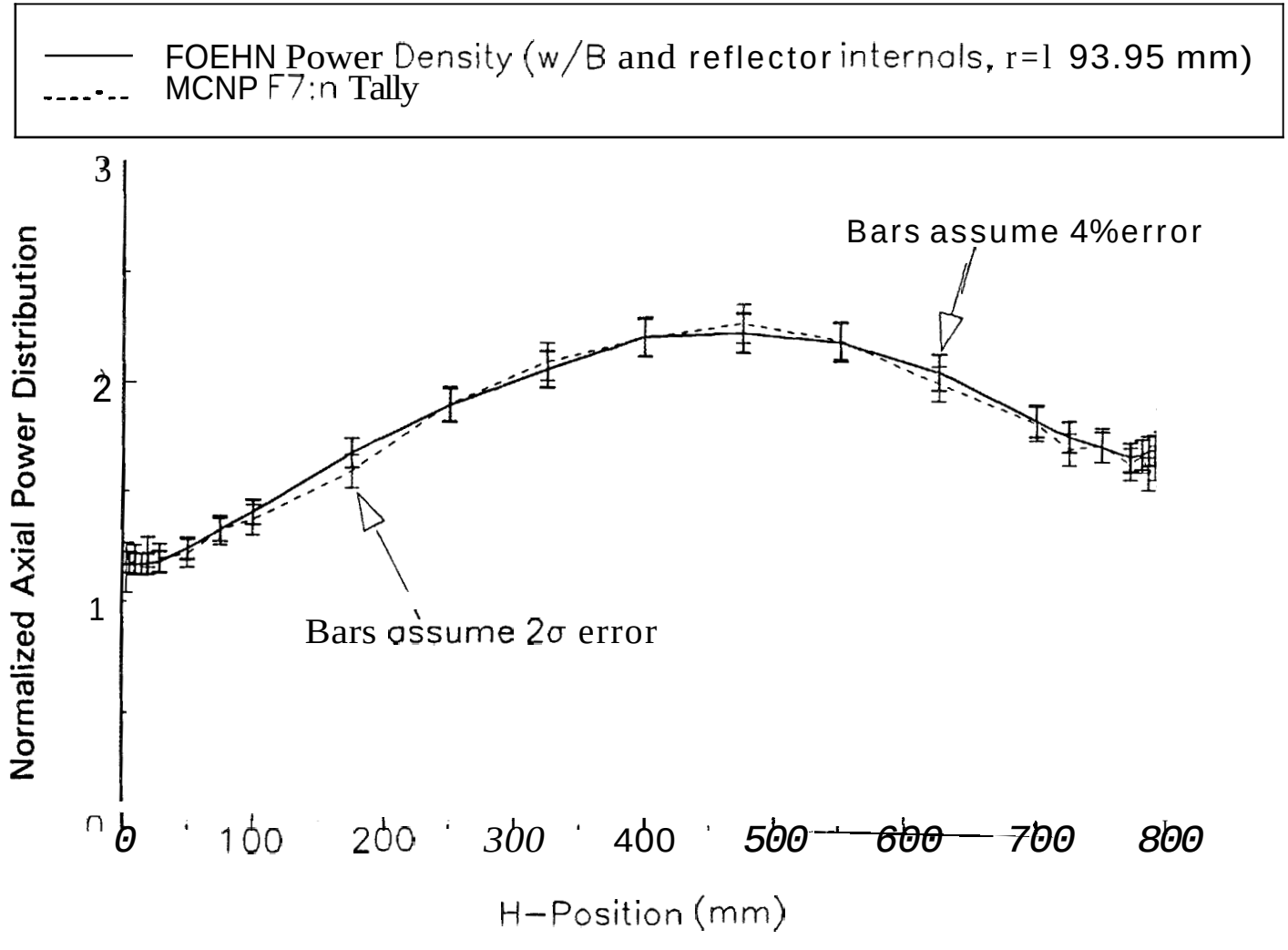

Fig. 4.26. Comparison of normalized experimental and computed axial power distribution in the lull-featured FOEHN configuration at r = 193.95 mm.

Table 4.17. Points of nonmatching power production density in the full complexity reactor configuration[a]

H/r (mm)	143.5	146.5	149.5	152.5	159.0	167.5	176.0	182.5	185.5	188.5	193.95
2.5	0	0	0	0	0	1	1	0	1	1	1
5.0											0
9.4	1										0
14.5	0					0					1
19.4	0					0					0
28.5	0					0					0
50.0	0	0	0	0	0	0	0	0	0	0	0
75.0	0					0					0
100.0	0					0					0
175.0	0	0	0	0	0	0	0	0	0	0	0
250.0	0					0					0
325.0	0					0					0
400.0	0	0	0	0	0	0	0	0	0	0	0
475.0	1					0					0
550.0	1					0					0
625.0	0	0	0	0	0	0	0	0	0	0	0
700.0	0					0					0
725.0	0					0					0
750.0	0	0	0	0	0	0	0	0	0	0	0
771.5	0					0					0
780.6	0					0					0
785.5	0					0					0
790.6	0										0
795.0											0
797.5	0	0	1	1	1	1	1	1	1	1	1

[a]125 data points, 18 misses (14.40%), 4 misses excluding top and bottom rows (3.20%).

production (based on gamma activity counting) is expected to be the greatest. The existence of a sharp flux gradient may also imply, for the measurement, a higher error than the ±4% used for the comparison performed in this work.

4.5 SUMMARY

In this chapter, the results of the MCNP simulations of all three FOEHN experiment configurations have been presented and discussed. It has been shown that all three models agree consistently with the experimental results within the limits of interpretation of the statistics inherent to the Monte Carlo approach. It was shown that the computed spatial distribution of the power production in the cores, the thermal flux distribution in the reflector, and the rendement agree very well with the corresponding experimental values. Where discrepancies between the models and the experiment occurred, they were fully correlated to (and explained by) the approximations made, the lack of precise information about the experimental setup, or the limitations of the version of the MCNP code used in this work.

5. CONCLUSIONS

Phase II of the validation of the neutronic design methods of the ANS reactor has been completed and presented in this report. The use of MCNP as a neutronics design code has been benchmarked against the FOEHN critical experiment. Many quantities of interest to the safe and efficient operation of a high-intensity neutron source reactor were computed and compared to their experimental counterparts. It was shown that for all quantities of importance (core power distribution, reflector fluxes, effective multiplication factor, and rendement figure of merit), the computational results reproduced the experimental ones within the error bounds defined by the statistics and the experimental errors. A notable exception pertains to the use of point detector tallies in MCNP for estimating fluxes in small regions. These MCNP tallies have been found to be inadequate for the design estimation of fluxes.

The results presented in this report document a successful benchmarking of the MCNP computer code against the FOEHN critical experiments and a significant, positive contribution to the validation of the neutronics design methodology for the ANS reactor.

In addition to the validation of the neutronics design methodology, the testing of the robustness of the design to small changes in some materials specifications was performed. Specifically, the AG3-NE alloy used as a structural material was replaced entirely by pure aluminum for some runs. It was found that changes in the effective multiplication factor and in some powers were larger than the computed statistical errors. It follows from this study that small changes in materials could have important effects on the neutronics of a reactor sharing some of the design characteristics of the FOEHN experiment. It is therefore recommended that, for a design for which requirements are rigid (such as the ANS reactor), a range of material compositions and of geometric specifications for which the performance remains within the ranges defined by the statistical bands (or by performance specifications) should be identified. Such a sensitivity analysis of the design would be a crucial step in the design effort, both to ensure a safe reactor and to contribute to reducing the cost of the project by identifying acceptable tolerance limits. An example of the type of artifacts that may arise in the design of the ANS reactor can be illustrated by one encountered inadvertently. It was found that small perturbations in some critical parameters significantly affect the performance of the reactor. Specifically, it was found that the mechanical tolerances within the core (i.e., fuel plate sizes, fit of core barrel components) affect the actual borated water content of the core. The improper distribution of this borated water was found to significantly distort the spatial distribution of the power production density. The knowledge of acceptable bounds for the mechanical tolerances may have important consequences on the safe and economical operation of the reactor. For example, the correlation of fuel manufacturing tolerances to power distribution would allow the definition of fuel manufacturing bounds for which the resulting reactor loading and power distribution would remain within the acceptable operational range. This would affect every reload and could result in recurrent savings.

A second issue that must be addressed in the design of the various facilities of the ANS reactor is the use of a version of MCNP capable of treating the $S(\alpha,\beta)$ interactions. It is recommended that for future models, the newest version of MCNP be used after it is quality-assurance certified.

The lack of complete and precise information about the FOEHN experiment caused a number of difficulties, of which many were resolved by experimenting with several plausible options. However, there still remain uncertainties about the positions of certain components in the core. Among the remaining unknowns are the exact location of the borated end caps, the azimuthal positions of the various fuel plates, and the thickness and exact location of the AG3-NE axial portion of the reactor bucket. One of these (the borated end caps location) may be the cause of the larger than average

discrepancy between experiment and model observed at the axial ends of the core. The use of a homogenized core was dictated by the lack of precise information about the azimuthal position of the fuel plates and the lack of a circular involute geometry option in the MCNP code. The potential error arising from this approximation has been previously quantified in the case of the ANS design for which the core D_2O is not borated. The effect in the presence of boron is uncertain. A short study aimed at quantifying the difference between a homogenous and an explicit heterogenous model in the presence of borated heavy water is currently under way.

6. REFERENCES

1. D. L. Selby et al., *The Advanced Neutron Source Research and Development Plan*, ORNL/TM-12249, Martin Marietta Energy Systems, Inc., Oak Ridge Natl. Lab., November 1992.

2. K. Scharmer and H. G. Eckert, *FOEHN: The Critical Experiment for the Franco-German High Flux Reactor*, ORNL/TR-91/23, Martin Marietta Energy Systems Inc., Oak Ridge Natl. Lab., 1991. English translation of K. Scharmer, H. G. Eckert, "FOEHN - Das kritische Experiment fur den Deutsch-Franzosischen Hochflussreaktor," KFK 1064, Dezember 1971. French version: Klaus Scharmer et Hans G. Eckert, "L'experience critique pour le reacteur a Haut-Flux Franco-Allemand," Institut Max von Laue-Paul Langevin, Grenoble, Gesellschaft fur Kernforschung, Commissariat a L'Energie Atomique, et Centre National de la Recherche Scientifique.

3. J. F. Breismeister, *MCNP Version 3b, Monte Carlo Neutron and Photon Transport Code System*, LA-7396-M, Rev. 2, Los Alamos Natl. Lab., September 1986.

4. J. M. Ryskamp, D. L. Selby, and R. T. Primm III, "Reactor Design of the Advanced Neutron Source," *Nucl. Tech.* **93**, 330–349, March 1991.

5. F. Gallmeier, *Verfizierung des dreidimensionalen Rechencodes MORSE-K durch Nachrechen des kritischen Experimentes FOEHN*, Technische Universität München, January 16, 1991.

6. A. Rohrmoser, Fakultät für Physik E21, Technische Universität München, private communication to John M. Ryskamp, Idaho Natl. Eng. Lab., December 1991.

7. R. D. Evans, *The Atomic Nucleus*, McGraw-Hill, New York, 1955.

8. P. J. Davies, *Interpolation and Approximation*, Dover Publications Inc., New York, 1975.

9. E. L. Redmond II and J. M. Ryskamp, "Monte Carlo Methods, Models, and Applications to the Advanced Neutron Source," *Nucl. Tech.* **95**, 272 (1991). See also E. L. Redmond II, *Monte Carlo Methods, Models, and Applications for the Advanced Neutron Source*, M.S. Thesis, Massachusetts Institute of Technology, June 1990.

10. A. Rohrmoser, *Verification of Data Generation, Two-Dimensional Transport Calculations and Diffusion and Burnup Calculations for the FRM-II Compact Core*, ORNL/OLS-92/12, translated from the German (Report No. 00119a issued by the Department of Physics E21, Technische Universität München, July 1991, 35 pages).

11. R. C. Thayer, E. L. Redmond II, and J. M. Ryskamp, "A Monte Carlo Method of Evaluating Heterogeneous Effects in Plate-Fueled Reactors," *Trans. Am. Nucl. Soc.* **63**, 445 (1991).

12. *CRC Handbook of Chemistry and Physics*, p. F-122, CRC Press, Inc., 62nd Edition, 1981-1982.

13. James T. West III, *SABRINA: An Interactive Three-Dimensional Geometry-Modeling Program for MCNP*, LA-10688-M, Los Alamos Natl. Lab., October 1986.

Appendix A. MCNP MODEL INPUT FILE

APPENDIX A

MCNP MODEL INPUT FILE

A full listing of the input for the MCNP model of the full complexity FOEHN configuration is given below.

```
message:   outp=frn800.o  runtpe=frn800.r  srctp=frn800.s  mctal=frn800.m

FRN800 - Complete model of the FOEHN reactor (the complete experiment)
c
c     Cell cards
c
c     The model was derived from information gathered from Glaser, et al.,
c     "Verifizierung des dreidimensionalen Rechencodes MORSE-K durch
c     nachrechnen des kritischen Experimentes FOEHN", dated Jan. 16, 1991,
c     and ORNL/TR-91/23 "FOEHN:The Critical Experiment for the Franco-German
c     High Flux Reactor", English version, (Dec. 1971).
c
c     ---------------------------------------------------------------------
c
c     Structures below the core
c
   1     1 0.099753   -1  12 -14          imp:n=1  $ D2o region
   2     1 0.099753    4  -8  12  -13     imp:n=1  $ D2o region
   3    12 0.047175    1  -2  12  -14     imp:n=1  $ Structural material - Al
   4    12 0.047175   -2  14 -16          imp:n=1  $ Structural material - Al
   5    12 0.047175    3 -10  13  -16     imp:n=1  $ Structural material - Al
   6    12 0.047175    8 -10  12  -13     imp:n=1  $ Structural material - Al
   7    12 0.047175    3  -4  12  -13     imp:n=1  $ Structural material - Al
   8    12 0.047175    2  -3  12  -15     imp:n=1  $ Structural material - Al
   9     1 0.099753   -2  16 -17          imp:n=1  $ D2o region
  10    10 9.13e-2     2  -3  15  -18     imp:n=1  $ Control rod - Nickel
  11     1 0.099753    3  -8  16 -163     imp:n=1  $ D2o region
  12    12 0.047175    8 -10  16  -17     imp:n=1  $ Structural material - Al
c
c     Structures even with the core
c
  13     1 0.099753   -2  17  -19         imp:n=1  $ D2o region
  14     1 0.099753    2  -3   18  -195  imp:n=1  $ Control rod - nickel
  15     1 0.099753    3  -4  163   -19  imp:n=1  $ D2o region
  16    12 0.047175    4  -5  163   -19  imp:n=1  $ Inner core tube - Al
  17     2 0.099763646 5  -6  163   -19  imp:n=1  $ Borated d2o
  19     2 0.099763646 7  -8  163   -19  imp:n=1  $ Borated d2o
  20    12 0.047175    8  -9   17   -19  imp:n=1  $ Inner tube w/borated d2o
  21     2 0.099763646 9 -900  17   -19  imp:n=1  $ borated d2o
  221   12 0.047175  900 -10   17   -19  imp:n=1  $ outer tank - Al
1131    12 0.047175   -7   6  151 -1138  imp:n=1  $ Top Al seal
1132    12 0.047175   -7   6 1164   -17  imp:n=1  $ Bottom Al seal
```

```
c
c     The beam tubes
c
  22     0            -20 21 -22          imp:n=1  $ Inside of beam tube1
  23    12 0.047175   -23 20  21 -22      imp:n=1  $ Outside of beam tube1
  24     0            -24 25 -26          imp:n=1  $ Inside of beam tube2
  25    12 0.047175   -27 24  25 -26      imp:n=1  $ Outside of beam tube2
  26     0            -28 29 -30          imp:n=1  $ Inside of beam tube3
  27    12 0.047175   -31 28  29 -30      imp:n=1  $ Outside of beam tube3
  28     0            -32 33 -34          imp:n=1  $ Inside of beam tube4
  29    12 0.047175   -35 32  33 -34      imp:n=1  $ Outside of beam tube4
  30     0            -36 37 -38 (43:-41:42:-40)
                                          imp:n=1  $ Inside of beam tube6
  31    12 0.047175   -39 36  37 -38 (43:-41:42)
                                          imp:n=1  $ Outside of beam tube6
  32     0            -40 41 -42          imp:n=1  $ Inside of beam tube7
  33    12 0.047175   -43 40  41 -42      imp:n=1  $ Outside of beam tube7
  34     0            -44 45 -46          imp:n=1  $ Inside of beam tube8
  35    12 0.047175   -47 44  45 -46      imp:n=1  $ Outside of beam tube8
  36     0            -48 49 -50          imp:n=1  $ Inside of beam tube9
  37    12 0.047175   -51 48  49 -50      imp:n=1  $ Outside of beam tube9
  38     0            -52 53 -54          imp:n=1  $ Inside of beam tube10
  39    12 0.047175   -55 52  53 -54      imp:n=1  $ Outside of beam tube10
  40     0            -56 57 -58          imp:n=1  $ Inside of beam tube11
  41    12 0.047175   -59 56  57 -58      imp:n=1  $ Outside of beam tube11
  42     0            -60 61 -62          imp:n=1  $ Inside of beam tube13
  43    12 0.047175   -63 60  61 -62      imp:n=1  $ Outside of beam tube13
c
c     Cold source - cell 14
c
  44    12 0.047175   -68 67   71  -75    imp:n=1  $ Outer bell covering
  45    12 0.047175   -67 66   71  -74    imp:n=1  $ Vessel
  46     0            -66 65   72  -73    imp:n=1  $ Vacuum inside vessel
  47    12 0.047175   -65 64   72  -73    imp:n=1  $ Rod inside vessel
  48     0            -64 72  -73         imp:n=1  $ Vacuum w/i rod w/i vessel
  49    12 0.047175   -66 71  -72         imp:n=1  $ Bottom of vessel
  50    12 0.047175   -69 70  -71         imp:n=1  $ Plug on bottom of vessel
  51    12 0.047175   -78 77   75 -195    imp:n=1  $ Outer tube on top of vessel
  52     0            -77 65   75 -195    imp:n=1  $ Vacuum between tube & rod
  53    12 0.047175   -65 64   75 -195    imp:n=1  $ Rod inside tube
  54     0            -64 75 -195         imp:n=1  $ Vacuum w/i rod w/i tube
  55    12 0.047175   -67 74  -75         imp:n=1  $ Top of outer bell covering
  56    12 0.047175   -66 73  -74         imp:n=1  $ Top of vessel
  57    12 0.047175   -79 80 -195 (-75:78) (69:-70:71) (68:-71:75)
                                          imp:n=1  $ Rest of cold source
c
c     Hot source - cell 15
c
  58    12 0.047175   -82  83 -195   85   imp:n=1  $ Outer guide tube
  59    12 0.047175   -85  87  -88        imp:n=1  $ Top lid of hot cell
  60     1 0.099753   -85  89   86  -87   imp:n=1  $ Between tube & cylinder
  61     9 0.0428042  -89  92   90  -91   imp:n=1  $ Inner cylinder
```

```
 62    0              -92  95   93  -94    imp:n=1  $ Void between cyl. & graphite
 63    7 1.67e-2      -95  96  -98 (100)   imp:n=1  $ Bottom half of  graphite
 64    1 0.099753      88 -85 -195         imp:n=1  $ D2o region on top of lid
 65    7 1.67e-2      -95  99  -97 (100)   imp:n=1  $ Top half of graphite
 66    0              -95  98  -99         imp:n=1  $ Horizontal split in graphite
 67    0             -100  96  -98         imp:n=1  $ Vertical split in graphite
 68   12 0.047175     -85  83  -86         imp:n=1  $ Bottom lid of hot cell
 69    9 0.0428042    -92  90  -93         imp:n=1  $ Bottom lid of inner cylinder
 70    9 0.0428042    -92 -91   94         imp:n=1  $ Top lid of inner cylinder
 71    0              -95  93  -96         imp:n=1  $ Bottom of void
 72    0              -95  97  -94         imp:n=1  $ Top of void
 73    1 0.099753     -89  86  -90         imp:n=1  $ Bottom - outer/inner tubes
 74    1 0.099753     -89  91  -87         imp:n=1  $ Top - outer/inner tubes
 75    0             -100  99  -97         imp:n=1  $ Vertical split in graphite
c
c      Rest of the beam tubes
c
 76    0            -101 102 -103          imp:n=1  $ Inside of beam tube16
 77   12 0.047175 -104 101  102 -103       imp:n=1  $ Outside of beam tube16
 78    0            -105 106 -103          imp:n=1  $ Inside of beam tube17
 79   12 0.047175 -108 105  106 -103       imp:n=1  $ Outside of beam tube17
 80    0            -109 110 -111          imp:n=1  $ Inside of beam tube19
 81   12 0.047175 -112 109  110 -111       imp:n=1  $ Outside of beam tube19
 82    0            -113 114 -115          imp:n=1  $ Inside of beam tube21
 83   12 0.047175 -116 113  114 -115       imp:n=1  $ Outside of beam tube21
 84    0            -117 118 -119          imp:n=1  $ Inside of beam tube22
 85   12 0.047175 -120 117  118 -119       imp:n=1  $ Outside of beam tube22
 86    0            -121 122 -195          imp:n=1  $ Inside of beam tube23
 87   12 0.047175 -124 121  122 -195       imp:n=1  $ Outside of beam tube23
 88    0            -125 126 -127          imp:n=1  $ Inside of beam tube24
 89   12 0.047175 -128 125  126 -127       imp:n=1  $ Outside of beam tube24
c
c      Safety rods
c
 90    1 0.099753  -129 12 -135 164        imp:n=1  $ Safety rod 1
 91    1 0.099753  -130 12 -135 169        imp:n=1  $ Safety rod 2
 92    1 0.099753  -131 12 -135 174        imp:n=1  $ Safety rod 3
 93    1 0.099753  -132 12 -135 179        imp:n=1  $ Safety rod 4
 94    1 0.099753  -133 12 -135 184        imp:n=1  $ Safety rod 5
 95    1 0.099753  -134 12 -135 189        imp:n=1  $ Safety rod 6
c
c      Area outside the safety rods and the core up to 40cm radius
c
 96    1 0.099753  198 -11 12 -19 (129:-12:135) (130:-12:135)
                  (133:-12:135) (132:-12:135) (131:-12:135)(10)
                  (134:-12:135) (31:-29) (108:-106) (35:-33)
                  (82:-83)              imp:n=1
c
c      The four quarters of the reactor-everything outside the tubes/cells
c
```

```
 97    1 0.099753  137 138 -194 12 -195 (11:19) (120:-118:119)
                  (82:-83) (39:-37) (108:-106) (43:-41) (55:-53:54)
                  (47:46) (51:-49:50) (63:-62:62) (116:-114) (39:-37)
                  (-2:197:195)          imp:n=1
 98    1 0.099753  137 -138 -194 12 -195 (11:19) (47:-45) (63:62)
                  (-2:197:195) (124:-122) (35:34) (112:111) (43:42)
                  (116:115) (39:38)     imp:n=1
 99    1 0.099753 -137 -138 -194 12 -195 (11:19) (35:-33:34) (-2:197:195)
                   (23:-21:22) (128:127) (27:-25) (31:30) (112:-110:111)
                   (63:-61)             imp:n=1
100    1 0.099753 -137 138 -194 12 -195 (11:19) (27:26) (128:-126)
                   (-2:197:195) (59:-57:58) (120:-118) (31:-29)
                   (104:-102) (79:-80)  imp:n=1
101    0    136                         imp:n=0
c
c      Top borated zone
c
102   14 0.0830797    -7 6 1138 -139    imp:n=1  $ top Aluminum seal
103   14 0.0830797    -7 6  139 -140    imp:n=1  $ Al plate
104   14 0.0830797    -7 6  140 -141    imp:n=1  $ Boron plate
105   14 0.0830797    -7 6  141 -142    imp:n=1  $ Al plate
106   14 0.0830797    -7 6  142 -143    imp:n=1  $ Al plate
107   14 0.0830797    -7 6  143 -144    imp:n=1  $ B plate
108   14 0.0830797    -7 6  144 -145    imp:n=1  $ Al plate
109   14 0.0830797    -7 6  145 -146    imp:n=1  $ Al plate
110   14 0.0830797    -7 6  146 -147    imp:n=1  $ B plate
111   14 0.0830797    -7 6  147 -148    imp:n=1  $ Al plate
112   14 0.0830797    -7 6  148 -149    imp:n=1  $ Al plate
113   14 0.0830797    -7 6  149 -150    imp:n=1  $ B plate
114   14 0.0830797    -7 6  150  -19    imp:n=1  $ Al plate
c
c      Bottom borated zone
c
115   14 0.0830797    -7 6 -1164 152    imp:n=1  $ Al plate
116   14 0.0830797    -7 6  -152 153    imp:n=1  $ B plate
117   14 0.0830797    -7 6  -153 154    imp:n=1  $ Al plate
118   14 0.0830797    -7 6  -154 155    imp:n=1  $ Al plate
119   14 0.0830797    -7 6  -155 156    imp:n=1  $ B plate
120   14 0.0830797    -7 6  -156 157    imp:n=1  $ Al plate
121   14 0.0830797    -7 6  -157 158    imp:n=1  $ Al plate
122   14 0.0830797    -7 6  -158 159    imp:n=1  $ B plate
123   14 0.0830797    -7 6  -159 160    imp:n=1  $ Al plate
124   14 0.0830797    -7 6  -160 161    imp:n=1  $ Al plate
125   14 0.0830797    -7 6  -161 162    imp:n=1  $ B plate
126   14 0.0830797    -7 6  -162 163    imp:n=1  $ Al plate
c
c      The inner rings of the safety rods
c
c      Safety rod 1
c
127    1 0.099753   -164  165 12 -135   imp:n=1  $ cadium region
128    1 0.099753   -165  166 12 -135   imp:n=1  $ inner cladding
```

```
 129    1 0.099753   -166  167 12 -135   imp:n=1  $ d2o channel
 130    1 0.099753   -167  168 12 -135   imp:n=1  $ Al guide tube
 131    1 0.099753   -168 -135 12        imp:n=1  $ d2o inside guide tube
c
c      Safety rod 2
c
 132    1 0.099753   -169  170 12 -135   imp:n=1  $ cadium region
 133    1 0.099753   -170  171 12 -135   imp:n=1  $ inner cladding
 134    1 0.099753   -171  172 12 -135   imp:n=1  $ d2o channel
 135    1 0.099753   -172  173 12 -135   imp:n=1  $ Al guide tube
 136    1 0.099753   -173 -135 12        imp:n=1  $ d2o inside guide tube
c
c      Safety rod 3
c
 137    1 0.099753   -174  175 12 -135   imp:n=1  $ cadium region
 138    1 0.099753   -175  176 12 -135   imp:n=1  $ inner cladding
 139    1 0.099753   -176  177 12 -135   imp:n=1  $ d2o channel
 140    1 0.099753   -177  178 12 -135   imp:n=1  $ Al guide tube
 141    1 0.099753   -178 -135 12        imp:n=1  $ d2o inside guide tube
c
c      Safety rod 4
c
 142    1 0.099753   -179  180 12 -135   imp:n=1  $ cadium region
 143    1 0.099753   -180  181 12 -135   imp:n=1  $ inner cladding
 144    1 0.099753   -181  182 12 -135   imp:n=1  $ d2o channel
 145    1 0.099753   -182  183 12 -135   imp:n=1  $ Al guide tube
 146    1 0.099753   -183 -135 12        imp:n=1  $ d2o inside guide  tube
c
c      Safety rod 5
c
 147    1 0.099753   -184  185 12 -135   imp:n=1  $ cadium region
 148    1 0.099753   -185  186 12 -135   imp:n=1  $ inner cladding
 149    1 0.099753   -186  187 12 -135   imp:n=1  $ d2o channel
 150    1 0.099753   -187  188 12 -135   imp:n=1  $ Al guide tube
 151    1 0.099753   -188 -135 12        imp:n=1  $ d2o inside guide tube
c
c      Safety rod 6
c
 152    1 0.099753   -189  190 12 -135   imp:n=1  $ cadium region
 153    1 0.099753   -190  191 12 -135   imp:n=1  $ inner cladding
 154    1 0.099753   -191  192 12 -135   imp:n=1  $ d2o channel
 155    1 0.099753   -192  193 12 -135   imp:n=1  $ Al guide tube
 156    1 0.099753   -193 -135 12        imp:n=1  $ d2o inside guide tube
c
c      The reflector tank
c
 157   12 0.047175   -196 194 12 -195 (104) (108)
                     (120:-118:119) (112:-110:111)
                     (116:-114:115)      imp:n=1
c
c      The encompassing sphere - outside the reflector tank
c
```

```
 158    0            -136 (196:-12:195) (104:-102:103)
                     (108:-102:103) (120:-118:119) (112:-110:111)
                     (116:-114:115)      imp:n=1
c
c      The structures above the core
c
 159   12 0.047175      4   -5  19 -201  imp:n=1  $ structure above core
 160    1 0.099753      5   -9  19 -199  imp:n=1  $ d20 region core
 161    1 0.099753     10 -197  19 -195  imp:n=1  $ structure above core
 162   12 0.047175      5  -10 199 -200  imp:n=1  $ structure above core
 163    1 0.099753      5  -10 200 -201  imp:n=1  $ d2o region above core
 164    1 0.099753      3  -10 201 -195  imp:n=1  $ d2o region above core
 165    1 0.099753     10 -198  17  -19  imp:n=1  $ outer tank
 166   12 0.047175      9  -10  19 -199  imp:n=1  $ outer tank
 167    1 0.099753     10 -198  12  -17  imp:n=1  $ d2o outside lower core
c
c      Cells used for core power distribution tallies
c
 614    6 0.083382617    6 -306  17 -151 imp:n=1  $ radius 14.20cm
 615    6 0.083382617  306 -307  17 -261 imp:n=1  $ radius 14.50 z=71.50 - tally
 616    6 0.083382617  306 -307 261 -262 imp:n=1
 617    6 0.083382617  306 -307 262 -263 imp:n=1  $ z=71.69 - tally
 618    6 0.083382617  306 -307 263 -264 imp:n=1
 619    6 0.083382617  306 -307 264 -265 imp:n=1  $ z=72.70 - tally
 620    6 0.083382617  306 -307 265 -267 imp:n=1  $ z=73.20 - tally
 621    6 0.083382617  306 -307 267 -268 imp:n=1
 622    6 0.083382617  306 -307 268 -269 imp:n=1  $ z=74.10 - tally
 623    6 0.083382617  306 -307 269 -270 imp:n=1
 624    6 0.083382617  306 -307 270 -271 imp:n=1  $ z=76.25 - tally
 625    6 0.083382617  306 -307 271 -272 imp:n=1
 626    6 0.083382617  306 -307 272 -273 imp:n=1  $ z=78.75 - tally
 627    6 0.083382617  306 -307 273 -274 imp:n=1
 628    6 0.083382617  306 -307 274 -275 imp:n=1  $ z=81.25 - tally
 629    6 0.083382617  306 -307 275 -276 imp:n=1
 630    6 0.083382617  306 -307 276 -277 imp:n=1  $ z=88.75 - tally
 631    6 0.083382617  306 -307 277 -278 imp:n=1
 632    6 0.083382617  306 -307 278 -279 imp:n=1  $ z=96.75 - tally
 633    6 0.083382617  306 -307 279 -280 imp:n=1
 634    6 0.083382617  306 -307 280 -281 imp:n=1  $ z=103.75 - tally
 635    6 0.083382617  306 -307 281 -282 imp:n=1
 636    6 0.083382617  306 -307 282 -283 imp:n=1  $ z=111.25 - tally
 637    6 0.083382617  306 -307 283 -284 imp:n=1
 638    6 0.083382617  306 -307 284 -285 imp:n=1  $ z=118.25 - tally
 639    6 0.083382617  306 -307 285 -286 imp:n=1
 640    6 0.083382617  306 -307 286 -287 imp:n=1  $ z=126.25 - tally
 641    6 0.083382617  306 -307 287 -288 imp:n=1
 642    6 0.083382617  306 -307 288 -289 imp:n=1  $ z=133.75 - tally
 643    6 0.083382617  306 -307 289 -290 imp:n=1
 644    6 0.083382617  306 -307 290 -291 imp:n=1  $ z=141.25 - tally
 645    6 0.083382617  306 -307 291 -292 imp:n=1
 646    6 0.083382617  306 -307 292 -293 imp:n=1  $ z=143.75 - tally
 647    6 0.083382617  306 -307 293 -294 imp:n=1
```

```
648    6 0.083382617  306 -307 294 -295 imp:n=1  $ z=146.25 - tally
649    6 0.083382617  306 -307 295 -296 imp:n=1
650    6 0.083382617  306 -307 296 -297 imp:n=1  $ z=148.40 - tally
651    6 0.083382617  306 -307 297 -298 imp:n=1
652    6 0.083382617  306 -307 298 -299 imp:n=1  $ z=149.31 - tally
653    6 0.083382617  306 -307 299 -300 imp:n=1  $ z=149.81 - tally
654    6 0.083382617  306 -307 300 -303 imp:n=1  $ z=150.31 - tally
655    6 0.083382617  306 -307 303 -304 imp:n=1
656    6 0.083382617  306 -307 304 -151 imp:n=1  $ z=151.00 - tally
c
657    6 0.083382617  307 -308  17 -261 imp:n=1  $ radius 14.80 z=71.50 - tally
658    6 0.083382617  307 -308 261 -262 imp:n=1
659    6 0.083382617  307 -308 262 -263 imp:n=1  $ z=71.69 - tally
660    6 0.083382617  307 -308 263 -264 imp:n=1
661    6 0.083382617  307 -308 264 -265 imp:n=1  $ z=72.70 - tally
662    6 0.083382617  307 -308 265 -267 imp:n=1  $ z=73.20 - tally
663    6 0.083382617  307 -308 267 -268 imp:n=1
664    6 0.083382617  307 -308 268 -269 imp:n=1  $ z=74.10 - tally
665    6 0.083382617  307 -308 269 -270 imp:n=1
666    6 0.083382617  307 -308 270 -271 imp:n=1  $ z=76.25 - tally
667    6 0.083382617  307 -308 271 -272 imp:n=1
668    6 0.083382617  307 -308 272 -273 imp:n=1  $ z=78.75 - tally
669    6 0.083382617  307 -308 273 -274 imp:n=1
670    6 0.083382617  307 -308 274 -275 imp:n=1  $ z=81.25 - tally
671    6 0.083382617  307 -308 275 -276 imp:n=1
672    6 0.083382617  307 -308 276 -277 imp:n=1  $ z=88.75 - tally
673    6 0.083382617  307 -308 277 -278 imp:n=1
674    6 0.083382617  307 -308 278 -279 imp:n=1  $ z=96.75 - tally
675    6 0.083382617  307 -308 279 -280 imp:n=1
676    6 0.083382617  307 -308 280 -281 imp:n=1  $ z=103.75 - tally
677    6 0.083382617  307 -308 281 -282 imp:n=1
678    6 0.083382617  307 -308 282 -283 imp:n=1  $ z=111.25 - tally
679    6 0.083382617  307 -308 283 -284 imp:n=1
680    6 0.083382617  307 -308 284 -285 imp:n=1  $ z=118.25 - tally
681    6 0.083382617  307 -308 285 -286 imp:n=1
682    6 0.083382617  307 -308 286 -287 imp:n=1  $ z=126.25 - tally
683    6 0.083382617  307 -308 287 -288 imp:n=1
684    6 0.083382617  307 -308 288 -289 imp:n=1  $ z=133.75 - tally
685    6 0.083382617  307 -308 289 -290 imp:n=1
686    6 0.083382617  307 -308 290 -291 imp:n=1  $ z=141.25 - tally
687    6 0.083382617  307 -308 291 -292 imp:n=1
688    6 0.083382617  307 -308 292 -293 imp:n=1  $ z=143.75 - tally
689    6 0.083382617  307 -308 293 -294 imp:n=1
690    6 0.083382617  307 -308 294 -295 imp:n=1  $ z=146.25 - tally
691    6 0.083382617  307 -308 295 -296 imp:n=1
692    6 0.083382617  307 -308 296 -297 imp:n=1  $ z=148.40 - tally
693    6 0.083382617  307 -308 297 -298 imp:n=1
694    6 0.083382617  307 -308 298 -299 imp:n=1  $ z=149.31 - tally
695    6 0.083382617  307 -308 299 -300 imp:n=1  $ z=149.81 - tally
696    6 0.083382617  307 -308 300 -303 imp:n=1  $ z=150.31 - tally
697    6 0.083382617  307 -308 303 -304 imp:n=1
698    6 0.083382617  307 -308 304 -151 imp:n=1  $ z=151.00 - tally
```

```
c
 699    6 0.083382617  308 -309  17 -261 imp:n=1  $ radius 15.10 z=71.50 - tally
 700    6 0.083382617  308 -309 261 -262 imp:n=1
 701    6 0.083382617  308 -309 262 -263 imp:n=1  $ z=71.69 - tally
 702    6 0.083382617  308 -309 263 -264 imp:n=1
 703    6 0.083382617  308 -309 264 -265 imp:n=1  $ z=72.70 - tally
 704    6 0.083382617  308 -309 265 -267 imp:n=1  $ z=73.20 - tally
 705    6 0.083382617  308 -309 267 -268 imp:n=1
 706    6 0.083382617  308 -309 268 -269 imp:n=1  $ z=74.10 - tally
 707    6 0.083382617  308 -309 269 -270 imp:n=1
 708    6 0.083382617  308 -309 270 -271 imp:n=1  $ z=76.25 - tally
 709    6 0.083382617  308 -309 271 -272 imp:n=1
 710    6 0.083382617  308 -309 272 -273 imp:n=1  $ z=78.75 - tally
 711    6 0.083382617  308 -309 273 -274 imp:n=1
 712    6 0.083382617  308 -309 274 -275 imp:n=1  $ z=81.25 - tally
 713    6 0.083382617  308 -309 275 -276 imp:n=1
 714    6 0.083382617  308 -309 276 -277 imp:n=1  $ z=88.75 - tally
 715    6 0.083382617  308 -309 277 -278 imp:n=1
 716    6 0.083382617  308 -309 278 -279 imp:n=1  $ z=96.75 - tally
 717    6 0.083382617  308 -309 279 -280 imp:n=1
 718    6 0.083382617  308 -309 280 -281 imp:n=1  $ z=103.75 - tally
 719    6 0.083382617  308 -309 281 -282 imp:n=1
 720    6 0.083382617  308 -309 282 -283 imp:n=1  $ z=111.25 - tally
 721    6 0.083382617  308 -309 283 -284 imp:n=1
 722    6 0.083382617  308 -309 284 -285 imp:n=1  $ z=118.25 - tally
 723    6 0.083382617  308 -309 285 -286 imp:n=1
 724    6 0.083382617  308 -309 286 -287 imp:n=1  $ z=126.25 - tally
 725    6 0.083382617  308 -309 287 -288 imp:n=1
 726    6 0.083382617  308 -309 288 -289 imp:n=1  $ z=133.75 - tally
 727    6 0.083382617  308 -309 289 -290 imp:n=1
 728    6 0.083382617  308 -309 290 -291 imp:n=1  $ z=141.25 - tally
 729    6 0.083382617  308 -309 291 -292 imp:n=1
 730    6 0.083382617  308 -309 292 -293 imp:n=1  $ z=143.75 - tally
 731    6 0.083382617  308 -309 293 -294 imp:n=1
 732    6 0.083382617  308 -309 294 -295 imp:n=1  $ z=146.25 - tally
 733    6 0.083382617  308 -309 295 -296 imp:n=1
 734    6 0.083382617  308 -309 296 -297 imp:n=1  $ z=148.40 - tally
 735    6 0.083382617  308 -309 297 -298 imp:n=1
 736    6 0.083382617  308 -309 298 -299 imp:n=1  $ z=149.31 -  tally
 737    6 0.083382617  308 -309 299 -300 imp:n=1  $ z=149.81 - tally
 738    6 0.083382617  308 -309 300 -303 imp:n=1  $ z=150.31 - tally
 739    6 0.083382617  308 -309 303 -304 imp:n=1
 740    6 0.083382617  308 -309 304 -151 imp:n=1  $ z=151.00 - tally
c
 741    6 0.083382617  309 -313  17 -261 imp:n=1  $ radius 15.40,z=71.50 - tally
 742    6 0.083382617  309 -313 261 -262 imp:n=1
 743    6 0.083382617  309 -313 262 -263 imp:n=1  $ z=71.69 - tally
 744    6 0.083382617  309 -313 263 -264 imp:n=1
 745    6 0.083382617  309 -313 264 -265 imp:n=1  $ z=72.70 - tally
 746    6 0.083382617  309 -313 265 -267 imp:n=1  $ z=73.20 - tally
 747    6 0.083382617  309 -313 267 -268 imp:n=1
 748    6 0.083382617  309 -313 268 -269 imp:n=1  $ z=74.10 - tally
```

```
749    6 0.083382617  309 -313 269 -270 imp:n=1
750    6 0.083382617  309 -313 270 -271 imp:n=1  $ z=76.25 - tally
751    6 0.083382617  309 -313 271 -272 imp:n=1
752    6 0.083382617  309 -313 272 -273 imp:n=1  $ z=78.75 - tally
753    6 0.083382617  309 -313 273 -274 imp:n=1
754    6 0.083382617  309 -313 274 -275 imp:n=1  $ z=81.25 - tally
755    6 0.083382617  309 -313 275 -276 imp:n=1
756    6 0.083382617  309 -313 276 -277 imp:n=1  $ z=88.75 - tally
757    6 0.083382617  309 -313 277 -278 imp:n=1
758    6 0.083382617  309 -313 278 -279 imp:n=1  $ z=96.75 - tally
759    6 0.083382617  309 -313 279 -280 imp:n=1
760    6 0.083382617  309 -313 280 -281 imp:n=1  $ z=103.75 - tally
761    6 0.083382617  309 -313 281 -282 imp:n=1
762    6 0.083382617  309 -313 282 -283 imp:n=1  $ z=111.25 - tally
763    6 0.083382617  309 -313 283 -284 imp:n=1
764    6 0.083382617  309 -313 284 -285 imp:n=1  $ z=118.25 - tally
765    6 0.083382617  309 -313 285 -286 imp:n=1
766    6 0.083382617  309 -313 286 -287 imp:n=1  $ z=126.25 - tally
767    6 0.083382617  309 -313 287 -288 imp:n=1
768    6 0.083382617  309 -313 288 -289 imp:n=1  $ z=133.75 - tally
769    6 0.083382617  309 -313 289 -290 imp:n=1
770    6 0.083382617  309 -313 290 -291 imp:n=1  $ z=141.25 - tally
771    6 0.083382617  309 -313 291 -292 imp:n=1
772    6 0.083382617  309 -313 292 -293 imp:n=1  $ z=143.75 - tally
773    6 0.083382617  309 -313 293 -294 imp:n=1
774    6 0.083382617  309 -313 294 -295 imp:n=1  $ z=146.25 - tally
775    6 0.083382617  309 -313 295 -296 imp:n=1
776    6 0.083382617  309 -313 296 -297 imp:n=1  $ z=148.40 -  tally
777    6 0.083382617  309 -313 297 -298 imp:n=1
778    6 0.083382617  309 -313 298 -299 imp:n=1  $ z=149.31 - tally
779    6 0.083382617  309 -313 299 -300 imp:n=1  $ z=149.81 - tally
780    6 0.083382617  309 -313 300 -303 imp:n=1  $ z=150.31 - tally
781    6 0.083382617  309 -313 303 -304 imp:n=1
782    6 0.083382617  309 -313 304 -151 imp:n=1  $ z=151.00 - tally
c
783    6 0.083382617  313 -314  17 -151 imp:n=1  $ radius 15.75
784    6 0.083382617  314 -315  17 -261 imp:n=1  $ radius 16.05,z=71.50 - tally
785    6 0.083382617  314 -315 261 -262 imp:n=1
786    6 0.083382617  314 -315 262 -263 imp:n=1  $ z=71.69 - tally
787    6 0.083382617  314 -315 263 -264 imp:n=1
788    6 0.083382617  314 -315 264 -265 imp:n=1  $ z=72.70 - tally
789    6 0.083382617  314 -315 265 -267 imp:n=1  $ z=73.20 - tally
790    6 0.083382617  314 -315 267 -268 imp:n=1
791    6 0.083382617  314 -315 268 -269 imp:n=1  $ z=74.10 - tally
792    6 0.083382617  314 -315 269 -270 imp:n=1
793    6 0.083382617  314 -315 270 -271 imp:n=1  $ z=76.25 - tally
794    6 0.083382617  314 -315 271 -272 imp:n=1
795    6 0.083382617  314 -315 272 -273 imp:n=1  $ z=78.75 - tally
796    6 0.083382617  314 -315 273 -274 imp:n=1
797    6 0.083382617  314 -315 274 -275 imp:n=1  $ z=81.25 - tally
798    6 0.083382617  314 -315 275 -276 imp:n=1
799    6 0.083382617  314 -315 276 -277 imp:n=1  $ z=88.75 - tally
```

```
800    6 0.083382617  314 -315 277 -278 imp:n=1
801    6 0.083382617  314 -315 278 -279 imp:n=1  $ z=96.75 - tally
802    6 0.083382617  314 -315 279 -280 imp:n=1
803    6 0.083382617  314 -315 280 -281 imp:n=1  $ z=103.75 - tally
804    6 0.083382617  314 -315 281 -282 imp:n=1
805    6 0.083382617  314 -315 282 -283 imp:n=1  $ z=111.25 - tally
806    6 0.083382617  314 -315 283 -284 imp:n=1
807    6 0.083382617  314 -315 284 -285 imp:n=1  $ z=118.25 - tally
808    6 0.083382617  314 -315 285 -286 imp:n=1
809    6 0.083382617  314 -315 286 -287 imp:n=1  $ z=126.25 - tally
810    6 0.083382617  314 -315 287 -288 imp:n=1
811    6 0.083382617  314 -315 288 -289 imp:n=1  $ z=133.75 - tally
812    6 0.083382617  314 -315 289 -290 imp:n=1
813    6 0.083382617  314 -315 290 -291 imp:n=1  $ z=141.25 - tally
814    6 0.083382617  314 -315 291 -292 imp:n=1
815    6 0.083382617  314 -315 292 -293 imp:n=1  $ z=143.75 - tally
816    6 0.083382617  314 -315 293 -294 imp:n=1
817    6 0.083382617  314 -315 294 -295 imp:n=1  $ z=146.25 - tally
818    6 0.083382617  314 -315 295 -296 imp:n=1
819    6 0.083382617  314 -315 296 -297 imp:n=1  $ z=148.40 - tally
820    6 0.083382617  314 -315 297 -298 imp:n=1
821    6 0.083382617  314 -315 298 -299 imp:n=1  $ z=149.31 - tally
822    6 0.083382617  314 -315 299 -300 imp:n=1  $ z=149.81 - tally
823    6 0.083382617  314 -315 300 -303 imp:n=1  $ z=150.31 - tally
824    6 0.083382617  314 -315 303 -304 imp:n=1
825    6 0.083382617  314 -315 304 -151 imp:n=1  $ z=151.00 - tally
c
826    6 0.083382617  315 -316  17 -151 imp:n=1  $ radius 16.60
827    6 0.083382617  316 -317  17 -261 imp:n=1  $ radius 16.90 z=71.50 - tally
828    6 0.083382617  316 -317 261 -262 imp:n=1
829    6 0.083382617  316 -317 262 -263 imp:n=1  $ z=71.69 - tally
830    6 0.083382617  316 -317 263 -264 imp:n=1
831    6 0.083382617  316 -317 264 -265 imp:n=1  $ z=72.70 - tally
832    6 0.083382617  316 -317 265 -267 imp:n=1  $ z=73.20 - tally
833    6 0.083382617  316 -317 267 -268 imp:n=1
834    6 0.083382617  316 -317 268 -269 imp:n=1  $ z=74.10 - tally
835    6 0.083382617  316 -317 269 -270 imp:n=1
836    6 0.083382617  316 -317 270 -271 imp:n=1  $ z=76.25 - tally
837    6 0.083382617  316 -317 271 -272 imp:n=1
838    6 0.083382617  316 -317 272 -273 imp:n=1  $ z=78.75 - tally
839    6 0.083382617  316 -317 273 -274 imp:n=1
840    6 0.083382617  316 -317 274 -275 imp:n=1  $ z=81.25 - tally
841    6 0.083382617  316 -317 275 -276 imp:n=1
842    6 0.083382617  316 -317 276 -277 imp:n=1  $ z=88.75 - tally
843    6 0.083382617  316 -317 277 -278 imp:n=1
844    6 0.083382617  316 -317 278 -279 imp:n=1  $ z=96.75 - tally
845    6 0.083382617  316 -317 279 -280 imp:n=1
846    6 0.083382617  316 -317 280 -281 imp:n=1  $ z=103.75 - tally
847    6 0.083382617  316 -317 281 -282 imp:n=1
848    6 0.083382617  316 -317 282 -283 imp:n=1  $ z=111.25 - tally
849    6 0.083382617  316 -317 283 -284 imp:n=1
850    6 0.083382617  316 -317 284 -285 imp:n=1  $ z=118.25 - tally
```

```
851    6 0.083382617  316 -317 285 -286 imp:n=1
852    6 0.083382617  316 -317 286 -287 imp:n=1  $ z=126.25 - tally
853    6 0.083382617  316 -317 287 -288 imp:n=1
854    6 0.083382617  316 -317 288 -289 imp:n=1  $ z=133.75 - tally
855    6 0.083382617  316 -317 289 -290 imp:n=1
856    6 0.083382617  316 -317 290 -291 imp:n=1  $ z=141.25 - tally
857    6 0.083382617  316 -317 291 -292 imp:n=1
858    6 0.083382617  316 -317 292 -293 imp:n=1  $ z=143.75 - tally
859    6 0.083382617  316 -317 293 -294 imp:n=1
860    6 0.083382617  316 -317 294 -295 imp:n=1  $ z=146.25 - tally
861    6 0.083382617  316 -317 295 -296 imp:n=1
862    6 0.083382617  316 -317 296 -297 imp:n=1  $ z=148.40 - tally
863    6 0.083382617  316 -317 297 -298 imp:n=1
864    6 0.083382617  316 -317 298 -299 imp:n=1  $ z=149.31 - tally
865    6 0.083382617  316 -317 299 -300 imp:n=1  $ z=149.81 - tally
866    6 0.083382617  316 -317 300 -303 imp:n=1  $ z=150.31 - tally
867    6 0.083382617  316 -317 303 -304 imp:n=1
868    6 0.083382617  316 -317 304 -151 imp:n=1  $ z=151.00 - tally
c
869    6 0.083382617  317 -318  17 -151 imp:n=1  $ radius 17.45
870    6 0.083382617  318 -319  17 -261 imp:n=1  $ radius 17.75 z=71.50 - tally
871    6 0.083382617  318 -319 261 -262 imp:n=1
872    6 0.083382617  318 -319 262 -263 imp:n=1  $ z=71.69 - tally
873    6 0.083382617  318 -319 263 -264 imp:n=1
874    6 0.083382617  318 -319 264 -265 imp:n=1  $ z=72.70 - tally
875    6 0.083382617  318 -319 265 -267 imp:n=1  $ z=73.20 - tally
876    6 0.083382617  318 -319 267 -268 imp:n=1
877    6 0.083382617  318 -319 268 -269 imp:n=1  $ z=74.10 - tally
878    6 0.083382617  318 -319 269 -270 imp:n=1
879    6 0.083382617  318 -319 270 -271 imp:n=1  $ z=76.25 - tally
880    6 0.083382617  318 -319 271 -272 imp:n=1
881    6 0.083382617  318 -319 272 -273 imp:n=1  $ z=78.75 - tally
882    6 0.083382617  318 -319 273 -274 imp:n=1
883    6 0.083382617  318 -319 274 -275 imp:n=1  $ z=81.25 - tally
884    6 0.083382617  318 -319 275 -276 imp:n=1
885    6 0.083382617  318 -319 276 -277 imp:n=1  $ z=88.75 - tally
886    6 0.083382617  318 -319 277 -278 imp:n=1
887    6 0.083382617  318 -319 278 -279 imp:n=1  $ z=96.75 - tally
888    6 0.083382617  318 -319 279 -280 imp:n=1
889    6 0.083382617  318 -319 280 -281 imp:n=1  $ z=103.75 - tally
890    6 0.083382617  318 -319 281 -282 imp:n=1
891    6 0.083382617  318 -319 282 -283 imp:n=1  $ z=111.25 - tally
892    6 0.083382617  318 -319 283 -284 imp:n=1
893    6 0.083382617  318 -319 284 -285 imp:n=1  $ z=118.25 - tally
894    6 0.083382617  318 -319 285 -286 imp:n=1
895    6 0.083382617  318 -319 286 -287 imp:n=1  $ z=126.25 - tally
896    6 0.083382617  318 -319 287 -288 imp:n=1
897    6 0.083382617  318 -319 288 -289 imp:n=1  $ z=133.75 -  tally
898    6 0.083382617  318 -319 289 -290 imp:n=1
899    6 0.083382617  318 -319 290 -291 imp:n=1  $ z=141.25 - tally
900    6 0.083382617  318 -319 291 -292 imp:n=1
901    6 0.083382617  318 -319 292 -293 imp:n=1  $ z=143.75 - tally
```

```
902    6 0.083382617  318 -319 293 -294 imp:n=1
903    6 0.083382617  318 -319 294 -295 imp:n=1  $ z=146.25 - tally
904    6 0.083382617  318 -319 295 -296 imp:n=1
905    6 0.083382617  318 -319 296 -297 imp:n=1  $ z=148.40 - tally
906    6 0.083382617  318 -319 297 -298 imp:n=1
907    6 0.083382617  318 -319 298 -299 imp:n=1  $ z=149.31 - tally
908    6 0.083382617  318 -319 299 -300 imp:n=1  $ z=149.81 - tally
909    6 0.083382617  318 -319 300 -303 imp:n=1  $ z=150.31 - tally
910    6 0.083382617  318 -319 303 -304 imp:n=1
911    6 0.083382617  318 -319 304 -151 imp:n=1  $ z=151.00 - tally
c
912    6 0.083382617  319 -320  17 -151 imp:n=1  $ radius 18.10
913    6 0.083382617  320 -321  17 -261 imp:n=1  $ radius 18.40 z=71.50 - tally
914    6 0.083382617  320 -321 261 -262 imp:n=1
915    6 0.083382617  320 -321 262 -263 imp:n=1  $ z=71.69 - tally
916    6 0.083382617  320 -321 263 -264 imp:n=1
917    6 0.083382617  320 -321 264 -265 imp:n=1  $ z=72.70 - tally
918    6 0.083382617  320 -321 265 -267 imp:n=1  $ z=73.20 - tally
919    6 0.083382617  320 -321 267 -268 imp:n=1
920    6 0.083382617  320 -321 268 -269 imp:n=1  $ z=74.10 - tally
921    6 0.083382617  320 -321 269 -270 imp:n=1
922    6 0.083382617  320 -321 270 -271 imp:n=1  $ z=76.25 - tally
923    6 0.083382617  320 -321 271 -272 imp:n=1
924    6 0.083382617  320 -321 272 -273 imp:n=1  $ z=78.75 - tally
925    6 0.083382617  320 -321 273 -274 imp:n=1
926    6 0.083382617  320 -321 274 -275 imp:n=1  $ z=81.25 - tally
927    6 0.083382617  320 -321 275 -276 imp:n=1
928    6 0.083382617  320 -321 276 -277 imp:n=1  $ z=88.75 - tally
929    6 0.083382617  320 -321 277 -278 imp:n=1
930    6 0.083382617  320 -321 278 -279 imp:n=1  $ z=96.75 - tally
931    6 0.083382617  320 -321 279 -280 imp:n=1
932    6 0.083382617  320 -321 280 -281 imp:n=1  $ z=103.75 - tally
933    6 0.083382617  320 -321 281 -282 imp:n=1
934    6 0.083382617  320 -321 282 -283 imp:n=1  $ z=111.25 - tally
935    6 0.083382617  320 -321 283 -284 imp:n=1
936    6 0.083382617  320 -321 284 -285 imp:n=1  $ z=118.25 - tally
937    6 0.083382617  320 -321 285 -286 imp:n=1
938    6 0.083382617  320 -321 286 -287 imp:n=1  $ z=126.25 -  tally
939    6 0.083382617  320 -321 287 -288 imp:n=1
940    6 0.083382617  320 -321 288 -289 imp:n=1  $ z=133.75 - tally
941    6 0.083382617  320 -321 289 -290 imp:n=1
942    6 0.083382617  320 -321 290 -291 imp:n=1  $ z=141.25 - tally
943    6 0.083382617  320 -321 291 -292 imp:n=1
944    6 0.083382617  320 -321 292 -293 imp:n=1  $ z=143.75 - tally
945    6 0.083382617  320 -321 293 -294 imp:n=1
946    6 0.083382617  320 -321 294 -295 imp:n=1  $ z=146.25 - tally
947    6 0.083382617  320 -321 295 -296 imp:n=1
948    6 0.083382617  320 -321 296 -297 imp:n=1  $ z=148.40 - tally
949    6 0.083382617  320 -321 297 -298 imp:n=1
950    6 0.083382617  320 -321 298 -299 imp:n=1  $ z=149.31 - tally
951    6 0.083382617  320 -321 299 -300 imp:n=1  $ z=149.81 - tally
952    6 0.083382617  320 -321 300 -303 imp:n=1  $ z=150.31 - tally
```

```
 953    6 0.083382617  320 -321 303 -304 imp:n=1
 954    6 0.083382617  320 -321 304 -151 imp:n=1  $ z=151.00 - tally
c
 955    6 0.083382617  321 -322  17 -261 imp:n=1  $ radius 18.70 z=71.50 - tally
 956    6 0.083382617  321 -322 261 -262 imp:n=1
 957    6 0.083382617  321 -322 262 -263 imp:n=1  $ z=71.69 - tally
 958    6 0.083382617  321 -322 263 -264 imp:n=1
 959    6 0.083382617  321 -322 264 -265 imp:n=1  $ z=72.70 - tally
 960    6 0.083382617  321 -322 265 -267 imp:n=1  $ z=73.20 - tally
 961    6 0.083382617  321 -322 267 -268 imp:n=1
 962    6 0.083382617  321 -322 268 -269 imp:n=1  $ z=74.10 - tally
 963    6 0.083382617  321 -322 269 -270 imp:n=1
 964    6 0.083382617  321 -322 270 -271 imp:n=1  $ z=76.25 - tally
 965    6 0.083382617  321 -322 271 -272 imp:n=1
 966    6 0.083382617  321 -322 272 -273 imp:n=1  $ z=78.75 - tally
 967    6 0.083382617  321 -322 273 -274 imp:n=1
 968    6 0.083382617  321 -322 274 -275 imp:n=1  $ z=81.25 - tally
 969    6 0.083382617  321 -322 275 -276 imp:n=1
 970    6 0.083382617  321 -322 276 -277 imp:n=1  $ z=88.75 - tally
 971    6 0.083382617  321 -322 277 -278 imp:n=1
 972    6 0.083382617  321 -322 278 -279 imp:n=1  $ z=96.75 - tally
 973    6 0.083382617  321 -322 279 -280 imp:n=1
 974    6 0.083382617  321 -322 280 -281 imp:n=1  $ z=103.75 - tally
 975    6 0.083382617  321 -322 281 -282 imp:n=1
 976    6 0.083382617  321 -322 282 -283 imp:n=1  $ z=111.25 - tally
 977    6 0.083382617  321 -322 283 -284 imp:n=1
 978    6 0.083382617  321 -322 284 -285 imp:n=1  $ z=118.25 -  tally
 979    6 0.083382617  321 -322 285 -286 imp:n=1
 980    6 0.083382617  321 -322 286 -287 imp:n=1  $ z=126.25 - tally
 981    6 0.083382617  321 -322 287 -288 imp:n=1
 982    6 0.083382617  321 -322 288 -289 imp:n=1  $ z=133.75 - tally
 983    6 0.083382617  321 -322 289 -290 imp:n=1
 984    6 0.083382617  321 -322 290 -291 imp:n=1  $ z=141.25 - tally
 985    6 0.083382617  321 -322 291 -292 imp:n=1
 986    6 0.083382617  321 -322 292 -293 imp:n=1  $ z=143.75 - tally
 987    6 0.083382617  321 -322 293 -294 imp:n=1
 988    6 0.083382617  321 -322 294 -295 imp:n=1  $ z=146.25 - tally
 989    6 0.083382617  321 -322 295 -296 imp:n=1
 990    6 0.083382617  321 -322 296 -297 imp:n=1  $ z=148.40 - tally
 991    6 0.083382617  321 -322 297 -298 imp:n=1
 992    6 0.083382617  321 -322 298 -299 imp:n=1  $ z=149.31 - tally
 993    6 0.083382617  321 -322 299 -300 imp:n=1  $ z=149.81 - tally
 994    6 0.083382617  321 -322 300 -303 imp:n=1  $ z=150.31 - tally
 995    6 0.083382617  321 -322 303 -304 imp:n=1
 996    6 0.083382617  321 -322 304 -151 imp:n=1  $ z=151.00 - tally
c
 997    6 0.083382617  322 -323  17 -261 imp:n=1  $ radius 19.00 z=71.50 - tally
 998    6 0.083382617  322 -323 261 -262 imp:n=1
 999    6 0.083382617  322 -323 262 -263 imp:n=1  $ z=71.69 - tally
1000    6 0.083382617  322 -323 263 -264 imp:n=1
1001    6 0.083382617  322 -323 264 -265 imp:n=1  $ z=72.70 - tally
1002    6 0.083382617  322 -323 265 -267 imp:n=1  $ z=73.20 - tally
```

```
1003    6 0.083382617  322 -323 267 -268 imp:n=1
1004    6 0.083382617  322 -323 268 -269 imp:n=1  $ z=74.10 - tally
1005    6 0.083382617  322 -323 269 -270 imp:n=1
1006    6 0.083382617  322 -323 270 -271 imp:n=1  $ z=76.25 - tally
1007    6 0.083382617  322 -323 271 -272 imp:n=1
1008    6 0.083382617  322 -323 272 -273 imp:n=1  $ z=78.75 - tally
1009    6 0.083382617  322 -323 273 -274 imp:n=1
1010    6 0.083382617  322 -323 274 -275 imp:n=1  $ z=81.25 - tally
1011    6 0.083382617  322 -323 275 -276 imp:n=1
1012    6 0.083382617  322 -323 276 -277 imp:n=1  $ z=88.75 - tally
1013    6 0.083382617  322 -323 277 -278 imp:n=1
1014    6 0.083382617  322 -323 278 -279 imp:n=1  $ z=96.75 - tally
1015    6 0.083382617  322 -323 279 -280 imp:n=1
1016    6 0.083382617  322 -323 280 -281 imp:n=1  $ z=103.75 - tally
1017    6 0.083382617  322 -323 281 -282 imp:n=1
1018    6 0.083382617  322 -323 282 -283 imp:n=1  $ z=111.25 -  tally
1019    6 0.083382617  322 -323 283 -284 imp:n=1
1020    6 0.083382617  322 -323 284 -285 imp:n=1  $ z=118.25 - tally
1021    6 0.083382617  322 -323 285 -286 imp:n=1
1022    6 0.083382617  322 -323 286 -287 imp:n=1  $ z=126.25 - tally
1023    6 0.083382617  322 -323 287 -288 imp:n=1
1024    6 0.083382617  322 -323 288 -289 imp:n=1  $ z=133.75 - tally
1025    6 0.083382617  322 -323 289 -290 imp:n=1
1026    6 0.083382617  322 -323 290 -291 imp:n=1  $ z=141.25 - tally
1027    6 0.083382617  322 -323 291 -292 imp:n=1
1028    6 0.083382617  322 -323 292 -293 imp:n=1  $ z=143.75 - tally
1029    6 0.083382617  322 -323 293 -294 imp:n=1
1030    6 0.083382617  322 -323 294 -295 imp:n=1  $ z=146.25 - tally
1031    6 0.083382617  322 -323 295 -296 imp:n=1
1032    6 0.083382617  322 -323 296 -297 imp:n=1  $ z=148.40 - tally
1033    6 0.083382617  322 -323 297 -298 imp:n=1
1034    6 0.083382617  322 -323 298 -299 imp:n=1  $ z=149.31 - tally
1035    6 0.083382617  322 -323 299 -300 imp:n=1  $ z=149.81 - tally
1036    6 0.083382617  322 -323 300 -303 imp:n=1  $ z=150.31 - tally
1037    6 0.083382617  322 -323 303 -304 imp:n=1
1038    6 0.083382617  322 -323 304 -151 imp:n=1  $ z=151.00 - tally
c
1039    6 0.083382617  323 -324  17 -151 imp:n=1  $ radius 19.20
1040    6 0.083382617  324 -7   325 -262 imp:n=1  $ radius 19.50 z=71.50 - tally
1041    6 0.083382617  324 -7    17 -325 imp:n=1
1042    6 0.083382617  324 -7   262 -263 imp:n=1  $ z=71.69 - tally
1043    6 0.083382617  324 -7   263 -264 imp:n=1
1044    6 0.083382617  324 -7   264 -265 imp:n=1  $ z=72.70 - tally
1045    6 0.083382617  324 -7   265 -267 imp:n=1  $ z=73.20 - tally
1046    6 0.083382617  324 -7   267 -268 imp:n=1
1047    6 0.083382617  324 -7   268 -269 imp:n=1  $ z=74.10 - tally
1048    6 0.083382617  324 -7   269 -270 imp:n=1
1049    6 0.083382617  324 -7   270 -271 imp:n=1  $ z=76.25 - tally
1050    6 0.083382617  324 -7   271 -272 imp:n=1
1051    6 0.083382617  324 -7   272 -273 imp:n=1  $ z=78.75 - tally
1052    6 0.083382617  324 -7   273 -274 imp:n=1
1053    6 0.083382617  324 -7   274 -275 imp:n=1  $ z=81.25 - tally
```

```
1054    6 0.083382617  324 -7   275 -276 imp:n=1
1055    6 0.083382617  324 -7   276 -277 imp:n=1  $ z=88.75 - tally
1056    6 0.083382617  324 -7   277 -278 imp:n=1
1057    6 0.083382617  324 -7   278 -279 imp:n=1  $ z=96.75 - tally
1058    6 0.083382617  324 -7   279 -280 imp:n=1
1059    6 0.083382617  324 -7   280 -281 imp:n=1  $ z=103.75 - tally
1060    6 0.083382617  324 -7   281 -282 imp:n=1
1061    6 0.083382617  324 -7   282 -283 imp:n=1  $ z=111.25 - tally
1062    6 0.083382617  324 -7   283 -284 imp:n=1
1063    6 0.083382617  324 -7   284 -285 imp:n=1  $ z=118.25 - tally
1064    6 0.083382617  324 -7   285 -286 imp:n=1
1065    6 0.083382617  324 -7   286 -287 imp:n=1  $ z=126.25 - tally
1066    6 0.083382617  324 -7   287 -288 imp:n=1
1067    6 0.083382617  324 -7   288 -289 imp:n=1  $ z=133.75 - tally
1068    6 0.083382617  324 -7   289 -290 imp:n=1
1069    6 0.083382617  324 -7   290 -291 imp:n=1  $ z=141.25 - tally
1070    6 0.083382617  324 -7   291 -292 imp:n=1
1071    6 0.083382617  324 -7   292 -293 imp:n=1  $ z=143.75 - tally
1072    6 0.083382617  324 -7   293 -294 imp:n=1
1073    6 0.083382617  324 -7   294 -295 imp:n=1  $ z=146.25 - tally
1074    6 0.083382617  324 -7   295 -296 imp:n=1
1075    6 0.083382617  324 -7   296 -297 imp:n=1  $ z=148.40 - tally
1076    6 0.083382617  324 -7   297 -298 imp:n=1
1077    6 0.083382617  324 -7   298 -299 imp:n=1  $ z=149.31 - tally
1078    6 0.083382617  324 -7   299 -300 imp:n=1  $ z=149.81 - tally
1079    6 0.083382617  324 -7   300 -303 imp:n=1  $ z=150.31 - tally
1080    6 0.083382617  324 -7   326 -151 imp:n=1
1081    6 0.083382617  324 -7   303 -326 imp:n=1  $ z=151.00 - tally

c
c      Surface cells
c
   1  cz   9.0
   2  cz   12.1
   3  cz   12.6
   4  cz   13.36
   5  cz   13.97
   6  cz   14.0
   7  cz   19.5
   8  cz   19.61
   9  cz   20.22
 900  cz   20.28
  10  cz   20.78
  11  cz   40.0
  12  pz   0.0
  13  pz   35.0
  14  pz   40.0
  15  pz   13.9
  16  pz   53.0
  17  pz   71.0
  18  pz   113.9
  19  pz   154.629
```

```
c
c    Beam tube 1
c
  20  gq   1.2842759e-1 8.7157241e-1 1.0 6.6913061e-1 1.439452e-15
           -3.7499006e-15 3.9392669e1 1.0262141e2 -1.72e2 1.0360484e4
  21  p    -9.3358043e-1 3.5836795e-1 -2.0083436e-15 8.6802007
  22  p    -9.3358043e-1 3.5836795e-1 -2.0083436e-15 9.1680201e1
  23  gq   1.2842759e-1 8.7157241e-1 1.0 6.6913061e-1 1.439452e-15
           -3.7499006e-15 3.9392669e1 1.0262141e2 -1.72e2 1.0357444e4
c
c    Beam tube 2
c
  24  gq   3.126967e-1 6.873033e-1 1.0 9.2718385e-1 1.0536957e-15
           -1.5621681e-15 5.1328843e1 7.609814e1 -1.72e2 9.4773943e3
  25  p    -8.2903757e-1 5.591929e-1 -9.4215763e-16 2.4408518e1
  26  p    -8.2903757e-1 5.591929e-1 -9.4215763e-16 1.0090852e2
  27  gq   3.126967e-1 6.873033e-1 1.0 9.2718385e-1 1.0536957e-15
           -1.5621681e-15 5.1328843e1 7.609814e1 -1.72e2 9.4753543e3
c
c    Beam tube 3
c
  28  gq   9.9969541e-1 3.048649e-4 1.0 3.4899497e-2 -6.858948e-15
           1.1972403e-16 8.5588899e1 1.4939598 -2.72e2 2.0302923e4
  29  p    1.7452406e-2 -9.998477e-1 -3.4300148e-15 -6.047901
  30  p    1.7452406e-2 -9.998477e-1 -3.4300148e-15 9.5152099e1
  31  gq   9.9969541e-1 3.0458649e-4 1.0 3.4899497e-2 -6.8589848e-15
           1.1972403e-16 8.5588899e1 1.4939598 -2.72e2 2.0300883e4
c
c    Beam tube 4
c
  32  gq   7.9389263e-1 2.0610737e-1 1.0 8.0901699e-1 -2.7190548e-15
           1.3854276e-15 8.0036531e1 4.0780649e1 -2.22e2 1.4313227e4
  33  p    4.539905e-1 -8.9100652e-1 -1.5258333e-15 1.5821156
  34  p    4.539905e-1 -8.9100652e-1 -1.5258333e-15 9.2582116e1
  35  gq   7.9389263e-1 2.0610737e-1 1.0 8.0901699e-1 -2.7190548e-15
           1.3854276e-15 8.0036531e1 4.0780649e1 -2.22e2 1.4311187e4
c
c    Beam tube 6
c
   36  gq   6.3781868e-1 3.6218132e-1 1.0 9.612617e-1 -1.0976368e-15
           8.2712862e-16 -7.8218928e1 -5.894219e1 -2.42e2 1.7014096e4
  37  p    6.0181502e-1 -7.9863551e-1 -6.8719506e-16 1.3111231e1
  38  p    6.0181502e-1 -7.9863551e-1 -6.8719506e-16 1.0111123e2
  39  gq   6.3781868e-1 3.6218132e-1 1.0 9.612617e-1 -1.0976368e-15
           8.2712862e-16 -7.8218928e1 -5.894219e1 -2.42e2 1.7012056e4
c
c    Beam tube 7
c
  40  gq   9.1451879e-1 8.5481214e-2 1.0 5.591929e-1 -4.433639e-15
           1.3554995e-15 -8.59927e1 -2.6290607e1 -2.52e2 1.7872485e4
  41  p    2.923717e-1 -9.5630476e-1 -2.3181099e-15 5.4849705
  42  p    2.923717e-1 -9.5630476e-1 -2.3181099e-15 1.0298497e2
```

```
  43  gq   9.1451879e-1 8.5481214e-2 1.0 5.591929e-1 -4.433639e-15
           1.3554995e-15 -8.59927e1 -2.6290607e1 -2.52e2 1.7870445e4
c
c    Beam tube 8
c
  44  gq   4.1317591e-1 5.8682409e-1 1.0 -9.8480775e-1 -6.3236299e-15
           -7.5362086e-15 -6.086621e1 7.2537524e1 -1.72e2 9.612597e3
  45  p    7.6604444e-1 6.4278761e-1 4.9189108e-15 -8.264593e-1
  46  p    7.6604444e-1 6.4278761e-1 4.9189108e-15 8.747354e1
  47  gq   4.1317591e-1 5.8682409e-1 1.0 -9.8480775e-1 -6.3236299e-15
           -7.5362086e-15 -6.086621e1 7.2537524e1 -1.72e2 9.610557e3
c
c    Beam tube 9
c
  48  gq   2.2040355e-1 7.7959645e-1 1.0 -8.2903757e-1 -4.433639e-15
           -8.3384622e-15 1.0625745e1 -1.998412e1 -2.52e2 1.5979068e4
  49  p    8.8294759e-1 4.6947156e-1 4.7219463e-15 6.4344558e1
  50  p    8.8294759e-1 4.6947156e-1 4.7219463e-15 1.1314456e2
  51  gq   2.2040355e-1 7.7959645e-1 1.0 -8.2903757e-1 -4.433639e-15
           -8.3384622e-15 1.0625745e1 -1.998412e1 -2.52e2 1.5977028e4
c
c    Beam tube 10
c
  52  gq   9.9513403e-1 4.8659656e-3 1.0 1.391731e-1 -6.4630636e-15
           4.5194143e-16 -8.3130253e1 -5.8130336 -2.52e2 1.7587108e4
  53  p    -6.9756474e-2 9.9756405e-1 3.2394228e-15 4.6807504e1
  54  p    -6.9756474e-2 9.9756405e-1 3.2394228e-15 1.000075e2
  55  gq   9.9513403e-1 4.8659656e-3 1.0 1.391731e-1 -6.4630636e-15
            4.5194143e-16 -8.3130253e1 -5.8130336 -2.52e2 1.7585068e4
c
c    Beam tube 11
c
  56  gq   7.1658198e-1 2.7414644e-1 1.0 9.0712729e-1 -1.9013903-15
           1.1881205e-15 -8.6309466 -6.0130121 -1.82e2 8.3011438e3
  57  p    -5.2991926e-1 8.480481e-1 1.1107409e-15 4.9544795e1
  58  p    -5.2991926e-1 8.480481e-1 1.1107409e-15 1.0834479e2
  59  gq   7.1658198e-1 2.7414644e-1 1.0 9.0712729e-1 -1.9013903e-15
           1.1881205e-15 -8.6105367 -6.0456754 -1.82e2 8.3000121e3
c
c    Beam tube 13
c
  60  gq   2.5e-1 7.5e-1 1.0 -8.660254e-1 -4.7694522e-15
           -8.2609336e-15 -5.8232221e1 1.0086117e2 -1.62e2 9.9269916e3
  61  p    8.660254e-1 5.0e-1 4.7694522e-15 -8.9738835e1
  62  p    8.660254e-1 5.0e-1 4.7694522e-15 8.8661165e1
  63  gq   2.5e-1 7.5e-1 1.0 -8.660254e-1 -4.7694522e-15
           -8.2609336e-15 -5.8232221e1 1.0086117e2 -1.62e2 9.9249516e3
c
c    Cold source - cell 14
c
  64  c/z  -6.18e1 3.28e1 1.5
  65  c/z  -6.18e1 3.28e1 1.6
```

```
  66  c/z  -6.18e1 3.28e1 1.95e1
  67  c/z  -6.18e1 3.28e1 2.0e1
  68  c/z  -6.18e1 3.28e1 2.04e1
  69  c/z  -6.18e1 3.28e1 4.5
  70  pz   1.065e2
  71  pz   1.105e2
  72  pz   1.11e2
  73  pz   1.6e2
  74  pz   1.605e2
  75  pz   1.609e2
  77  c/z  -6.18e1 3.28e1 9.25
  78  c/z  -6.18e1 3.28e1 9.5
  79  c/z  -6.18e1 3.28e1 2.05e1
  80  pz   1.064e2
c
c    Hot source - cell 15
c
  82  c/z  3.75e1 3.25e1 1.55e1
  83  pz   1.01e2
  85  c/z  3.75e1 3.25e1 1.5e1
  86  pz   1.02e2
  87  pz   1.44e2
  88  pz   1.45e2
  89  c/z  3.75e1 3.25e1 1.35e1
  90  pz   1.03e2
  91  pz   1.43e2
  92  c/z  3.75e1 3.25e1 1.32e1
  93  pz   1.033e2
  94  pz   1.427e2
  95  c/z  3.75e1 3.25e1 1.0e1
  96  pz   1.08e2
  97  pz   1.38e2
  98  pz   1.22e2
  99  pz   1.24e2
 100  c/z  3.75e1 3.25e1 1.00
c
c    Beam tube 16
c
 101  c/z  -5.22e1 7.45e1 2.0
 102  pz   1.11e2
 103  pz   2.31e2
 104  c/z  -5.22e1 7.45e1 2.2
c
c    Beam tube 17
c
 105  c/z  3.9 3.73e1 2.0
 106  pz   1.31e2
 108  c/z  3.9 3.73e1 2.2
c
c    Beam tube 19 - from 19a results
c
 109  gq   8.9755635e-1 1.5267081e-1 9.4977284e-1 5.8924867e-1 4.1259636e-1
```

```
          -1.4346363e-1 1.0120434e2 -2.4350297e1 -2.4454883e2 1.7634846e4
 110  p    3.200682e-1 -9.2050485e-1 2.2411417e-1 6.1243727e1
 111  p    3.200682e-1 -9.2050485e-1 2.2411417e-1 1.4124373e2
 112  gq   8.9755635e-1 1.5267081e-1 9.4977284e-1 5.8924867e-1 4.1259636e-1
          -1.4346363e-1 1.0120434e2 -2.4350297e1 -2.4454883e2 1.7632806e4
c
c    Beam tube 21 - from 21a results
c
 113  gq   6.7620392e-1 4.8255025e-1 8.4124583e-1 8.1865304e-1 5.7322703e-1
          -4.5344891e-1 -2.3517413e1 -1.3604388e2 -2.1202619e2 1.5979028e4
 114  p    5.6903082e-1 -7.193398e-1 3.9843967e-1 6.7731469e1
 115  p    5.6903982e-1 -7.193398e-1 3.9843967e-1 1.6103147e2
 116  gq   6.7620392e-1 4.8255025e-1 8.4124583e-1 8.1865304e-1 5.7322703e-1
          -4.5344891e-1 -2.3517413e1 -1.3604388e2 -2.1202619e2 1.5976988e4
c
c    Beam tube 22 - from 22a results
c
 117  gq   6.878947e-1 4.6512176e-1 8.469777e-1 -8.1715663e-1 -5.7217923e-1
          -4.3707697e-1 1.1929125e2 1.8823231e1 -2.0555643e2  1.4184522e4
 118  p    5.5866035e-1 7.313537e-1 3.9117819e-1 8.4926917e1
 119  p    5.5866035e-1 7.313537e-1 3.9117819e-1 1.6892692e2
 120  gq   6.878343e-1 4.6512176e-1 8.469481e-1 -8.1715663e-1 -5.7217923e-1
          -4.3716155e-1 1.1930128e2 1.8823231e1 -2.0554941e2 1.4182065e4
c
c    Beam tube 23
c
 121  c/z  3.75e1 -6.49e1 10.0
 122  pz   1.0
 124  c/z  3.75e1 -6.49e1 1.02e1
c
c    Beam tube 24 - from 24a results
c
 125  gq   7.227548e-1 4.1317591e-1 8.6406929e-1 -8.0670728e-1 5.6486252e-1
          3.8825835e-1 7.0420299e1 -1.5074281e2 -2.1263661e2 1.8199186e4
 126  p    -5.2654078e-1 -7.6604444e-1 3.6868783e-1 8.05063e1
 127  p    -5.2654078e-1 -7.6604444e-1 3.6868783e-1 1.155063e2
 128  gq   7.227548e-1 4.1317591e-1 8.6406929e-1 -8.0670728e-1 5.6486252e-1
          3.8825835e-1 7.0420299e1 -1.5074281e2 -2.1263661e2 1.8197146e4
c
c    Safety rod 1 (just the rod - bottom is surface 12 and top of the
c                  safety rods is surface 134)
c
c    The top and bottom of the rod is the same for all the rods.
c    These are the outer diameter of the cladding.
c
 129  gq   1.0 1.0 2.4380884e-29 1.110223e-16 6.9829627e-15
          6.9829627e-15 -6.2019713e1 2.2573329e1 -1.3772631e-13 1.06875e3
c
c    Safety rod 2
c
 130  gq   1.0 1.0 2.4380884e-29 0.0 6.9829627e-15
          6.9829627e-15 -5.0558933e1 -4.2423982e1 -3.2464812e-13 1.06875e3
```

```
c
c    Safety rod 3
c
 131  gq   1.0 1.0 2.4380884e-29 1.110223e-16 6.9829627e-15
           6.9829627e-15 6.2019713e1 -2.2573329e1 1.3772631e-13 1.06875e3
c
c    Safety rod 4
c
 132  gq   1.0 1.0 2.4380884e-29 -5.5511151e-17 6.9829627e-15
           6.9829627e-15 1.146078e1 -6.4997312e1 -1.869218e-13  1.06875e3
c
c    Safety rod 5
c
 133  gq   1.0 1.0 2.4380884e-29 0.0 6.9829627e-15
           6.9829627e-15 5.0558933e1 4.2423982e1 3.2464812e-13 1.06875e3
c
c    Safety rod 6
c
 134  gq   1.0 1.0 2.4380884e-29 -5.5511151e-17 6.9829627e-15
           6.9829627e-15 -1.146078e1 6.4997312e1 1.869218e-13 1.06875e3
 135  pz   100.0
c
c    The encompassing sphere around everything to check geometry
c
 136  so   500
 137  px   0.0
 138  py   0.0
c
c    The borated regions on top and below the core
c
1138  pz   151.6
 139  pz   151.833
 140  pz   152.066
 141  pz   152.299
 142  pz   152.532
 143  pz   152.765
 144  pz   152.998
 145  pz   153.231
 146  pz   153.464
 147  pz   153.697
 148  pz   153.93
 149  pz   154.163
 150  pz   154.396
 151  pz   151.00
 152  pz   70.167
 153  pz   69.934
 154  pz   69.701
 155  pz   69.468
 156  pz   69.235
 157  pz   69.002
 158  pz   68.769
 159  pz   68.536
```

```
 160  pz   68.303
 161  pz   68.070
 162  pz   67.837
 163  pz   67.604
1164  pz   70.4
c
c      The inside rings of the safety rods
c
c      Safety rod 1 (all the safety rods will follow the same  pattern
c                   for the surfaces as seen below)
c
c      Inner diameter of outer cladding/outer diameter of cadium
c
 164  gq   1.0 1.0 2.4380884e-29 1.110223e-16 6.9829627e-15
           6.9829627e-15 -6.2019713e1 2.2573329e1 -1.3772631e-13 1.0691975e3
c
c      Inner diameter of cadium/outer diameter of inner cladding
c
 165  gq   1.0 1.0 2.4380884e-29 1.110223e-16 6.9829627e-15
           6.9829627e-15 -6.2019713e1 2.2573329e1 -1.3772631e-13 1.0709375e3
c
c      Inner diameter of inner cladding/outer diameter of d2o channel
c
 166  gq   1.0 1.0 2.4380884e-29 1.110223e-16 6.9829627e-15
           6.9829627e-15 -6.2019713e1 2.2573329e1 -1.3772631e-13 1.07136e3
c
c      Inner diameter of d2o channel/outer diameter of Al guide tube
c
 167  gq   1.0 1.0 2.4380884e-29 1.110223e-16 6.9829627e-15
           6.9829627e-15 -6.2019713e1 2.2573329e1 -1.3772631e-13 1.085e3
c
c      Inner diameter of Al guide tube/inner cylinder of d2o
c
 168  gq   1.0 1.0 2.4380884e-29 1.110223e-16 6.9829627e-15
           6.9829627e-15 -6.2019713e1 2.2573329e1 -1.3772631e-13 1.08644e3
c
c      Safety rod 2
c
 169  gq   1.0 1.0 2.4380884e-29 0.0 6.9829627e-15
           6.9829627e-15 -5.0558933e1 -4.2423982e1 -3.2464812e-13 1.0691975e3
 170  gq   1.0 1.0 2.4380884e-29 0.0 6.9829627e-15
           6.9829627e-15 -5.0558933e1 -4.2423982e1 -3.2464812e-13 1.0709375e3
 171  gq   1.0 1.0 2.4380884e-29 0.0 6.9829627e-15
           6.9829627e-15 -5.0558933e1 -4.2423982e1 -3.2464812e-13 1.07136e3
 172  gq   1.0 1.0 2.4380884e-29 0.0 6.9829627e-15
           6.9829627e-15 -5.0558933e1 -4.2423982e1 -3.2464812e-13 1.085e3
 173  gq   1.0 1.0 2.4380884e-29 0.0 6.9829627e-15
           6.9829627e-15 -5.0558933e1 -4.2423982e1 -3.2464812e-13 1.08644e3
c
c      Safety rod 3
 c
 174  gq   1.0 1.0 2.4380884e-29 1.110223e-16 6.9829627e-15
```

```
            6.9829627e-15 6.2019713e1 -2.2573329e1 1.3772631e-13 1.0691975e3
 175  gq    1.0 1.0 2.4380884e-29 1.110223e-16 6.9829627e-15
            6.9829627e-15 6.2019713e1 -2.2573329e1 1.3772631e-13 1.0709375e3
 176  gq    1.0 1.0 2.4380884e-29 1.110223e-16 6.9829627e-15
            6.9829627e-15 6.2019713e1 -2.2573329e1 1.3772631e-13 1.07136e3
 177  gq    1.0 1.0 2.4380884e-29 1.110223e-16 6.9829627e-15
            6.9829627e-15 6.2019713e1 -2.2573329e1 1.3772631e-13 1.085e3
 178  gq    1.0 1.0 2.4380884e-29 1.110223e-16 6.9829627e-15
            6.9829627e-15 6.2019713e1 -2.2573329e1 1.3772631e-13 1.08644e3
c
c      Safety rod 4
c
 179  gq    1.0 1.0 2.4380884e-29 -5.5511151e-17 6.9829627e-15
            6.9829627e-15 1.146078e1 -6.4997312e1 -1.869218e-13 1.0691975e3
 180  gq    1.0 1.0 2.4380884e-29 -5.5511151e-17 6.9829627e-15
            6.9829627e-15 1.146078e1 -6.4997312e1 -1.869218e-13 1.0709375e3
 181  gq    1.0 1.0 2.4380884e-29 -5.5511151e-17 6.9829627e-15
            6.9829627e-15 1.146078e1 -6.4997312e1 -1.869218e-13 1.07136e3
 182  gq    1.0 1.0 2.4380884e-29 -5.5511151e-17 6.9829627e-15
            6.9829627e-15 1.146078e1 -6.4997312e1 -1.869218e-13 1.085e3
 183  gq    1.0 1.0 2.4380884e-29 -5.5511151e-17 6.9829627e-15
            6.9829627e-15 1.146078e1 -6.4997312e1 -1.869218e-13 1.08644e3
c
c      Safety rod 5
c
 184  gq    1.0 1.0 2.4380884e-29 0.0 6.9829627e-15
            6.9829627e-15 5.0558933e1 4.2423982e1 3.2464812e-13 1.0691975e3
 185  gq    1.0 1.0 2.4380884e-29 0.0 6.9829627e-15
            6.9829627e-15 5.0558933e1 4.2423982e1 3.2464812e-13 1.0709375e3
 186  gq    1.0 1.0 2.4380884e-29 0.0 6.9829627e-15
            6.9829627e-15 5.0558933e1 4.2423982e1 3.2464812e-13 1.07136e3
 187  gq    1.0 1.0 2.4380884e-29 0.0 6.9829627e-15
            6.9829627e-15 5.0558933e1 4.2423982e1 3.2464812e-13 1.085e3
 188  gq    1.0 1.0 2.4380884e-29 0.0 6.9829627e-15
            6.9829627e-15 5.0558933e1 4.2423982e1 3.2464812e-13 1.08644e3
c
c      Safety rod 6
 c
 189  gq    1.0 1.0 2.4380884e-29 -5.5511151e-17 6.9829627e-15
            6.9829627e-15 -1.146078e1 6.4997312e1 1.869218e-13 1.0691975e3
 190  gq    1.0 1.0 2.4380884e-29 -5.5511151e-17 6.9829627e-15
            6.9829627e-15 -1.146078e1 6.4997312e1 1.869218e-13 1.0709375e3
 191  gq    1.0 1.0 2.4380884e-29 -5.5511151e-17 6.9829627e-15
            6.9829627e-15 -1.146078e1 6.4997312e1 1.869218e-13 1.07136e3
 192  gq    1.0 1.0 2.4380884e-29 -5.5511151e-17 6.9829627e-15
            6.9829627e-15 -1.146078e1 6.4997312e1 1.869218e-13 1.085e3
 193  gq    1.0 1.0 2.4380884e-29 -5.5511151e-17 6.9829627e-15
            6.9829627e-15 -1.146078e1 6.4997312e1 1.869218e-13 1.08644e3
c
c      The reflector tank
c
 194  cz    115                    $ inner diameter
```

```
 195  pz   221                    $ height
 196  cz   116                    $ outer diameter
c
c      The structures above the core
c
 197  cz   21.5                   $ outer diameter of more outer tank per drawing
 198  cz   21.7                   $ outer diameter of more outer tank per drawing
 199  pz   175                    $ bottom of cross beam per drawing
 200  pz   180                    $ top of cross beam per drawing
 201  pz   185                    $ top of inner cylinder per drawing
c
c      Surfaces for the core power distribution tallies
c
 261  pz   71.50
 262  pz   71.69
 263  pz   72.19
 264  pz   72.20
 265  pz   72.70
 267  pz   73.20
 268  pz   73.60
 269  pz   74.10
 270  pz   75.75
 271  pz   76.25
 272  pz   78.25
 273  pz   78.75
 274  pz   80.75
 275  pz   81.25
 276  pz   88.25
 277  pz   88.75
 278  pz   95.75
 279  pz   96.25
 280  pz   103.25
 281  pz   103.75
 282  pz   110.75
 283  pz   111.25
 284  pz   118.25
 285  pz   118.75
 286  pz   125.75
 287  pz   126.25
 288  pz   133.25
 289  pz   133.75
 290  pz   140.75
 291  pz   141.25
 292  pz   143.25
 293  pz   143.75
 294  pz   145.75
 295  pz   146.25
 296  pz   147.90
 297  pz   148.40
 298  pz   148.81
 299  pz   149.31
 300  pz   149.81
```

```
 303  pz   150.31
 304  pz   150.50
 306  cz   14.20
 307  cz   14.50
 308  cz   14.80
 309  cz   15.10
 313  cz   15.40
 314  cz   15.75
 315  cz   16.05
 316  cz   16.60
 317  cz   16.90
 318  cz   17.45
 319  cz   17.75
 320  cz   18.10
 321  cz   18.40
 322  cz   18.70
 323  cz   19.00
 324  cz   19.20
 325  pz   71.19
 326  pz   150.81

c
c
c      MCNP Control Information
c
c
kcode  10000 1.0 5 80
c
prdmp  80 10 80
c
ksrc   14.2 0 79       12 12 92       0 -19.3 79      -14.2 0 131
       19.3 0 157      -19.3 0 105    0 -14.2 144     -12 -12 79
       -12 12 118      0 19.3 105     0 -19.3 157     14.2 0 92
        -12 12 79       12 -12 105     0 -14.2 92      0 -14.2 118
       12 -12 131      -19.3 0 131    0 14.2 79       0 19.3 157
       -12 12 105      19.3 0 92      12 12 144       0 -14.2 131
       19.3 0 79       0 19.3 144     12 -12 144      12 12 105
       14.2 0 157      0 -14.2 79     0 -19.3 131     -14.2 0 92
       12 -12 157      0 14.2 118     -12 12 92       19.3 0 131
       0 -19.3 118     19.3 0 144     -12 -12 105     -14.2 0 105
       0 19.3 79       12 12 131      14.2 0 118      0 14.2 157
       -12 -12 92      -19.3 0 79     0 -14.2 157     14.2 0 105
       -12 12 144      19.3 0 118     0 -19.3 92      12 12 79
       -14.2 0 157     -12 -12 118    14.2 0 144      12 -12 118
       -19.3 0 92      0 -19.3 144    -14.2 0 79      -12 12 157
       12 -12 79       14.2 0 131     -19.3 0 118     0 -14.2 105
       0 19.3 92       -19.3 0 157    -12 12 131      12 -12 92
       0 19.3 131      -12 -12 131    0 14.2 92       -12 -12 157
       -14.2 0 144     0 14.2 144     0 -19.3 105     12 12 157
       -12 -12 144     19.3 0 105     0 14.2 131      12 12 118
       -19.3 0 144     0 19.3 118     0 14.2 105      -14.2 0 118
c
```

```
c     ------------------------------------------------------------------ -----
c
mode   n
c
c
c      The material compositions were taken from the report by Glaser, et.al.
c      "Verifizierung des dreidimensionalen Rechencodes MORSE-K durch
c       Nachrechen des kritischen Experimentes FOEHN", dated Jan. 16, 1991.
c
c      The elements are defined by atomic density in units of barns/cm,
c      Except in the case of materials 4 and 5, which are single elements.
c      Therefore an atomic fraction of 1 was used.
c
c
c      Material 1 - unborated d2o
c
m1      1002.55c 0.06637     1001.50c 0.000133    8016.50c 0.03325
mt1    hwtr.01t
c
c      Material 2 - borated d2o
c
m2      1002.55c 0.06637     1001.50c 0.000133    8016.50c 0.03325
        5010.50c 1.0646e-5
mt2    hwtr.01t
c
c      Material 3 - element Aluminum used for structural material
c
m3     13027.50c 0.031673    1002.55c 0.0103347   8016.50c  0.0051673
       27059.50c 2.1221e-8  24000.50c 6.493e-5   25055.50c 1.1323e-4
       26000.55c 6.9681e-5  28000.50c 6.6513e-7  29000.50c 6.3346e-7
       31000.50c 4.4342e-6  73181.50c 3.1673e-10 90232.50c 4.751e-9
mt3    hwtr.01t
c
c      Material 4 - boron used for the end plates
c
m4      5010.50c 1.0
c
c      Material 5 - cadium used in the safety rods
c
m5     48000.50c 1.0
c
c      Material 6 - fuel zone - the core
c
m6     92235.50c 0.0004736  92238.50c 0.0000468   1001.50c 0.000078
        8016.50c 0.019432    1002.55c 0.038786   13027.50c 0.02456
       27059.50c 1.6455e-8  24000.50c 5.0348e-5  25055.50c 8.7801e-5
       26000.55c 5.4032e-5  28000.50c 5.1576e-7  29000.50c 4.912e-7
       31000.50c 3.4384e-6  73181.50c 2.456e-10  90232.50c 3.684e-9
        5010.50c 6.3578e-6
mt6    hwtr.01t
c
c      Material 7 - graphite used in the hot cell
```

```
c
m7      6000.50c 1.67e-2
mt7    grph.08t
c
c      Material 8 - aluminum with borated water-outer wall of core tube
c
m8     13027.50c 0.02654     1001.50c 0.735e-4    1002.55c 0.036682
        8016.50c  0.01838    5010.50c 5.8841e-6  27059.50c 1.6455e-8
       24000.50c 5.0348e-5  25055.50c 8.7801e-5  26000.55c 5.4032e-5
       28000.50c 5.1576e-7  29000.50c 4.912e-7   31000.50c 3.4384e-6
       73181.50c 2.456e-10  90232.50c 3.684e-9
mt8    hwtr.01t
c
c      Material 9 - zircaloy-4
c
m9     26000.55c 1.695e-4   40000.50c 4.21162e-2 50000.35c 5.185e-4
c
c      Material 10 - nickel - used in the control rod
c
m10    28000.50c 9.13e-2
c
 c      Material 11 - stainless steel - safety rod cladding
c
m11    24000.50c 1.4156e-2  25055.50c 9.77323e-4 26000.55c 5.70399e-2
       28000.50c 1.09566e-2 42000.50c 1.60059e-3
c
c      Material 12 - 100% aluminum for piping/tankwalls/cells/etc.
c
m12    13027.50c 0.047175   27059.50c 4.0334e-8  24000.50c 1.2341e-4
       25055.50c 2.15215e-4 26000.55c 1.3244e-4  28000.50c 1.2642e-6
       29000.50c 1.204e-6   31000.50c 8.4280e-6  73181.50c 6.020e-10
       90232.50c 9.030e-9
c
c      Material 13 - inner core tank wall/outer tank wall w/o boron
c
m13    13027.50c 0.02654     1001.50c 0.735e-4    1002.55c 0.036682
       27059.50c 1.6455e-8  24000.50c 5.0348e-5  25055.50c 8.7801e-5
       26000.55c 5.4032e-5  28000.50c 5.1576e-7  29000.50c 4.912e-7
       31000.50c 3.4384e-6  73181.50c 2.456e-10  90232.50c 3.684e-9
        8016.50c 0.01838
mt13   hwtr.01t
c
c      Material 14 - solid boron zone - material #56 from eckert
c
m14     1002.55c 0.03867     8016.50c 0.01938     1001.50c 0.000078
       13027.50c 0.0248      5010.50c 1.517e-4   27059.50c 1.5376e-8
       24000.50c 4.7047e-5  25055.50c 8.2045e-5  26000.55c 5.0490e-5
       28000.50c 4.8195e-7  29000.50c 4.590e-7   31000.50c 3.2130e-6
       73181.50c 2.295e-10  90232.50c 3.4425e-9
mt14   hwtr.01t
c
c      TALLY INPUT
```

```
c
c
c       Tallies for power at radius 14.50,14.80,15.10 cm at various heights
c
f7:n    615 617 619 620 622 624 626 628 630 632 634 636 638 640 642 644 646
        648 650 652 653 654 656 657 659 661 662 664 666 668 670 672 674 676 678
        680 682 684 686 688 690 692 694 695 696 698 699 701 703 704 706 708 710
        712 714 716 718 720 722 724 726 728 730 732 734 736 737 738 740
c
c       Tallies for power at radius 15.4 , 16.05,16.6 cm at various heights
 c
f17:n   741 743 745 746 748 750 752 754 756 758 760 762 764 766 768 770 772
        774 776 778 779 780 782 784 786 788 789 791 793 795 797 799 801 803 805
        807 809 811 813 815 817 819 821 822 823 825 827 829 831 832 834 836 838
        840 842 844 846 848 850 852 854 856 858 860 862 864 865 866 868
c
c       Tallies for power at radius 17.75,18.40,18.70 cm at various heights
c
f27:n   870 872 874 875 877 879 881 883 885 887 889 891 893 895 897 899 901
        903 905 907 908 909 911 913 915 917 918 920 922 924 926 928 930 932 934
        936 938 940 942 944 946 948 950 951 952 954 955 957 959 960 962 964 966
        968 970 972 974 976 978 980 982 984 986 988 990 992 993 994 996
c
c       Tallies for power at radius 19.0, 19.2 cm at various heights
c
f37:n    997  999 1001 1002 1004 1006 1008 1010 1012 1014 1016 1018 1020
        1022 1024 1026 1028 1030 1032 1034 1035 1036 1038 1040 1042 1044 1045
        1047 1049 1051 1053 1055 1057 1059 1061 1063 1065 1067 1069 1071 1073
        1075 1077 1078 1079 1081
```

INTERNAL DISTRIBUTION

1. J. L. Anderson
2. B. R. Appleton
3. R. S. Booth
4–5. J. H. Campbell
6. R. D. Cheverton
7. H. L. Dodds
8. W. W. Engle
9. G. F. Flanagan
10. F. Gallmeier
11. J. C. Gehin
12–13. M. L. Gildner
14. R. M. Harrington
15. J. B. Hayter
16. D. T. Ingersoll
17–20. R. L. Johnson
21. K. H. King-Jones
22. R. A. Lillie
23. J. A. March-Leuba
24. T. J. McManamy
25. J. T. Mihalczo
26. T. F. Orlin
27. C. C. Queen
28. J. P. Renier
29–33. D. L. Selby
34. P. B. Thompson
35. A. W. Trivelpiece
36. C. D. West
37. G. L. Yoder
38. ORNL Patent Office
39. Central Research Library, Document Reference Section
40. Y-12 Technical Library
41–42. Laboratory Records
43. Laboratory Records (RC)

EXTERNAL DISTRIBUTION

44. R. Awan, Division of Energy Research Reactors, Office of Nuclear Energy, Department of Energy, NE-473, Washington, DC 20585
45. P. Ageron, Institut Laue Langevin, 156X 38042, Grenoble Cedex, France
46. K. Böning, Fakultät für Physik E21, Technische Universität München, D-8046, Garching, Germany
47. J. Carew, Brookhaven National Laboratory, Building 475-B, Upton, NY 11973
48. J. Hendricks, Los Alamos National Laboratory, Group X6, P.O. Box 1663, Los Alamos, NM 87545
49. A. F. Henry, Professor, Department of Nuclear Engineering, Massachusetts Institute of Technology, 77 Massachusetts Avenue, Cambridge, MA 02139
50. H. C. Honeck, Computer Application Technology, Inc., 621 Colleton Avenue SE, Aiken, SC 29801
51. R. A. Hunter, Director, Office of Facilities, Fuel Cycle/Test Programs, Department of Energy, NE-47, Washington, DC 20585
52. J. A. Lake, Manager, Nuclear Engineering and Reactor Design, Idaho National Engineering Labortory, P.O. Box 1625, Idaho Falls, ID 83415
53. R. F. Lidstone, Atomic Energy of Canada, Ltd., Whiteshell Nuclear Research Establishment, Pinawa, Manitoba, ROE 1L0, Canada

54. R. C. Little, Los Alamos National Laboratory, Group X6, P.O. Box 1663, Los Alamos, NM 87545
55. T. F. Luera, PhD Manager, Program Development, Reactor Engineering Center, Sandia National Laboratories, Dept. 65006, P.O. Box 5800, Albuquerque, NM 87185
56. M. Milgram, Atomic Energy of Canada, Ltd., Research Company, Chalk River Nuclear Laboratories, Chalk River, Ontario, K0J 1J0, Canada
57. A. M. Ougouag, Idaho National Engineering Laboratory, P.O. Box 1625, Idaho Falls, ID 83415
58. E. Redmond, Department of Nuclear Engineering, Massachusetts Institute of Technology, 77 Massachusetts Avenue, Cambridge, MA 02139
59. A. Rohrmoser, Fakultät für Physik E21, Technische Universität München, D-8046, Garching, Germany
60. G. A. Rubio, Idaho National Engineering Laboratory, P.O. Box 1625, Idaho Falls, ID 83415

61–95. J. M. Ryskamp, Idaho National Engineering Laboratory, P.O. Box 1625, Idaho Falls, ID 83415

96. E. Shirai, Department of Research Reactor Operations, Japan Atomic Energy Research Institute, Toki-mura, Naka-gun, Ibaraki-ken 319-11, Tokyo, Japan
97. C. A. Wemple, Idaho National Engineering Laboratory, P.O. Box 1625, Idaho Falls, ID 83415
98. J. G. Williams, Engineering Building, Room 104A, University of Arizona, Tucson, AZ 85719

99–103. ANS Project Office, U. S. Department of Energy, Oak Ridge Field Office, FEDC, MS-8218, P. O. Box 2009, Oak Ridge, TN 37831-8218

104. Office of Assistant Manager for Energy Research and Development, U.S. Department of Energy, Oak Ridge Field Office, P.O. Box 2001, Oak Ridge, TN 37831-2001
105. Office of Honors and Awards, P. King, P.O. Box 2008, Building 2518, MS-6324, Oak Ridge, TN 37831-6324

106–107. Office of Scientific and Technical Information P.O. Box 62, Oak Ridge, TN 37831